Volcanic glass- an ideal paleomagnetic recording material?

Annika Ferk

München 2012

Volcanic glass- an ideal paleomagnetic recording material?

Annika Ferk

Dissertation
an der Fakultät für Geowissenschaften
der Ludwig–Maximilians–Universität
München

vorgelegt von
Annika Ferk
aus Memmingen

München, den 27.02.2012

Erstgutachter: Prof. Dr. Donald B. Dingwell
Zweitgutachter: Dr. habil. Roman Leonhardt
Tag der mündlichen Prüfung: 17.07.2012

Contents

List of Figures

List of Tables

Summary

Volcanic glass is often considered an ideal recording material for paleointensities. Experiments to determine the ancient field intensity are time consuming and mostly have low success rates. Studies have shown that the usage of glassy samples can increase success rates very much as the remanence carriers are in or close to the single domain range. Further, effects like magnetic anisotropy and cooling rate correction can be corrected for. The aim of this thesis is to clarify whether an ideal behavior can be expected when working on volcanic glass. Studies were done on samples of different compositions (phonolite, pantellerite and rhyolite) and varying degrees of devitrification/hydration. Rock magnetic measurements were done to determine the remanence carriers of remelted glass samples of phonolitic composition. Single domain (SD) titanomagnetites were identified to carry the stable remanence and in the course of paleointensity experiments the validity of a cooling rate correction method that makes use of the natural cooling rate of the samples as determined from relaxation geospeedometry was shown. After correction the samples reproduce the intensity of the previously applied field. For the unhydrated samples from Montaña Blanca, Tenerife (phonolitic composition, 2 ka old) and from Mayor Island, New Zealand (pantelleritic composition, 8 ka old) remanence carriers in or close to the SD range were found and high quality well defined paleointensities were obtained. Success rates of the paleointensity experiments were $\geq$70%. The results compare very well with other paleointensities from close-by studies at the respective times. These data support the ideal recording behavior of volcanic glass. Yet, rock magnetic and paleointensity experiments on devitrified and hydrated samples give contrary results: It was found that hydration and devitrification result in a loss of magnetic stability and remanence carriers, an increase in grain size of magnetic particles and a decrease of the "apparent" paleointensity. A possible explanation for these obsevations is a partial or full overprint of the original thermoremanent magnetization by a chemical remanence. It is therefore obvious that suchlike altered glasses are far from being ideal recorders. Great care has thus to be taken when sampling volcanic glass. If pristine glass is sampled, an ideal behavior during paleointensity experiments is probable and - as the here presented data suggest - a good estimate of the ancient field intensity is likely to be gained. If, however, the glass is unknowingly altered the determined paleointensities are prone to underestimate the true field value.

Chapter 1

Introduction and Overview

High quality paleointensity data is essential to address many geoscientific problems: the evolution of the Earth's magnetic field [e.g. Genevey and Gallet, 2002, Heller et al., 2003, Prévot et al., 1990, Tarduno et al., 2007] , its state during long lasting magnetic quiet zones like the Cretaceous normal superchron [Tauxe and Staudigel, 2004, Cottrell and Tarduno, 2000], dating of burned archeological artifacts by comparing archeointensity determinations with known historic intensity evolution curves [Pavón-Carrasco et al., 2008] and the development of high quality geomagnetic field models for the past and present [Korte and Constable, 2005, Leonhardt and Fabian, 2007] are just some examples. However, while determinations of paleodirections are of assuredly high quality, paleointensities are often less reliable. There are many potential problems that one might come across when conducting paleointesity experiments. These are for example anisotropy of thermoremanence (TRM) [Veitch et al., 1984], magnetic domain state bias [Leonhardt et al., 2004a], alteration during geological time or during the laboratory experiment itself [Valet et al., 1996] and different cooling histories in laboratory and nature [Fox and Aitken, 1980, Papusoi, 1972, Leonhardt et al., 2006]. As a consequence success rates of paleointensity experiments are low [Biggin, 2003, Dekkers and Böhnel, 2006]. During the last years it was tried to deal with the above mentioned problems and to improve the quality of paleointensity data in two ways: First, development of new paleointensity methods [Dekkers and Böhnel, 2006, Fabian and Leonhardt, 2010, Muxworthy and Heslop, 2011] that are thought to be less prone to domain state bias than the commonly used Thellier method [Thellier and Thellier, 1959] and variants of it [e.g. Coe, 1967, Shaw, 1974, Leonhardt et al., 2004, Yu and Tauxe, 2005]. Second, systematic choice of samples that have remanence carriers in the single domain (SD) range and for which corrections of some of the biasing effects are possible. Single silicate crystals with magnetic inclusions [Cottrell and Tarduno, 1999, Tarduno et al., 2007] and volcanic glass [e.g. Pick and Tauxe, 1993, Bowles et al., 2005, Leonhardt et al., 2006] have been proposed to be such ideal materials. As the remanence carriers in volcanic glass are mainly in the SD or small pseudo-single-domain (PSD) range [Geissman et al., 1983, Juárez et al., 1998, Smirnov and Tarduno, 2003, Leonhardt et al., 2006] magnetic domain state bias can largely be excluded. Further, alterations in geological time and in laboratory experiments of some glasses are small [Pick and Tauxe, 1993]. Both, the

mainly SD remanence carriers and the absence of alterations improve the success rates of paleointensity experiments remarkably [e.g. Pick and Tauxe, 1993, Leonhardt et al., 2006]. Further, with additional measurements of the TRM along three orthognonal axes one can correct for magnetic anisotropy [e.g. Leonhardt et al., 2006]. Last, but not least it is possible to consider cooling rate effects which can rarely be done for other volcanic rocks. A cooling rate correction technique for volcanic glass that is based on the thermal "memory" of volcanic glasses has been proposed [Bowles et al., 2005, Leonhardt et al., 2006]. The physical state of glass contains a thermal history which is locked in at the glass transition [Dingwell and Webb, 1990, Dingwell, 1995]. Thus, natural glasses contain a record of their natural cooling rates. By using relaxation geospeedometry [Wilding et al., 1995, Gottsmann and Dingwell, 2001b, Potuzak et al., 2008, Nichols et al., 2009] natural cooling rates of glasses can be reconstructed. Further, laboratory cooling rates can be measured and the magnetic cooling rate dependence of the TRM is determined experimentally. Using a linear extrapolation function - as theoretically predicted for the cooling rate dependence of TRM for SD remanence carriers [Halgedahl et al., 1980] - it is possible to obtain cooling rate corrected paleointensity values.

Although these advantages of volcanic glass for paleointensity studies are observed, there are still some critical voices. Smirnov and Tarduno [2003] found that laboratory alteration during paleointensity experiments plays an important role when the glass transition temperature T_g occurs below the blocking temperatures T_B of the thermoremanence. Heating in the laboratory above this region can lead to what they call "neocrystallization", an alteration that is not necessarily detected by the commonly performed alteration checks. Fortunately, the glass transition temperature can be determined in the course of relaxation geospeedometry experiments and this kind of alteration can thus be ruled out by comparison with blocking or Curie temperatures. For submarine basaltic glasses (SBG) it has further been questioned whether the remanence is a primary and total TRM [Heller, 2002], but recent studies suggest that low-Ti titanomagnetite is formed at temperatures above both the glass and Curie temperature [Burgess et al., 2010, Bowles et al., 2011]. Therefore the remanence is considered a total TRM. Another problem that can be encountered when working on sub-aerial glasses is emplacement rotation. Obsidians often are blocky lava flows. In such cases it is mostly difficult to determine in the field whether a block has cooled in-situ or rotated after or even during cooling. Maybe the biggest concerns when dealing with volcanic glasses are devitrification, hydration and perlitization, which in the field are visually identified by crystallinity or perlitic beads and arcuate fractures [McPhie et al., 1993]. It is important to know whether such "alterations" have an impact on the magnetic remanence carriers and the reliability of the recorded paleodirections and -intensities.

The goal of this dissertation is on the one hand to check as to what extent volcanic glass can be considered an ideal recording material and on the other hand to add high quality paleointensity data to the paleomagnetic data base. First, six samples of remelted phonolitic volcanic glass were investigated (chapter 2). They were cooled under increasingly faster cooling conditions in a known magnetic field. Then the paleointensity and the influence of cooling rate were determined and the related overestimate of the paleofield strength

quantified. As the true paleointensity was yielded only after correction, it was thereby shown that cooling rate correction is working and is essential to obtain the true field value. In another publication (chapter 3) it was tried to use the gained knowledge about cooling rate correction to get high quality paleointensity data for a 8 ka pantelleritic obsidian flow from Mayor Island, New Zealand. Paleomagnetic data is not evenly distributed around the globe. For the southern hemisphere only few archeomagnetic data from mainly Peru exist, but additional data from the South Pacific Region is needed to add accuracy to geomagnetic field models. Obsidians that are more or less evenly distributed around the globe give the possibility to add valueable data to the so far unbalanced data base. Alteration during the repeated heatings to high temperatures during the paleointensity experiments on Mayor Island samples made cooling rate correction impossible. Nonetheless, a good upper paleointensity estimate of the field strength 8 ka ago for the South Pacific Region was obtained. In a third study (chapter 4) two of the above mentioned problems were examined: the emplacement rotation and break-up of a 2 ka obsidian block and the devitrification of a 750 ka flow and its influence on the recorded paleointensity. The rotated block was shown to give the same intensity value as other sites from the same eruption. Taken together these data give a high quality field value for Tenerife 2 ka years ago. The devitrification, however, was found to have a great influence on the reliability of the magnetic record. Rock magnetic measurements showed a loss of remanence carriers and magnetic stability with increasing devitrification. Further, a decrease of "apparent" paleointensity with degree of devitrification was found and it was not possible to distinguish between right and wrong paleointensity values as the quality of the two did not differ. To analyze the problems connected to hydration/alteration of volcanic glasses in more detail samples from Iceland that showed varying degrees of perlitization were studied (chapter 5). Again a loss of magnetic stability and remanence carriers as well as a decrease of "apparent" paleointensity together with increasing perlitization were found. The finding of these two studies might have a strong impact on the reliability of paleointensities from SBG as for example Helo et al. [2011] reported post-eruptive hydration of SBG. If such hydration is common for SBG, a systematic underestimation of the true paleointensity has to be taken into account when dealing with data from SBG.

Chapter 2

A cooling rate bias in paleointensity determination from volcanic glass: an experimental demonstration.

This chapter was published in the Journal of Geophysical Research in 2010 [Ferk et al., 2010]. Co-authors are F. W. von Aulock, R. Leonhardt, K.-U. Hess, and D. B. Dingwell.

Abstract

The suitability of volcanic glass for paleointensity determinations is the basis of many studies. The dominant single domain (SD) magnetic remanence carriers, the pristine character of volcanic glass, the possibility to correct paleointensity data for cooling rate dependence using relaxation geospeedometry are all arguments that have been made in favor of this technique. In the present study the validity of cooling rate correction is tested using remelted volcanic glass. To obtain a stable multicomponent glass, with ideal magnetic properties, a natural phonolitic glass from Tenerife was remelted in air to avoid heterogeneity and degassing in later experiments. Further, it was tempered for altogether 10 hours at 900°C to yield a sufficient concentration of magnetic remanence carriers. To exclude nucleation or crystallization 6 samples were then heated to about 60°C above the calorimetric glass transition temperature (≈660°C) and quenched at different rates from 0.1 to 15 K/min. Rock magnetic measurements show that low titanium titanomagnetite in the SD range is the main remanence carrier. After performing paleointensity experiments using a modified Thellier method, the dependence of the thermoremanence on cooling rate was investigated. Using the synthesis cooling rates and the experimentally determined magnetic cooling rate dependencies we were able to correct the data and obtained a mean paleointensity of 46.9±1.3μT, which reflects the ambient field of 48μT within error. The uncorrected mean paleointensity corresponds to a 18% larger value of 56.5±0.9μT. Therefore, application of a cooling rate correction is essential to obtain the correct ancient magnetic field intensity from SD assemblages in volcanic glass.

2.1 Introduction

Obtaining accurate values of absolute paleomagnetic field strength is of central interest for a variety of geoscientific problems, ranging from the Earth's deep interior to the magnetosphere. Based on paleointensity information two preferred states of the geodynamo were postulated, a low-field and a high-field state [Shcherbakov et al., 2002, Heller et al., 2003], suggesting significantly distinct field generation processes within the Earth's core. The predominant field intensity state during long lasting magnetic quiet zones, like the Cretaceous normal superchron, has been studied deeply [Prévot et al., 1990, Pick and Tauxe, 1993, Cottrell and Tarduno, 2000]. The evolution of the Archaean magnetic field strength is investigated for the evolution of the magnetosphere, shielding the early Earth's atmosphere from solar-wind erosion [Tarduno et al., 2007]. Even dating of burned archeological artifacts can be achieved by comparing archeointensity determinations with known historic intensity evolution curves [Pavón-Carrasco et al., 2008].
Unfortunately reliable paleointensity values are difficult to obtain because many factors can bias the results. One of these biasing mechanisms, which is only seldom considered, is related to a difference between cooling rates in nature and during the laboratory paleointensity experiment. It has been shown theoretically and experimentally that single domain (SD) particles, which are usually thought to provide the best paleointensity record according to other magnetic-domain-state-related biasing factors, are most strongly affected by cooling rate differences. Often, significant overestimates of the geomagnetic field are observed [Halgedahl et al., 1980, Fox and Aitken, 1980, McClelland-Brown, 1984, Chauvin et al., 2000, Leonhardt et al., 2006]. Therefore, a technique to enable correcting the cooling rate effect, is essential to obtain accurate paleointensity data.
For archeological materials, mostly burned artifacts like potsherds, such corrections are sometimes conducted using heating/cooling cycles, which are thought to resemble the original ancient burning condition [Fox and Aitken, 1980, Chauvin et al., 2000, Genevey and Gallet, 2002]. For volcanic rocks, however, cooling rates are rarely considered for [Bowles et al., 2005]. Based on historical dated obsidians from Lipari, Italy, Leonhardt et al. [2006] proposed a cooling rate correction technique, which can be applied to volcanic glasses. The physical state of glass contains a thermal history which is locked in at the glass transition [Dingwell and Webb, 1990, Dingwell, 1995]. Thus natural glasses contain a record of their natural cooling rates. By using relaxation geospeedometry [Wilding et al., 1995, Gottsmann and Dingwell, 2001b, Potuzak et al., 2008, Nichols et al., 2009] natural cooling rates of glasses can be reconstructed. Laboratory cooling rates are known and the magnetic cooling rate dependence of the thermoremanent magnetization (TRM) is determined experimentally. Using a linear extrapolation function, the absolute paleointensity values of the pristine, SD dominated glass can then be determined.
The validity of the cooling rate correction technique and its inherent assumptions are tested in this study. Six samples of remelted volcanic glass are investigated, which were quenched under increasingly faster cooling conditions and acquired their remanent magnetization in a known magnetic field. Thus, an analysis of the influence of different cooling histories on the determined paleointensity is possible and the extent of any field overestimate can be

quantified.

2.2 Sample preparation

Samples were prepared at the Department of Earth and Environmental Sciences of the University of Munich. To obtain a stable multicomponent glass with ideal magnetic properties, circa 500g of a natural phonolitic glass from Lavas Negras on the north side of Teide, Tenerife, was remelted in a thin-walled platinum crucible (Fig. 2.1a) using a Nabertherm HT14/07 furnace operating at 1600°C in air. The sample was held at these conditions for circa 12 hours to ensure homogeneity, volatile escape and fining of bubbles. Rock magnetic experiments for the glassy products of this fusion showed only paramagnetic contributions. Therefore, the sample was tempered at 900°C in air to yield a sufficient concentration of magnetic remanence carriers. In preliminary qualitative DTA (Differential Thermal Analysis) measurements an exothermal peak at 835°C was interpreted as the beginning of crystallization. Thus, in order to ensure limited growth yet significant nucleation of crystals the annealing temperature was chosen to lie slightly above these first signs of crystallization. The sample was heated with ≈7.5 K/min up to 900°C and held there for 2 hours, then subsequently cooled down by switching off the electrical power of the oven and opening its door. This procedure was repeated twice with annealing of 3 hours and 5 hours, respectively. After each annealing step, rock magnetic experiments showed an increasing abundance of magnetic minerals and a sufficient concentration was found after the 5 h step. Next, the glass transition temperature T_g was determined by relaxation geospeedometry. For this purpose, the heat capacity c_p of the glass was measured in a Differential Scanning Calorimeter (DSC) and the peak in c_p was taken as T_g. Detailed descriptions of the experimental procedures can be found in Wilding et al. [1995], Gottsmann and Dingwell [2001b], Potuzak et al. [2008] and Nichols et al. [2009]. For one sample, that had previously been cooled with 5 K/min, $T_g = 663$°C was determined. To exclude further nucleation or crystallization six miniature cores of 5mm diameter were then heated in air in a Netzsch 402C dilatometer with 10 K/min to circa 60°C above T_g at around 720°C, kept at this temperature for five minutes and each quenched at one of the following cooling rates: 0.1, 0.5, 1, 5, 10 and 15 K/min. Measurement of the magnetic field intensity inside the bifilar wound Netzsch dilatometer using a fluxgate sensor showed that it is identical to the ambient magnetic field at Munich, i.e. 48 μT. Sample names (e.g. LNN3-600-0.1) indicate the natural sample from which the remelted glass was derived (LNN3: Lavas Negras North, sample 3), holding time at 900°C (600 min) and quench rate (e.g. 0.1 K/min).

2.3 Magnetic mineralogy and domain state

Rock magnetic measurements to identify the magnetic mineralogy and its domain state were done at a Variable Field Translation Balance and analyzed using the RockmagAnalyzer software [Leonhardt, 2006]. Isothermal remanent magnetization (IRM) acquisition,

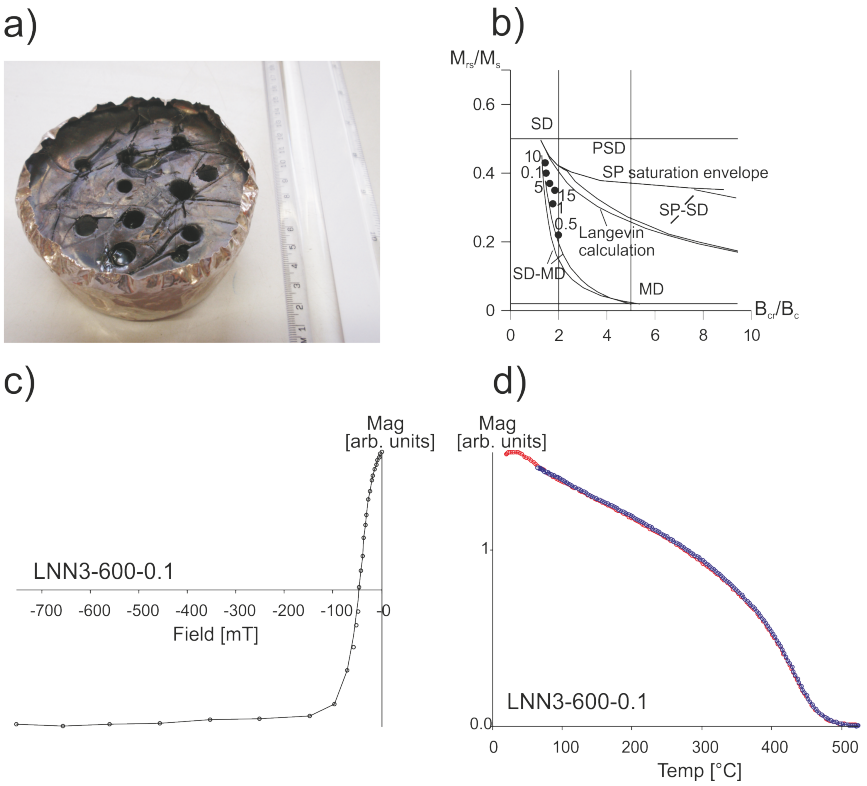

Figure 2.1: (a) Picture of the remelted glass in the platinum crucible, (b) hysteresis parameters of the different samples (indicated by the respective cooling rates), shown in a Day plot [Day et al., 1977] with domain state related boundaries and mixing lines by Dunlop [2002], (c) and (d), representative backfield and thermomagnetic (reduced for paramagnetism) curve (sample LNN3-600-0.1).

isothermal backfield curves (Fig. 2.1c) and hysteresis loops at room temperature as well as thermomagnetic curves (applied field: about 400 mT, Fig. 2.1d) were measured in that order on specimens belonging to the same miniature cores as those used for paleointensity experiments. In addition, sample LNN3-600-0.1 was stepwise heated to 420°C, 480°C and 530°C and after each of these thermomagnetic measurements, the backfield and hysteresis measurements were repeated at room temperature to test for thermal stability.

Curie temperatures, hysteresis and backfield parameters as well as tail and quality parameters of the later paleointensity experiments can be found in Tab. A.1 of the appendix. Heating and cooling curves of the thermomagnetic measurements are reversible, indicating an absence of alteration (Fig. 2.1d). This is further supported by the almost identical hysteresis and backfield parameters of sample LNN3-600-0.1 after the different heating steps. Determinations of second derivatives for the thermomagnetic curves of all samples indicate a Curie temperature T_C between 410 and 460°C, corresponding to titanomagnetite ($Fe_{3-x}Ti_xO_4$) with titanium contribution of $x \approx 0.22$. Between 70 and 90°C a very small kink is found in the thermomagnetic curves of all samples. Buddington and Lindsley [1964]

have shown that in silicic melts low-titanium titanomagnetite can coexist only with high-titanium hemoilmenite, but not with high-titanium titanomagnetite. Thus, the low T_C of about 80°C would relate to titanium contribution $y \approx 0.6$ in hemoilmenites ($Fe_{2-y}Ti_yO_3$). This hemoilmenite fraction, however, has a negligible contribution to the whole magnetization.
T_C and therefore also the blocking temperatures T_b lie well below T_g of ≈660°C, excluding any bias to paleointensity determination related to the glass transition [Smirnov and Tarduno, 2003]. Fast saturating IRM curves as well as Bloemendal S_{300} values [Bloemendal et al., 1992] close to 1 are indicative for magnetically soft material, as expected for titanomagnetite as main remanence carrier. Hysteresis parameters analyzed according to Dunlop [2002] show close to SD behavior, although minor variations along the SD-MD mixing line are observed (Fig. 2.1b). IRM and backfield data plotted as suggested by Henkel [1964] lie close to the line for ideal Stoner-Wohlfarth particles, further supporting a predominant SD character of the remanence carrying particles (see Fig. A.1 in the appendix). This conclusion is underlined by repeated thermal demagnetizations during the Thellier-Thellier experiments. Hereby the absence of any magnetization tails (Fig. 2.2) confirms SD behavior of the remanence carrying fraction.
There is no obvious trend in hysteresis, backfield and/or T_C data that can be related to the varying cooling rates. All measurement parameters are very similar. This supports our hypothesis that by heating only to about 60°C above the glass transition temperature before quenching under different cooling conditions, new nucleation or growth of crystals can be neglected. Thus, in this manner, rock magnetically very similar samples containing SD titanomagnetites have been obtained, which differ essentially only in their cooling histories.

2.4 Paleointensity determination

All paleointensity determinations were conducted in a MMTD20 thermal demagnetizer at the paleomagnetic laboratory of LMU Munich in Niederlippach. Laboratory fields of 30±0.1 μT were used for all measurements and applied during heating and cooling. Intensity measurements were done using the modified Thellier-technique MT4 [Leonhardt et al., 2004], which is a zero-field first method that includes partial TRM (pTRM) checks (in-field), additivity checks (zero-field) [Krása et al., 2003], and pTRM-tail checks (zero-field) [Riisager and Riisager, 2001]. Directional differences between the applied field and the natural remanent magnetization (NRM) of the pTRM-tail check are taken into account according to Leonhardt et al. [2004a]. All determinations were analyzed using the ThellierTool4.21 software and its default criteria [Leonhardt et al., 2004]. The samples do not show any magnetic anisotropy as was indicated by anisotropy of magnetic susceptibility (AMS) being well below the signal of the sample holder and B_{cr} values of about 40 mT. An isotropic behavior of the samples is reasonable as during the production of the remelted glass no anisotropy "source", such as the flow direction of a natural obsidian deposit, was present, i.e. no differential stresses or resulting strains obtained during the synthesis.

Table 2.1: Paleointensity results and correction

Sample	q	$H_{UC} \pm \sigma_{UC}$ [μT]	f_{CR}	$H_{CR} \pm \sigma_{CR}$ [μT]
LNN3-600-0.1	20.7	54.7±1.6	1.194±0.038	45.8±3.7
LNN3-600-0.5	20.0	57.1±1.3	1.396±0.028	40.9±2.9
LNN3-600-1	26.5	59.6±1.6	1.199±0.016	49.7±2.6
LNN3-600-5	25.4	53.4±1.0	1.260±0.029	42.4±2.5
LNN3-600-10	88.5	57.6±0.3	1.181±0.008	48.8±0.7
LNN3-600-15	33.0	54.3±0.8	1.138±0.009	47.7±1.3
weighted average		*56.5±0.9*		*46.9±1.3*

Sample names contain the original sample reference of the remelted glass (LNN3: Lavas Negras North, sample 3), the tempering time at 900°C (600 min) and the quench rate in K/min (e.g. 0.1 K/min). H_{UC} and H_{CR} are the paleointensity values of the different samples with associated errors for the uncorrected and cooling rate corrected determinations, respectively. Uncertainties are determined by error propagation and include the scatter about the straight line segment and the uncertainty related to the cooling rate correction factor f_{CR}. Also shown are weighted averages of the intensity values and associated uncertainties. The quality factor q was chosen as weighting parameter for H_{UC} and $1/\sigma_{CR}$ for H_{CR}.

The quality of individual paleointensity determinations is very good. Linear trends covering a fraction of the NRM $f \geq 93\%$ were analyzed for all samples. Quality factors q exceed 20, no alteration is present (difference ratio DRAT $< 2.4\%$) and, as mentioned before, magnetization tails are small. Uncorrected paleointensity results range from 53.4±1.0 to 59.6±1.6 μT, giving a mean weighted paleointensity of 56.5±0.9 μT (Tab. 2.1; weighting factor q), which exceeds the ambient field during experimental cooling by about 18%. NRM/TRM plots and decay plots of three samples with cooling rates of 0.1, 1 and 15 K/min are shown in Fig. 2.2.

2.5 Cooling rate dependency

Although a dominating SD behavior is found, hysteresis and pTRM tail measurements suggest slightly varying domain states of the different samples. Due to domain state variations, also a varying cooling rate dependency of the TRM is to be expected [McClelland-Brown, 1984] and a direct correlation between paleointensity and cooling is hampered. Following Leonhardt et al. [2006], the magnetic cooling rate dependency was measured. A field of 30±0.1 μT was applied. For fast cooling the cooling fan of the MMTD20 furnace was used just like during the paleointensity experiments, while slow cooling was obtained through cooling without fan operation. Laboratory cooling rates were determined from basaltic

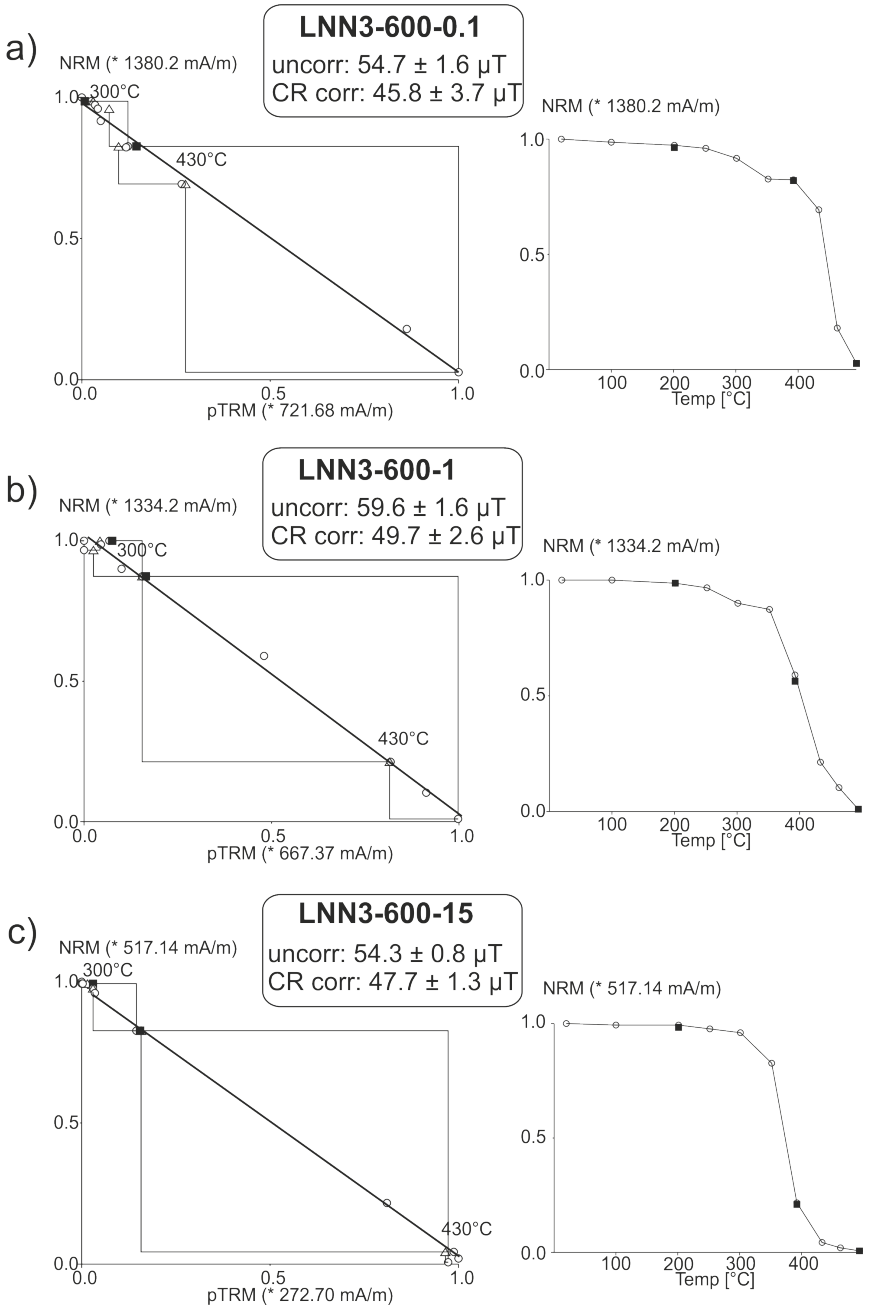

Figure 2.2: NRM/pTRM diagrams (triangles: alteration checks, squares: additivity checks) and respective decay plots of demagnetization steps (squares: tail checks) for three of the remelted samples with cooling rates of (a) 0.1, (b) 1 and (c) 15 K/min. Temperatures in both plots indicate temperatures on the display of the Shaw oven; especially at higher steps, sample temperatures are significantly lower. Intensity results are given for uncorrected and cooling rate (CR) corrected analysis.

samples that have the same size and volume as the studied miniature cores between 700°C and 600°C. This temperature range was chosen, because it includes the glass transition at about 660°C and determination of natural cooling rates is only possible at the glass transition. Although the change in cooling rates down from the glass transtion to blocking temperatures may not be exactly the same in nature and in the laboratory, this is so far the closest one can get to a comparison between natural and laboratory cooling. To get the mean cooling rates of our furnace in this temperature range the temperature decrease, measured by a thermocouple inside one of the basaltic samples, was monitored versus time. An initial fast heating/cooling cycle with a cooling rate of ≈410 K/min was used to imply a TRM ($TRM_{f,1}$). Then a 74-fold slower heating/cooling cycle with a cooling rate of ≈5.5 K/min ($TRM_{s,1}$) and again a higher one ($TRM_{f,2}$) in order to check for alterations during the experiment, were performed. $TRM_{f,1}$ and $TRM_{f,2}$ differ by $\leq 2\%$, confirming that alteration is absent. These differences are also used as error estimate for inaccuracy in determination of both $TRM_{s,1}$ and $TRM_{f,1}$. A conservative estimate of the uncertainty in cooling rate determination is 10% for fast cooling and 5% for slow cooling.

For slow cooling experiments the TRM intensity is 11% to 26% larger than for fast cooling, as would be expected for a non-interacting SD assemblage [Halgedahl et al., 1980, Dodson and McClelland-Brown, 1980]. The magnetic cooling rate dependency is extra-/interpolated to the original cooling rates as used during the synthesis of the remelted glasses. The laboratory measured $TRM_{f,1}$ and $TRM_{s,1}$, both normalized to $TRM_{f,1}$, are plotted versus $\ln(\dot{T}_{f,1}/\dot{T})$ (Fig. 2.3). A linear extra-/interpolation is valid according to Halgedahl et al. [1980], if non-interacting SD particles, dominantly blocking close to the respective blocking temperature, are the remanence carriers. As our samples are at least close to SD and unblock sharply within about 50°C, these conditions are fulfilled. The previous error estimates for inaccuracy of laboratory cooling rate and magnetization determination allow a minimum/maximum error propagation towards the natural cooling rates (Fig. 2.3). The obtained cooling rate correction factor $f_{CR} = \mathrm{TRM}/\mathrm{TRM}_{f,1}$ is then used to correct the paleointensity values H_{UC} (Tab. 2.1) by $H_{CR} = H_{UC}/f_{CR}$. Error propagation, including the uncertainties of the paleointensity experiments and of the cooling rate correction factor determination, gives the total uncertainty σ_{CR} of the individual cooling rate corrected paleointensity values. Application of cooling rate correction significantly reduces the paleointensities to a mean value of 46.9±1.3 μT (weighting factor $1/\sigma_{CR}$, Tab. 2.1). This reflects the ambient field value of 48 μT very good and verifies the need for cooling rate correction in SD dominated materials.

2.6 Discussion and Conclusion

Rapid laboratory cooling during paleointensity determination, opposed by slow cooling during ancient NRM acquisition, leads to paleointensity overestimates and hence a strong bias towards erroneously higher field values in SD-dominated paleointensity recorders. In this study, laboratory experiments were conducted on remelted volcanic glass with known cooling histories during TRM acquisition, whose SD character is confirmed by rock mag-

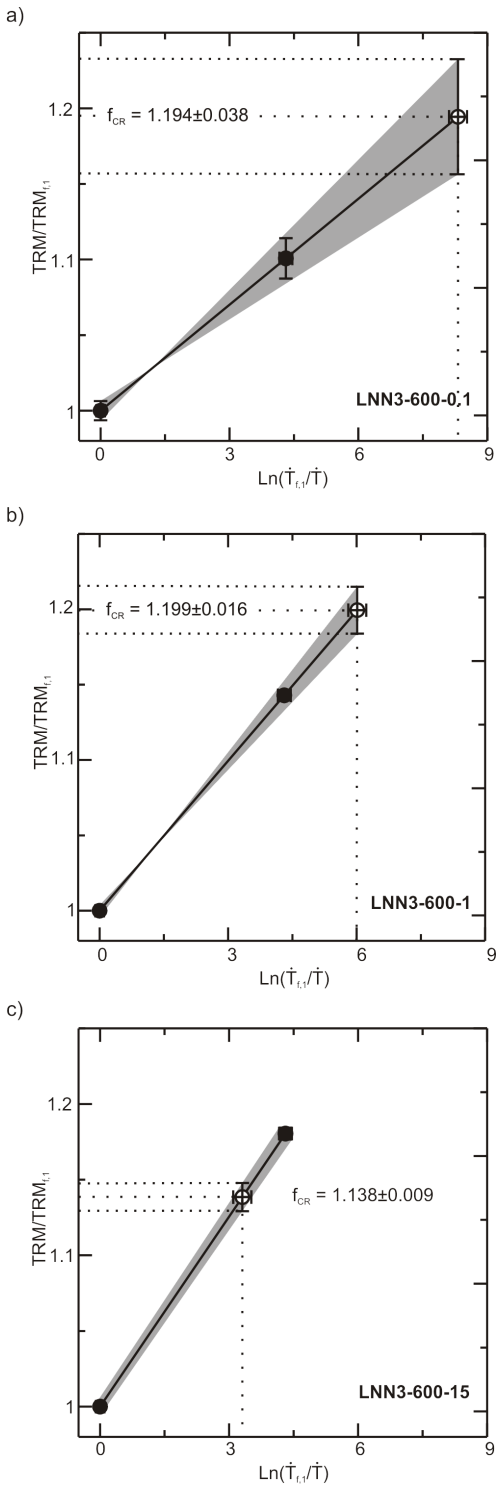

Figure 2.3: Cooling rate correction using the laboratory measured cooling rate dependency (solid symbols) and related uncertainties, as well as the linear extra-/interpolation of the TRM dependency to the synthesis cooling rates (open symbols). (a), (b) and (c) show the same samples as in Fig. 2.2, i.e. samples cooled with (a) 0.1 K/min, (b) 1 K/min, (c) 15 K/min.

netic measurements and small magnetization tails. A 75-fold lower cooling rate results in 11% to 26% higher TRM acquisition values, which exceeds the theoretically predicted magnetic cooling rate dependencies of SD magnetite which would be in the order of 10% [Halgedahl et al., 1980, Dodson and McClelland-Brown, 1980]. TRM overestimates exceeding the theoretically predicted values were also observed in other experimental studies on archeomagnetic materials [e.g Genevey and Gallet, 2002]. A possible reason for the here observed overestimates of 18% on average, could be related to titanomagnetites (TM20) as remanence carriers and not SD magnetite or hematite as used in the theoretical studies. Titanomagnetites are characterized by different magnetic parameters, of which in particular the blocking temperature relationship, relaxation times and anisotropy are relevant for cooling rate dependencies. It should also be mentioned that overcorrections of the expected paleointensity and largest TRM overestimates are found particularly for two samples LNN3-600-0.5 and LNN3-600-5. These two overcorrections give rise to sligthly larger uncertainties of the average cooling rate corrected field value compared to the uncorrected paleointensity estimate. Nevertheless the originally applied field is then correctly reproduced (Tab. 2.1). The reason for overcorrection in the two specimens remains elusive, because all determined rock magnetic parameters are similar to the other specimens. Only indications for slightly larger MD contributions are found for both samples (see Day plot of Fig. 2.1b and tails in Tab. A.1 in the appendix) although both samples are dominated by SD remanence. MD contribution, however, would be expected to reduce the TRM ratio [McClelland-Brown, 1984, Fabian and Leonhardt, 2009].

Cooling rates of 290 K/min during the Thellier experiment are larger than the cooling rates of 0.1 to 15 K/min used for initial TRM acquisition. These initial cooling rates correspond well to the middle range of naturally observed cooling rates in volcanic glasses (140 K/min to 0.001 K/min [Gottsmann et al., 2004, Gottsmann and Dingwell, 2002]), yet they are already sufficient to generate a maximum field overestimate about 18%. Similar overestimates of 22% are reported from natural volcanic glasses [Leonhardt et al., 2006]. These large overestimates clearly underline that cooling rate correction is necessary to obtain correct past geomagnetic field values in SD assemblages. Such correction involves two basic requirements: (1) knowledge of the natural cooling rate during NRM acquisition; (2) a known dependency between TRM and cooling rate if extra- or interpolation is necessary. The first requirement can be achieved for volcanic glass, where natural cooling rates can be determined by relaxation geospeedometry [Wilding et al., 1995]. This technique also yields the glass transition temperature (T_g), which marks the transition between a supercooled liquid and a solid glass. T_C of our samples ($\leq$440°C) is well below T_g of 660°C. Hence, the samples are suitable for paleointensity determination as TRM acquisition occurs in a solid-like state. Further, for archeomagnetic investigations on burned artifacts, results from experimental archeology can be consulted to determine the natural cooling rate [e.g Genevey and Gallet, 2002]. However, for the most widely used material in absolute paleointensity studies, basaltic rocks, an accurate determination of cooling history remains elusive. The second requirement, extra-/interpolation towards the natural cooling rate, requires a known magnetic cooling rate dependency. It has been shown theoretically [Halgedahl et al., 1980] that a linear extra-/interpolation as used in Fig. 2.3 is applicable

for a narrow unblocking spectra as observed in our samples. Magnetic cooling rate dependencies of wide unblocking spectra and PSD to MD dominated materials, which are usually considered as less reliable for paleointensity studies, will require further investigation.
The treatment of uncertainties of extra-/interpolation follows the outline of Leonhardt et al. [2006]. The errors for the laboratory cooling rates and uncertainties in the TRM acquisition experiment are conservative estimates. Thus, extra-/interpolation of these uncertainties towards the natural cooling rates (Fig. 2.3) gives a realistic upper limit for the uncertainties associated with cooling rate correction. The final accuracy of individual cooling rate corrected paleointensity determinations (σ_{CR}) is related to the sum of uncertainties caused by deviations from the straight line segment and the error of the correction factor f_{CR}. Therefore, σ_{CR} comprises the quality of all successive experiments for each sample. The weighted average paleointensity of the remelted glass samples is then determined using $1/\sigma_{CR}$ as weighting parameter.
After cooling rate correction our remelted glass samples give a paleointensity of 46.9±1.3 μT, which reflects the originally applied field value of 48 μT within its margins of error. Without the two overcorrected values, the applied field of 48 μT would be exactly obtained after correction (48.3±0.6 μT). The uncorrected average value of 56.5±0.9 μT exceeds the original field by 18%. Therefore, application of cooling rate correction is essential to retrieve the correct ancient field value in case of SD dominated material.

Acknowledgements

We thank P. Camps and an anonymous reviewer for their comments. Funding was provided by DFG grant Le1905/1-1 and FWF grant P21221-N14. D. B. Dingwell acknowledges the funding support of a LMUexcellent Research Professorship in experimental Volcanology (Bundesexzellenzinitiative). We also thank N. Petersen and R. Egli for many helpful discussions.

Chapter 3

Paleointensities on 8ka obsidian from Mayor Island, New Zealand

This chapter is a slightly modified version of a publication in Solid Earth from 2011 [Ferk et al., 2011a]. Co-authors are R. Leonhardt, K.-U. Hess, and D. B. Dingwell.

Abstract

The 8 ka B.P. (6050 BCE) pantelleritic obsidian flow on Mayor Island, Bay of Plenty, New Zealand, has been investigated using 30 samples from two sites. Due to a very high paramagnetic/ferromagnetic ratio it was not possible to determine the remanence carriers. This is despite the fact that the samples were studied intensively at low, room and high temperatures. We infer that a stable remanence within the samples is carried by single- or close to single-domain particles. Experiments to determine the anisotropy of thermoremanence tensor and the dependency on cooling rate were hampered due to alteration resulting from the repeated heating of the samples to temperatures just below the glass transition. Nonetheless, a well-defined mean paleointensity of 57.0±1.0 μT, based on individual high quality paleointensity determinations, was obtained. This field value compares very well to a paleointensity of 58.1±2.9 μT which Tanaka et al. [2009] obtained for 5500 BCE at a site 100 km distant. Agreement with geomagnetic field models, however, is poor. Thus, gathering more high-quality paleointensity data for the Pacific region and for the southern hemisphere in general to better constrain global field models is very important.

3.1 Introduction

The quality of global geomagnetic field models is always restricted by the quality and distribution of the included data. While the quality of paleodirections is assuredly high, paleointensities are thought to be less reliable. During the conduction of paleointensity experiments one must be aware of potential problems such as alteration during geological

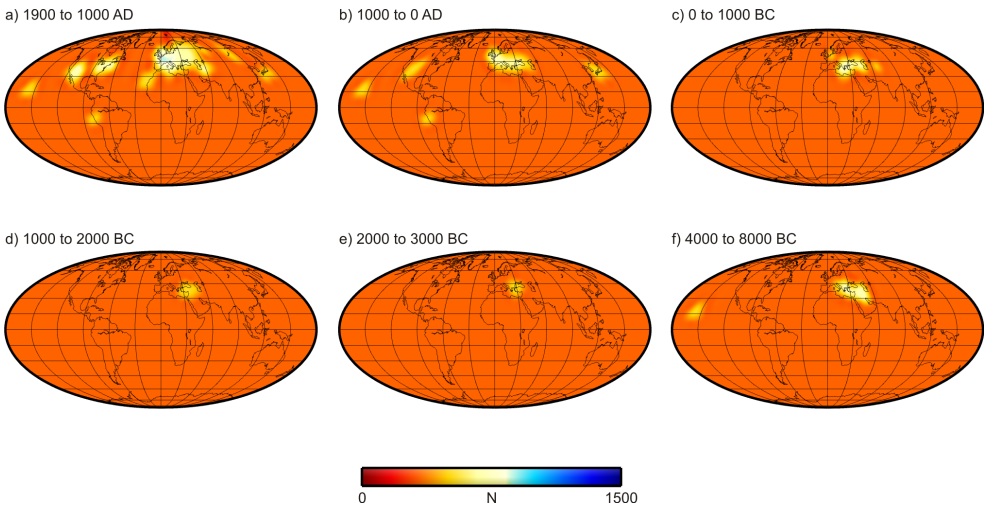

Figure 3.1: Global distribution of archeomagnetic data from Korte and Constable [2005], Genevey et al. [2008] for the last 10 ka.

time or even during the laboratory experiment itself [Valet et al., 1996], anisotropy of thermoremanence [Veitch et al., 1984], magnetic domain state bias [Leonhardt et al., 2004a] and different cooling histories in laboratory and nature [Fox and Aitken, 1980, Papusoi, 1972, Leonhardt et al., 2006]. Especially during the last few years, several studies have tried to deal with these problems and to improve the quality of paleointensity determination either by introducing new methods [Dekkers and Böhnel, 2006, Fabian and Leonhardt, 2010, Muxworthy and Heslop, 2011] or by using samples that have remanence carriers in the SD range and for which corrections of some of the biasing effects are possible. Volcanic glass [Pick and Tauxe, 1993, Bowles et al., 2005, Leonhardt et al., 2006] and single silicate crystals with magnetic inclusions [Cottrell and Tarduno, 1999, Tarduno et al., 2007] have been proposed to be such ideal materials. Paleomagnetic data is by no means evenly distributed around the globe. Fig. 3.1 shows the distribution of archeomagnetic and paleomagnetic data around the world for the last 10 ka [Korte and Constable, 2005, Genevey et al., 2008]. For example, the data set behind the global field model CALS7K by Korte and Constable [2005] consists mainly of data from Europe, Egypt and Japan plus some data points from North America and Peru. For the rest of the world, especially for the southern hemisphere, data is very sparse.

To address both of the problems noted above, i.e. quality and global distribution of data, a 8 ka B.P. pantelleritic obsidian flow from Mayor Island, Bay of Plenty, New Zealand has been analyzed. By studying pantelleritic volcanic glass one should be able to rule out and/or correct for most biasing and other restricting effects. In this manner high quality data would be obtained for a region in the southern Pacific for which, to date, very few paleomagnetic data exist. Unfortunately, alteration during the experiments hampered application of corrections for most samples. Nonetheless, high quality paleointensity data could be obtained as will be shown in the following sections.

3.2 Geology and sampling

Mayor Island (Tuhua) lies 26 km north of Tauranga, Bay of Plenty, New Zealand in a back-arc setting 100 km behind the Taupo Volcanic Zone (Fig. 3.2). It is a volcano of Quaternary age [Houghton and Wilson, 1986] with rocks of peralkaline rhyolite composition that span the comendite-pantellerite boundary of Macdonald's [1974] classification and are referred to as pantellerites by Stevenson et al. [1993]. It rises 700 m from the sea floor from a base of a 15 km wide composite shield. The island is 4.5 km wide and dominated by a 3 km wide composite caldera whose steep walls rise 250 to 350 m above sea level. The caldera was built from three collapse events [Houghton et al., 1992] with the most recent one obscuring the form of the others. The 8000±70 a B.P. (6050±70 BCE; radiocarbon-dated [Buck et al., 1981]) flow studied in this paper predates this last collapse event (6.3 ka [Houghton and Wilson, 1986]). The 8 ka deposit consists of a 1 m thick pumice fall bed that is overlain by a 20 to 70 m thick lava flow that drapes steeply over both the inner and outer walls of the caldera. Detailed petrographic and physical characteristics and the emplacement history of the flow can be found in Stevenson et al. [1993]. The deposit is made up of finely vesicular pumice that forms a surface carapace and represents the upper 10 m of the flow. Below this follows a upper obsidian layer (UOBS) that gradually changes downwards to a central crystalline rhyolite layer. Beneath this rhyolite layer a lower obsidian layer (LOBS) that incorporates a basal crumble layer is found above the already mentioned fall deposit [Stevenson et al., 1993]. The deposit has been interpreted by Stevenson et al. [1993] as a fountain-fed flow that deformed after emplacement.

All samples for this study were originally obtained by Gottsmann and Dingwell [2002] without orientation for their study on the thermal history of the 8 ka flow. A 70 cm thick vertical profile of LOBS (Fig. 6 in Gottsmann and Dingwell [2002]) was sampled at Hall's Pass which is an area where the flow drapes back into the caldera. Sample names indicate sample number and vertical position measured from top, i.e. LOBS2.13: sample 2, at depth of 13 cm. The sequence was taken above a crumble breccia containing disintegrated, sligthly fused pumices from the underlying pumice deposit and clasts of the overlying obsidian. Towards the central crystalline rhyolite on top of LOBS a decimetre thick transition zone with obsidian fragments is incorporated into the rhyolite or in layers of folded glass and rock bands. In this transition zone gas blisters of ∼10 cm are found. At Parikoura Point on the east coast of the island a horizontal profile was sampled through exposures of UOBS (Fig. 7 in Gottsmann and Dingwell [2002]). It consists of steeply inland dipping flow ridges and ramps. It was sampled at the northern cliff face along a slightly north-easterly inclined platform. The profile is ∼30 m long and comprises a sequence of anticlinal flow ridges and synclinal troughs between these ridges. Samples were taken from the exposed surfaces of the flow ridges. Sample names give horizontal profile distance in cm, e.g. sample UOBS1420 is at 14.20 m in the profile. One flow ridge was sampled in a 5.2 m long detailed profile with spacing of 20 to 50 cm (samples UOBS700 to UOBS1220). In the transition zone from the central crystalline rhyolite to the UOBS alternating bands of crystalline rhyolite and obsidian as well as an increase in bubble content are found. At the upper end of UOBS gas blisters and increasing vesicularity show the transition to the

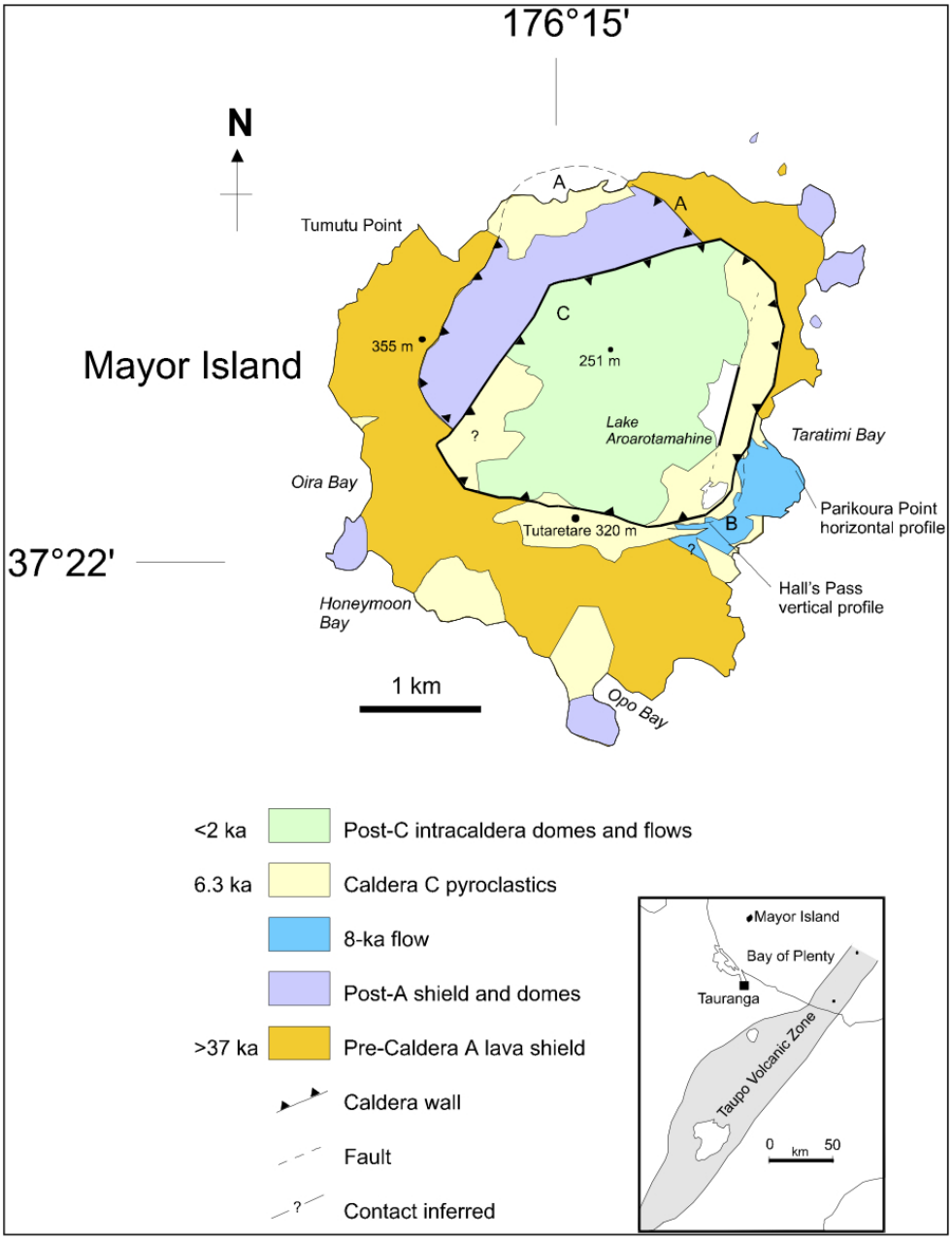

Figure 3.2: Location of Mayor Island and geology map including the identification of caldera parts A, B and C and location of investigated sites (LOBS: Hall's Pass, UOBS: Parikoura Point) within the 8 ka flow (blue). Taken from Gottsmann and Dingwell [2002].

finely vesicular pumice layer [Stevenson et al., 1993].
Samples of both LOBS and UOBS are very pristine with no indication of secondary hydration or alteration processes. Both layers show very similar chemical composition with an average $molAl_2O_3/mol[(Na_2O + K_2O)]$ of 1.54 [Gottsmann and Dingwell, 2002], which does not change with layer depth or horizontal sample location within the sites [Gottsmann and Dingwell, 2002].

3.3 Relaxation geospeedometry

Relaxation geospeedometry, i.e. measurements of the heat capacity at constant pressure c_p, can be used to determine both the glass transition temperature T_g and the natural cooling rate. The theoretical and mathematical background for this method has been dicussed in detail by e.g. Wilding et al. [1995] and Gottsmann and Dingwell [2001b]. Here we only shortly introduce the general concept: By passing through the glass transition, the melt changes from liquid-like viscous to solid-like brittle behavior [Dingwell and Webb, 1990]; it goes from a thermodynamic state of metastable equilibrium to one of disequilibrium. Thus, T_g depends not only on the composition of the melt, but also on the quench rate. This information becomes frozen into the glass structure and can be gained by measurement of a structure-dependent physical property such as heat capacity c_p, during reheating. Such relaxation geospeedometry had already been performed by Gottsmann and Dingwell [2002] on LOBS and UOBS samples. A detailed description of the experiments can be found there. Their measurements and modelling procedures resulted in modelled cooling rates ranging from 0.00072 K/min to 6.3 K/min and glass transition temperatures between 489 °C and 405 °C (Tab. 3.1). Within the vertical profile of LOBS cooling rates increase from 0.00072 K/min close to the crystalline rhyolite to 0.017 K/min at the contact to the basal crumble breccia (Tab. 3.1). The centre of LOBS shows uniform cooling rates of ∼0.001 K/min. Most of the samples of UOBS show cooling rates between 0.00102 K/min (UOBS1080, Tab. 3.1) and 0.01242 K/min (UOBS2650, Tab. 3.1). UOBS120 and UOBS2095 show much faster cooling rates of 6.3 K/min and 2.5 K/min, respectively.

3.4 Magnetic mineralogy and domain state

Rock magnetic measurements were performed to analyze magnetic mineralogy and domain state. Isothermal remanent magnetization (IRM) acquisition, isothermal backfield curves, hysteresis loops (all at room temperature) and thermomagnetic curves were measured on a Variable Field Translation Balance (VFTB) by Petersen Instruments at the University of Munich, Germany using 8 mm diameter miniature cores. Further, hysteresis and backfield curves (at low, room and high temperatures) were done on a low-temperature (LT) Vibrating Sample Magnetometer (VSM) and on a high-temperature (HT) VSM (both by Princeton Measurements). For some samples the temperature dependences of hysteresis

Table 3.1: Relaxation geospeedometry

Sample	limiting T_f [°C]	natural cooling rate [K/min]
LOBS1.4	407	0.00072
LOBS2.13	409	0.00084
LOBS3.23	409	0.00114
LOBS4.33	412	0.0012
LOBS5.42	411	0.00114
LOBS6.53	420	0.0012
LOBS7.63	425	0.00174
LOBS8.73	454	0.01692
UOBS0	429	0.00378
UOBS120^N	489	6.3
UOBS225^N	444	0.009
UOBS295	449	0.01122
UOBS700	411	0.0015
UOBS720^N	425	0.0051
UOBS750^N	454	0.00672
UOBS775^N	450	0.00726
UOBS837^N	447	0.00606
UOBS889^N	452	0.00588
UOBS925^N	412	0.00282
UOBS986^N	420	0.00144
UOBS1020^N	415	0.0012
UOBS1080^N	405	0.00102
UOBS1117^N	420	0.0012
UOBS1153^N	413	0.00114
UOBS1220	453	0.0057
UOBS1420	417	0.00192
UOBS1570	411	0.00174
UOBS1705^N	432	0.0063
UOBS1825	418	0.00336
UOBS1945	444	0.0087
UOBS2095^N	486	2.52
UOBS2245	419	0.00222
UOBS2380	430	0.00516
UOBS2650	448	0.01242

Limiting fictive temperatures T_f and natural cooling rates of indicated samples. The limiting fictive temperature T_f is used to represent T_g. It constitutes the temperature of the undercooled melt at which the glass structure is completely frozen in without any possibility for further structural relaxation, i.e. the lowest possible expression of T_g.

and backfield were also measured on LTVSM and/or HTVSM. Additionally, thermomagnetic curves were measured with the HTVSM. Last but not least, the following experiments were done on a Magnetic Properties Measurement System (MPMS) by Quantum Design. For low temperature experiments in the MPMS fields at room temperature (RT), at low temperature (LT, 10 K) or during cooling of 2.5 T were applied and the field was turned off during the measurement: A RTSIRM (room temperature saturation IRM) was imparted on samples LOBS4.33, UOBS295 and UOBS1945 and measured during cooling to 10 K, then a LTSIRM (low temperature SIRM) was imparted and measured during warming to RT . Sample UOBS1080 experienced a more detailed measurement procedure: After field-cooling (FC) to 10 K, this FC remanence was measured during warming to RT. After another cooling in zero field to 10 K a LTSIRM was imparted and measured during warming to RT. Then a RTSIRM was imparted and measured during cooling to 10 K and during warming to RT. LTVSM, HTVSM and MPMS experiments were done in the course of a visitor's fellowship at the Institute for Rock Magnetism at the University of Minneapolis, USA.

Three LOBS (1.4, 4.33, 8.73) and five UOBS (120, 295, 925, 1420, 2095) samples were measured in the VFTB and the data were analyzed using the RockMagAnalyzer software by Leonhardt [2006]. All three LOBS samples are mainly paramagnetic, but have a remanent content that is high enough to get good IRM and backfield curves (Fig. 3.3a i). For samples LOBS1.4 and 8.73 it is also possible to determine a Curie temperature T_C of ∼210 °C (Fig. 3.3a iii) even though the departure of the thermomagnetic curves from a curve calculated for the decrease in saturation magnetisation of paramagnetic particles (green line in Fig. 3.3a iii) is not very strong. For T_C determination this paramagnetic decrease was subtracted from the original thermomagnetic curve. Later remanence measurements (section 3.5) show unblocking of grains in LOBS8.73 up to at least 400 °C. This implies a contribution from remanence carriers that do not show in the thermomagnetic curves due to the high paramagnetic contribution. LOBS1.4 plots in and LOBS8.73 close to the single domain (SD) region of the Day plot [Day et al., 1977]. The hysteresis loop of sample LOBS4.33 is dominated by paramagnetic behavior and thus, no meaningful hysteresis parameters can be obtained. Samples from UOBS are even more paramagnetic than LOBS4.33. Hysteresis measurements show only a sligthly broadened straight line through the origin (Fig. 3.3b ii) and IRM and backfield measurements are very noisy even though a remanent contribution can clearly be seen (Fig. 3.3b i). For thermomagnetic curves deviations from the paramagnetic decrease are so small that no Curie temperatures can be determined (Fig. 3.3b iii).

As the very strong paramagnetic contribution mostly prevented obtaining meaningful data using the VFTB, further measurements were done on the more sensitive MPMS and VSMs. However, their higher sensitivity could not totally make up for the smaller sample sizes and so again mainly the strong paramagnetic contribution was monitored: Hysteresis and backfield data at room temperature (RT) were taken for every sample. Hysteresis plots are almost always dominated by the paramagnetic contribution (e.g. UOBS 1080 in Fig. 3.4a i). A small ferrimagnetic contribution can be seen when the loops are corrected for the high field slope (Fig. 3.4a ii), but the measurement noise is much too high to determine

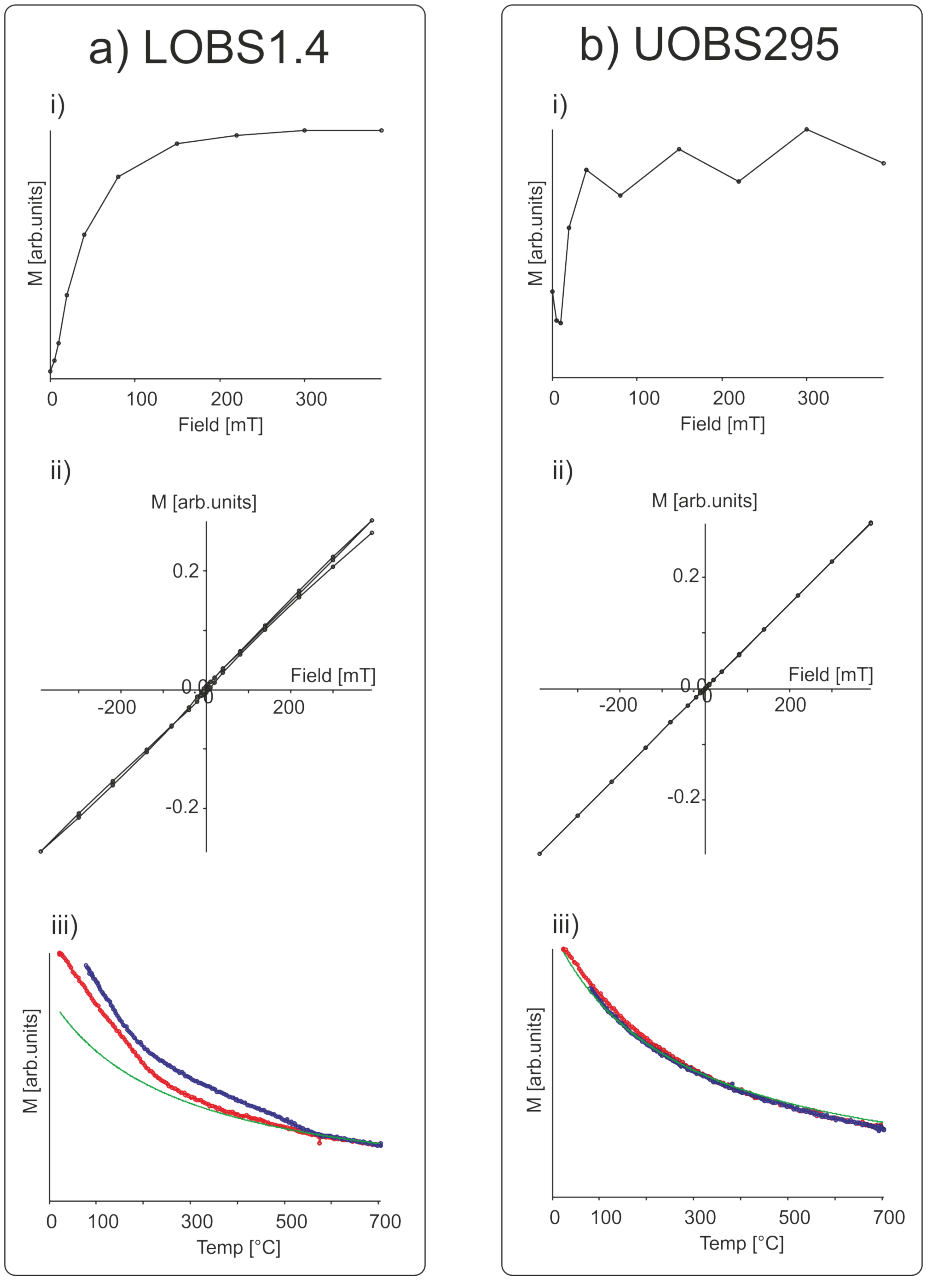

Figure 3.3: VFTB measurements for samples a) LOBS1.4 and b) UOBS295: i) IRM acquisition, ii) hysteresis loops and iii) thermomagnetic curves (red: heating, blue: cooling, green: paramagnetic decay).

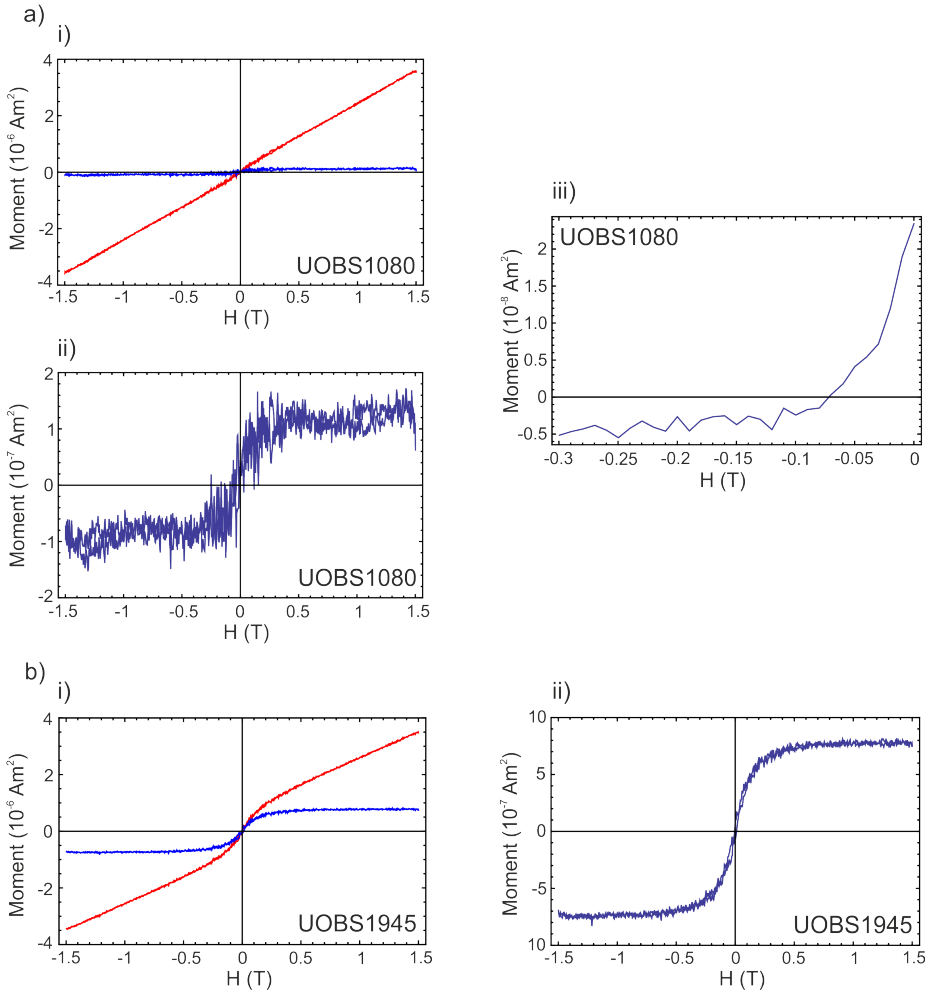

Figure 3.4: VSM measurements at 50 °C for a) UOBS1080 and b)UOBS1945. Graphs show i) hysteresis loops as measured (red) and corrected for the high field slope (>1T, blue) and ii) the corrected loops seperately in blow-ups. iii) gives an additional backfield curve for UOBS1080.

hysteresis parameters. Only sample UOBS1945 (Fig. 3.4b i) shows a stronger hysteresis, but is again too much dominated by paramagnetism to determine coercivity H_c (Fig. 3.4b ii). Further, it was impossible to determine coercivity of remanence H_{cr} values from the backfield curves as there is always some shift in the data: Fig. 3.4a iii shows that at the end of the measurement not the same absolute value in magnetization as before was obtained. For some samples the y-axis was not even crossed. It was not possible to find any reason for this shift and hence, no correction could be applied. For samples LOBS4.33, UOBS295 and UOBS1945 hysteresis and for UOBS1080 hysteresis and backfield curves were also measured in 10 °C steps from 10 K to room temperature and in 25 °C steps from room temperature to ∼450 °C. However, no further insights regarding the remanence carriers could be gained from these measurements as the paramagnetic contribution stayed dominant during the hysteresis loops, and backfield measurements were as erroneous as those at room temperature. Thermomagnetic curves for LOBS7.63 and UOBS700 are also similar to those of the VFTB. They only show slight deviations from paramagnetic decay. For UOBS700 a little kink below ∼400 °C implies a Curie temperature in this range, but the data is not very clear. MPMS data of LOBS4.33, UOBS295, UOBS1945 and UOBS1080 can be found in Fig. 3.5a, b, c and d, respectively. Neither at ∼262 K (Hematite Morin transition) nor at ∼120 K (Magnetite Verwey Transition) are any remarkable changes in the different remanent magnetizations observed. However, there is always a strong decrease in RTSIRM during cooling and a respective increase in LTSIRM below 50-75 K. This is most probably connected to the high paramagnetic/ferro(i)magnetic ratio: Within the MPMS the field is not perfectly zeroed. There seems to be a small negative residual field of ±1-2 μT. Paramagnetic susceptibility is inversely proportional to temperature and, thus, at low temperatures an induced negative magnetization partially cancels out the positive remanence. Sample UOBS295 (Fig. 3.5b) shows a more sharp decrease in RTSIRM during cooling which hints to ordering or a phase transition rather than to gradual increase in paramagnetic susceptibility. However, the LTSIRM warming curve does not show a sudden increase and an interpretation is therefore difficult. All warming curves show decreases above 50-75 K. Such decreases may have different reasons like unblocking of superparamagnetic (SP) grains or domain reorganization in MD high-Ti titanomagnetite [Moskowitz et al., 1998]. However, for our samples VFTB experiments have shown that we are dealing with SD or close to SD remanence carriers. Hence, the second possibility can be ruled out and instead it is followed that nanoparticles go from SP to stable SD. The difference between FC remanence and LTSIRM warming curves in Fig. 3.5d may be explained with a phase of extremly high coercivity which is either due to the presence of an imperfect antiferromagnetic phase with a low ordering temperature (50-100 K) that is magnetized more efficiently by field-cooling (strong-field TRM) than isothermally at 10 K or with the presence of low temperature partially oxidized nano-(titano-)magnetites.

An identification of remanence carriers is not possible based on the so far performed VFTB, VSM and MPMS experiments. The strong paramagnetic contribution constrains analysis of the ferro(i)magnetic particles. However, the small grain sizes and the small but clearly existing remanence suggest that paleointensity determination is worth a try.

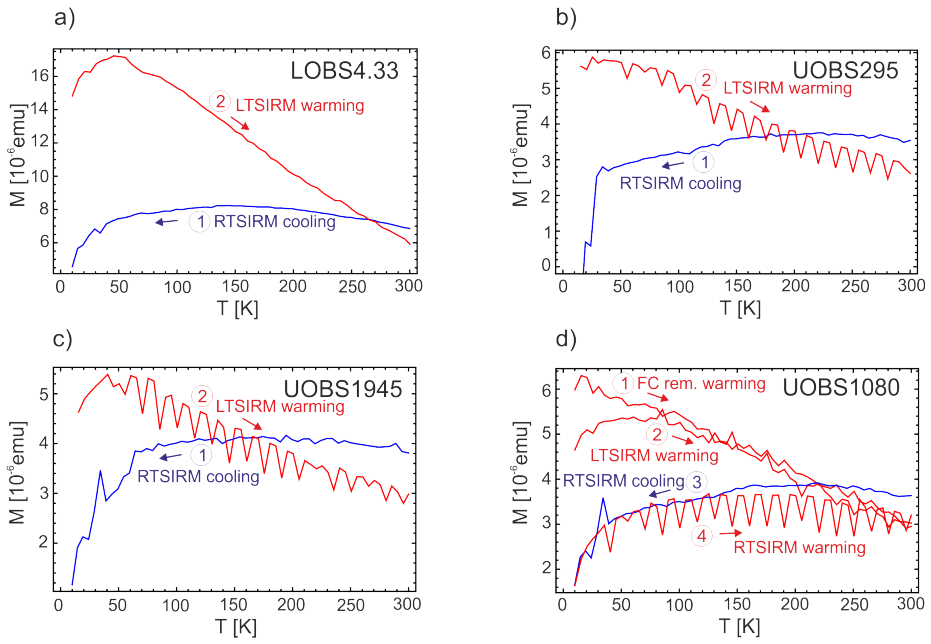

Figure 3.5: MPMS measurements for samples a) LOBS4.33, b) UOBS295, c) UOBS1945 and d) UOBS1080. a), b) and c) show 1. a room temperature (RT) SIRM measured during cooling and 2. a low temperature (LT, at 10K) SIRM measured during warming. d) shows 1. a field cooled remanence measured during warming, 2. a LTSIRM measured during warming, 3. a RTSIRM measured during cooling and 4. during warming. In all cases measurements were done in zero field and applied fields for RTSIRM, LTSIRM and field cooling were 2.5 T.

3.5 Paleointensity determination

3.5.1 Thellier-type experiments

Paleointensity experiments on 8 mm diameter miniature cores and on 1-in cores were done in a MMTD20 thermal demagnetizer in the paleomagnetic laboratory of the University of Munich, Germany in Niederlippach and in a MMTD60 thermal demangetizer in the laboratory of the Montan University Leoben, Austria in Gams. For in-field steps laboratory fields of 30 ± 0.1 μT were applied during heating and cooling. The experiments followed the modified Thellier-technique MT4 by Leonhardt et al. [2004] which is a zero-field first method that incorporates pTRM checks [Coe, 1967], additivity checks [Krása et al., 2003] and pTRM tail checks [Riisager and Riisager, 2001]. Directional differences between the applied field and the NRM of the pTRM-tail check are taken into account according to Leonhardt et al. [2004a]. All determinations were analyzed using the ThellierTool4.21 software [Leonhardt et al., 2004]. Paleointensity data are summarized in Tab. 3.2 with sample subscripts m, NL and G denoting minicores, Niederlippach and Gams, respectively, and different Arai plots are given in Fig. 3.6.
Measurements in Niederlippach proceeded to temperatures above T_g even though NRM_{left} had already been only ∼10% at ∼390 °C. Alteration of these samples gets very strong above T_g leading to departing checks (e.g. Fig. 3.6a). As this alteration is most likely connected to relaxation of the glass structure, only steps below T_g are considered for paleointensity determination, i.e. only steps up to 390 °C (7 steps), while higher temperature steps are disregarded. This accounts for the two miniature samples LOBS8.73 and UOBS2095 as well as for the 8 1-in cores measured in Niederlippach (subscript NL in Tab. 3.2). With this experience in mind, 24 samples (inch cores) in the Gams laboratory were heated up to 390 °C in 10 steps. Almost all samples were then demagnetized to at least 15%. Only samples UOBS889 (Fig. 3.6d), 1570 and 2380 had ∼20%, UOBS0 ∼40% and UOBS1945 and 2095 ∼50% left.
Paleointensity determinations are of good quality. In total, data from 24 of the 34 measured samples (70%) could be used with good values for different quality parameters (Tab. 3.2): Mostly fraction of the NRM f [Coe et al., 1978] and gap factor g [Coe et al., 1978] are greater than 0.7, quality factor q [Coe et al., 1978] ranges between 7.5 and 100, though mostly between 15 and 30. In many of the experiments an onset of alteration is observed at temperature steps above ∼300 °C which is probably related to the repeated heating to temperatures close to T_g. However, for the temperature intervals used for paleointensity determination, the difference ratio DRAT [Selkin and Tauxe, 2000], which measures deviations in pTRM checks, is typically ≤5.1, suggesting the data are reliable. Repeated thermal demagnetizations (one before and one after the pTRM acquisition of the respective temperature step) show only minor deviations (d(TR)≤2.1%, d(TR): Leonhardt et al. [2004]) indicative of SD remanence carriers for 63% of the samples and slightly higher values (up to d(TR)=5.5%) indicative of small PSD particles for the others although an unique interpretation in terms of domain size is hampered by the above mentioned alterations above ∼300 °C before the remanence is unblocked.

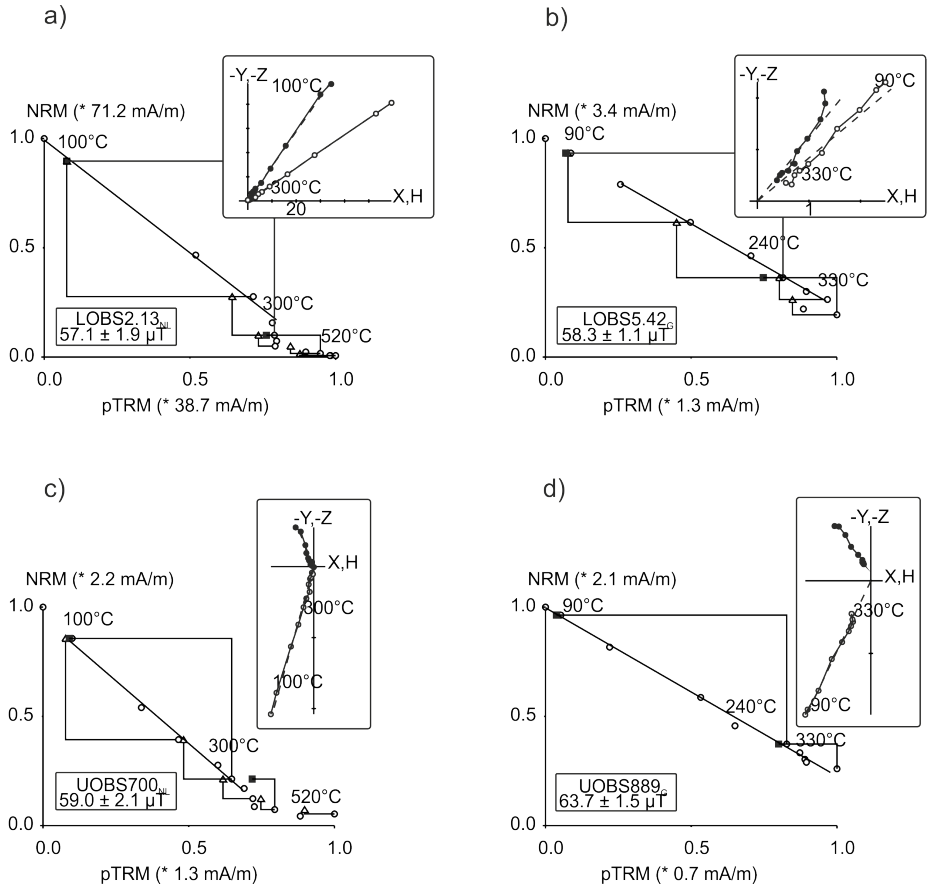

Figure 3.6: NRM/pTRM plots and respective orthogonal projections for a) LOBS2.13, b) LOBS5.42, c) UOBS700 and d) UOBS889. Triangles and squares in the NRM/pTRM plots indicate pTRM checks (CK) and additivity checks (AC), respectively.

Arithmetic means and standard deviations for LOBS and UOBS are 56.5±2.0 μT and 59.2±8.4 μT, respectively. For the whole 8 ka flow a weighted mean (using 1/(arithmetic standard deviation) as weighting factor) of 57.0±1.0 μT is calculated.

Table 3.2: Paleointensity results and correction

Sample	Uncorr. paleointensity	quality parameters					ATRM correction		CR correction	
	H_{UC} [μT]	f	g	q	DRAT	d(TR)	f_{ATRM}	H_{ATRM} [μT]	f_{CR}	$H_{ATRM,CR}$ [μT]
LOBS	**56.5±2.0**									
LOBS2.13$_{NL}$	57.1±1.9	0.83	0.63	15.5	4.2	2.9				
LOBS3.23$_{G}$										
LOBS4.33$_{NL}$	55.5±1.2	0.83	0.81	32.5	1.9	2.9				
LOBS5.42$_{G}$	58.3±1.1	0.54	0.75	21.1	3.0	2.1	(1.244±0.218)	(72.5±14.1)		
LOBS6.53$_{G}$										
LOBS6.53$_{NL}$	58.9±4.2	0.74	0.73	7.5	4.4	3.7				
LOBS7.63$_{G}$	53.5±0.9	0.69	0.72	28.5	2.3	0.9				
LOBS8.73$_{m}$										
LOBS8.73$_{NL}$	56.0±1.9	0.75	0.64	14.5	8.1	5.0				
UOBS	**59.2±8.4**							**61.1±8.9**		
UOBS0$_{G}$										
UOBS120$_{G}$	65.2±2.0	0.67	0.78	17.3	2.8	1.4				
UOBS225$_{G}$	68.7±2.9	0.85	0.83	16.6	2.0	2.5				
UOBS295$_{G}$	73.9±2.9	0.85	0.82	17.7	4.1	2.0				
UOBS700$_{G}$	42.3±0.4	0.69	0.73	60.1	3.4	0.4				
UOBS700$_{NL}$	59.0±2.1	0.72	0.72	14.2	1.6	1.8				
UOBS701$_{G}$										
UOBS720$_{G}$	46.9±2.5	0.76	0.75	10.6	2.5	3.4	(1.190±1.950)	(55.8±94.4)		
UOBS750$_{G}$	72.5±3.2	0.79	0.74	13.3	3.5	2.1				
UOBS775$_{G}$	56.6±0.4	0.93	0.77	100.2	1.6	1.4	(1.051±0.278)	(59.5±16.2)		
UOBS837$_{NL}$										
UOBS889$_{G}$	63.7±1.4	0.76	0.82	27.3	0.0	1.2	1.113±0.037	70.9±3.9	1.106±0.074	64.1±0.7
UOBS925$_{NL}$	54.6±2.4	0.82	0.68	12.5	1.1	3.9				
UOBS1020$_{G}$	58.0±2.7	0.97	0.77	15.9	6.2	5.5				
UOBS1080$_{NL}$	64.1±2.3	0.95	0.61	16.3	3.5	3.7				
UOBS1117$_{G}$										
UOBS1420$_{G}$										
UOBS1570$_{G}$	56.3±1.4	0.75	0.78	24.4	1.4	1.8	1.238±0.013	69.7±2.4		
UOBS1705$_{G}$	53.1±1.7	0.88	0.81	22.6	2.8	0.6	(1.067±0.119)	(56.6±8.1)		
UOBS1825$_{G}$										
UOBS1945$_{G}$	62.7±2.0	0.44	0.84	11.6	5.1	0.6	(0.929±0.239)	(58.2±16.8)		
UOBS2095$_{m}$										
UOBS2095$_{G}$	50.1±1.9	0.39	0.80	8.1	4.3	0.9	1.159±0.050	58.0±4.7		
UOBS2245$_{G}$	62.3±2.6	0.84	0.78	15.9	3.5	0.7				
UOBS2380$_{G}$	55.2±1.9	0.63	0.78	14.5	2.7	0.9				
8 ka flow	**57.0±1.0**							**59.3±2.2**		

H_{UC}, H_{ATRM} and $H_{ATRM,CR}$ are the paleointensity values of the individual samples with associated errors for the uncorrected, ATRM corrected and ATRM and cooling rate (CR) corrected determinations, respectively. H_{ATRM} errors are calculated as minimum-maximum errors including the uncertainty of the uncorrected paleointensity σ_{UC} and of the ATRM correction factor f_{ATRM}. $H_{ATRM,CR}$ errors are calculated via full error propagation using the uncertainties of H_{UC}, f_{ATRM} and f_{CR}. Also shown are arithmetic means and standard deviations of the different sites and weighted means for the whole 8 ka flow (using 1/(arithmetic standard deviation of site means) as weighting parameter). Additionally, the following quality parameters for the individual paleointensity determinations are given: fraction of NRM f [Coe et al., 1978], gap factor g [Coe et al., 1978], quality factor q [Coe et al., 1978], difference ratio DRAT [Selkin and Tauxe, 2000] and d(TR) [Leonhardt et al., 2004].

3.5.2 Anisotropy correction

As samples in Niederlippach had been heated too high, no anisotropy or cooling rate experiments (subsection 3.5.3) could be performed on these samples. Relaxation at the glass transition altered the samples and no meaningful results can be obtained.
However, for Gams samples these experiments could be carried out. If a rock is magnetically anisotropic this means that its ability to acquire a magnetization in a magnetic field depends on its orientation with respect to that field. The anisotropy tensor of TRM (ATRM tensor) can be obtained as weak field TRM is proportional to the field strength. Determinations of the ATRM tensor were done on the same samples as paleointensity determinations in the MMTD60 demagnetizer in the Gams laboratory. TRMs were imparted using in-field heating/cooling cycles to the upper end of the blocking spectra of the samples, i.e. up to 390 °C, subsequently in +z, +x, -x, +y, -y and -z direction. Additionally, the +z treatment was repeated in the end to check for alteration. The measurements were analyzed following the approach of Veitch et al. [1984] and the results are summarized in Tab. 3.2. After determining the ATRM tensor, a paleointensity scaling factor, f_{ATRM} ($H_{ATRM} = H_{UC} * f_{ATRM}$ (UC: uncorrected)), is calculated based on the directions of the ancient field and the laboratory field. f_{ATRM} is not only determined from the averaged axes components but also separately for positive (+x, +y, +z) and negative (-x, -y, -z) measurements, i.e. f^{pos}_{ATRM} and f^{neg}_{ATRM}. The uncertainty of f_{ATRM} is calculated by $\sigma(f_{ATRM}) = (|f^{pos}_{ATRM} - f^{neg}_{ATRM}|$. The uncertainty $\sigma(H_{ATRM})$ of the ATRM corrected paleointensity is a minimium-maximum error including the uncertainty of the uncorrected paleointensity $\sigma(H_{UC})$ and of the correction factor $\sigma(f_{ATRM})$.

For only 8 of the 24 samples was alteration small enough to correct for anisotropy. Fig. 3.7 shows that in most cases the two +z measurements at the beginning and at the end of the experiment varied by ≥5%. Therefore, anisotropy correction was tried only for samples LOBS5.42, UOBS720, 775, 889, 1570, 1705, 1945 and 2095. As mentioned above samples UOBS889, 1570, 1945 and 2095 still have $NRM_{left} > 15\%$ at 390 °C. As their T_g is in the same range as the one of the other samples, it was decided to stop heating them further and to determine the ATRM tensor at 390 °C. Vector subtraction of the TRM remaining at 390 °C from each step in the anisotropy experiment should yield a reasonable measure of the ATRM tensor. Although TRM capacity remained stable as has been shown by the ≤5% difference between the two +z measurements, very high relative errors $\sigma(f_{ATRM})/f_{ATRM}$ of 11-164% were found for most samples (data for f_{ATRM} and H_{ATRM} in brackets in Tab. 3.2). These high errors suggest that there was alteration during these experiments that was not monitored by the two +z measurements. Either alteration did not affect the tensor in this direction or it was just by chance that these two measurements showed similar values. Only samples UOBS889, 1570 and 2095 showed relative errors <5% that were thought to represent reliable measurements. Thus, for the anisotropy corrected paleointensity values of 61.1±8.9 μT for UOBS and 59.3±2.2 μT for the whole flow only corrected paleointensities of these three samples and uncorrected paleointensities of all other samples were used. In both cases the paleointensity is slightly increased but within error identical to the uncorrected mean values.

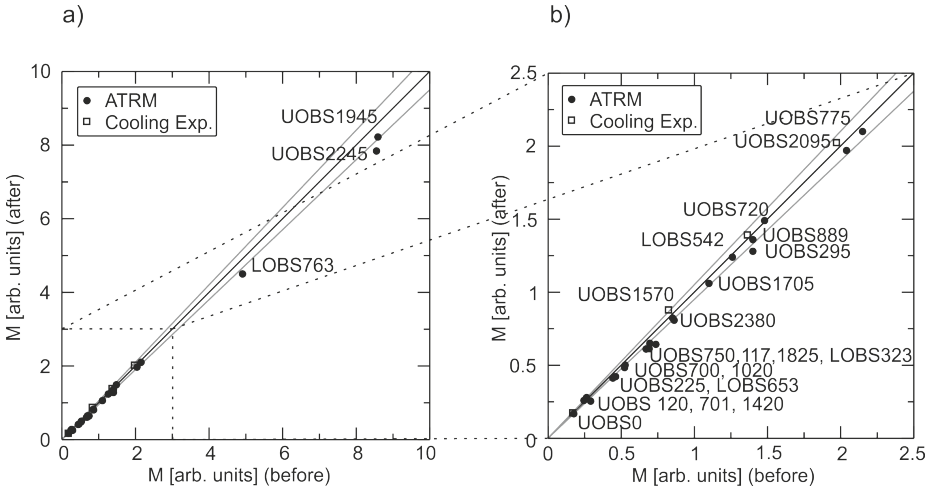

Figure 3.7: Comparison of magnetization before and after the ATRM (filled circle) and cooling rate (open square) experiments. Diagonal in the plots represents no alteration and grey cone around this line gives 5% deviation between the two measurements. b) shows close-up of lower left corner of a).

3.5.3 Corrections for cooling rate dependence

In the 1980s several studies [Halgedahl et al., 1980, Dodson and McClelland-Brown, 1980, Fox and Aitken, 1980, McClelland-Brown, 1984] have shown that non-interacting SD particles acquire a smaller TRM during faster cooling. How exactly the TRM depends on cooling rate varies, however, with slight changes in grain size and domain state. Hence, to correct overestimation of paleointensity [Leonhardt et al., 2006, Ferk et al., 2010] the TRM dependency on cooling rate as well as natural cooling rates (via relaxation geospeedometry) have to be determined. For these measurements the same samples as for Thellier-Thellier and anisotropy experiments are subjected to magnetic cooling rate dependency investigations in the MMTD60 using two laboratory cooling rates [Leonhardt et al., 2006]. As most of our samples had altered already during the anisotropy experiments only samples UOBS889, 1570 and 2095 that did not show remarkable alteration were subjected to cooling rate experiments. For fast cooling the cooling fan of the furnace was used like during the previous experiments, while for slow cooling the samples were cooled without fan operation. Laboratory cooling rates were determined on basaltic dummy samples across the glass transition intervals of our samples, i.e. between about 500 °C and 400 °C. A conservative estimate of the uncertainty in cooling rate determination is 10% for fast cooling and 5% for slow cooling. First, a fast heating/cooling cycle with a cooling rate of ≈55.6 K/min was used to induce a TRM ($TRM_{f,1}$). Then a heating/cooling cycle with a ca. 43-fold slower cooling rate of ≈1.3 K/min ($TRM_{s,1}$) and finally, another fast cycle ($TRM_{f,2}$) in order to check for alterations during the experiment, were performed. $TRM_{f,1}$ and $TRM_{f,2}$ of UOBS1570 differ by 7% indicating strong alterations (Fig. 3.7b). For UOBS2095 $TRM_{f,1}$ and $TRM_{f,2}$ are within 3% but $TRM_{f,2} > TRM_{s,1}$ which makes a cooling-rate correction

impossible. A reliable result was obtained only for UOBS889: $TRM_{f,1}$ and $TRM_{f,2}$ differ only by 2% indicating only very minor alteration. This difference between $TRM_{f,1}$ and $TRM_{f,2}$ is used as error estimates for $TRM_{s,1}$ and $TRM_{f,1}$. The TRM intensity for slow cooling is 6% larger than for fast cooling, as would be expected for non-interacting SD particles [Halgedahl et al., 1980, Dodson and McClelland-Brown, 1980]. Linear extrapolation of the magnetic cooling-rate dependency to the natural cooling rate as determined by relaxation geospeedometry is performed in order to correct the overestimation of H_{ATRM}. Such linear extrapolation is valid, if the remanence carriers are non-interacting SD particles that dominantly block close to the respective blocking temperature [Halgedahl et al., 1980]. As has been mentioned before, it was not possible to determine unambigiously the domain size of most LOBS and UOBS samples, as mostly rock magnetic measurements were not sensitive enough. However, both successful rock magnetic experiments for LOBS1.4 and 8.73 and thermal demagnetization steps (thermal repeat: TR) after imparting the pTRM during paleointensity determinations, i.e. the tail checks, imply SD or small PSD remanence carriers. Also TR steps of UOBS889 differ only by 1.2% suggesting SD particles. However, unblocking of the TRM occurs mainly over a temperature range of 200 °C. Thus, the second requirement is not strictly fulfilled. Nevertheless, as there is no other theory regarding cooling rate dependency for such samples, linear extrapolation was used as an approximation of cooling rate dependency. The previous error estimates for inaccuracy of laboratory cooling rate and magnetization determination allow a minimum-maximum error propagation towards the natural cooling rates. The obtained cooling rate (CR) correction factor $f_{CR} = \mathrm{TRM}/\mathrm{TRM}_{f,1}$ is then used to correct the paleointensity values H_{ATRM} by $H_{ATRM,CR} = H_{ATRM}/f_{CR}$. Full error propagation, including the uncertainties of the paleointensity experiments as well as those of f_{ATRM} and f_{CR} gives the uncertainty $\sigma(H_{ATRM,CR})$ of $H_{ATRM,CR}$. The resulting paleointensity, 64.1±0.7 μT for UOBS889 is practically identical to it's uncorrected value of 63.7±1.4 μT. Both are slightly higher than the mean values for the whole 8 ka flow.

3.6 Discussion

Even though many rockmagnetic experiments at low, room and high tempertures were performed, it was not possible to determine the remanence carriers due to the very high paramagnetic contribution. However, it was found that the samples carry a small but stable remanence that is carried by SD or close to SD remanence carriers. Further, most samples unblock clearly below T_g and alteration that is connected to unblocking above T_g [Smirnov and Tarduno, 2003] can be ruled out.
Thus, it should be possible to determine a reliable paleointensity value using these samples assuming that they carry a primary remanence. However, problems emerged due to heating of the samples: Heating above T_g of some samples and repeated heating to temperatures just below the glass transition introduced alteration into the experiments. Therefore, it was necessary to leave out data that was obtained above T_g and it was not possible to perform ATRM or CR correction on all samples. Nevertheless, the successful ATRM and

CR experiments indicate negligible difference to uncorrected data. The uncorrected mean paleointensity of 57.0±1.0 μT seems most reliable and can at least give a upper limit of the field strength 8 ka ago in New Zealand as faster cooling in the laboratory compared to nature leads to an overestimate of paleointensity when dealing with SD remanence carriers [Halgedahl et al., 1980, Dodson and McClelland-Brown, 1980]. Interestingly, a comparison with previous intensity data from the same region shows excellent agreement: Within error our Mayor Island paleointensity data for 6050±70 BCE is identical to the field value of 58.1±2.9 μT which Tanaka et al. [2009] obtained for a ∼500 year younger (5500 BCE) rhyolithic lava at Okataina Volcanic Center (OVC). OVC is a rhyolitic eruptive center within Taupo Volcanic Zone and just ∼100 km distant from Mayor Island. Tanaka et al. [2009] did not apply any cooling-rate correction. Normally one would expect different cooling rate dependencies. The match in the uncorrected data may be fortuitous especially when considering the 500 year age difference. However, it might also indicate that in these cases the cooling rate does not have a strong influence. Nonetheless, it was tried to approximate a cooling rate corrected paleointensity value by comparison with other data. First the f_{CR} of sample UOBS889 (∼1.10) was used to correct our mean value of 57.0±1.0 μT. This gives a corrected value of ∼52 μT. This approach is justified due to the very similar magnetic properties of the different samples. However, as we have shown earlier [Leonhardt et al., 2006, Ferk et al., 2010] already slight variations in domain states result in changes in the TRM dependency on cooling rate. Thus, this value is only an approximation. Additionally, our uncorrected mean value was corrected by the ∼15% overestimate as observed for an obsidian with SD remanence carriers from Lipari [Leonhardt et al., 2006]. Allthough these ∼15% come from another lava, they may be useful as they are a mean value for the whole flow. This yields a corrected value of ∼49 μT. Together these approximations suggest a cooling rate corrected paleointensity of ∼50 μT. Further studies will have to check whether the uncorrected or the corrected value is more likely.

In their study on rhyolithic lava from OVC Tanaka et al. [2009] have also compared their data to other volcanic and lake sediment data and to the geomagnetic field model CALS7K by Korte and Constable [2005]. While the paleointensity data itself agrees well with a world-wide trend with a moderate high at 7-8 ka [Yang et al., 2000], there is a very poor fit to CALS7K. This is reasonable considering the paucity of reliable paleointensity data in the Pacific region to date and the thereby induced strong weighting of sedimentary data in the model. Further, geomagnetic field models are always less free to develop close to boundary due to the necessary boundary conditions. This may introduce additional errors at locations with few data. A comparison of our data with CALS7K is not possible as the model does not go back far enough. Therefore, agreement of the data with the so far unpublished geomagnetic field model by Leonhardt et al. [2010] that goes back to 10 ka was tested. This model suggests a field value of only ∼43.5 μT for 6050±70 BCE at Mayor Island, which is closer to the cooling rate corrected value. However, due to the low number of data constraining the model at this time it is impossible to say whether this is true and more and better data are needed for the modelling procedures. Our new paleointensity value itself is of high quality. It is, therefore, an important first step towards a better global

distribution of high quality data and better-defined geomagnetic field models. Generally, obsidians may help to get a better data distribution as they are more evenly distributed about the globe than archeomagnetic data that so far is mainly used for last thousands of years. This and other studies [Pick and Tauxe, 1993, Bowles et al., 2005, Leonhardt et al., 2006] suggest that volcanic glasses give very good paleomagnetic results and they may, hence, help to obtain paleointensities and also -directions for areas with no archeomagnetic data.

Acknowledgements

We thank J. Bowles and A. Muxworthy for their thorough reviews that strongly helped to improve the manuscript. We are very thankful to J. Gottsmann for providing maps and figures of his study [Gottsmann and Dingwell, 2002]. Rock magnetic measurements at the Institute for Rock Magnetism were enabled by a Visiting Fellowship for A. Ferk. Our warmest thanks go to the whole IRM staff, especially to M. Jackson, for their help with the equipment and with interpretation of low temperature data. Further thanks to K. Fabian for help with Mathematica. Funding was provided by DFG grant Le1905/1-1 and FWF grant P21221-N14. D. B. Dingwell acknowledges the funding support of a LMUexcellent Research Professorship in experimental Volcanology (Bundesexzellenzinitiative) and ERC advanced grant EVOKES.

Chapter 4

Paleointensities of phonolitic obsidian: Influence of emplacement rotations and devitrification

This chapter is a slightly modified version of a paper that has been published in the Journal of Geophysical Research in 2011 [Ferk et al., 2011b]. Co-authors are R. Leonhardt, F. W. von Aulock, K.-U. Hess, and D. B. Dingwell.

Abstract

A paleomagnetic study on phonolitic obsidian from six sites in Tenerife, Spain is presented. Two sites are located at the 750 ka El Pasajiron at the southern wall of Las Cañadas Caldera. Four sites correspond to the 115±17 BCE Montaña Blanca Complex. Paleointensity determinations are performed with a modified Thellier technique using checks for alteration and domain state. Additionally, the anisotropy of the thermoremanence and the magnetic cooling rate dependency of each specimen are measured. It was not possible to obtain good quality paleointensity data for El Pasajiron. Thermal alteration was observed in most measurements. Systematic changes in rockmagnetic properties and paleointensities within the profile of one site also suggest the presence of a chemical remanence (CRM) which was probably acquired during devitrifiction of the upper part of the flow. This CRM cannot be seen in the Arai plots themselves but only by comparison of data from different samples. This underlines the importance of sampling only fresh glassy looking obsidians and not devitrified ones. Paleointensity determinations at Montaña Blanca are of very good quality leading to an high success rate of 82%. Samples at one site show acquistion of TRM during emplacement rotations. However, it could be shown that paleointensity data of rotated samples are reliable if the remanence carriers are in the single domain range. An ATRM (anisotropy tensor of thermoremanent magnetization) and cooling rate corrected paleointensity of 48.4±2.1 μT and a VDM of 9.64±0.42*10^{22}Am^2 were determined which are in very good agreement with other data from Spain and Morocco and to

various geomagnetic field models.

4.1 Introduction

Several studies [Pick and Tauxe, 1993, Selkin and Tauxe, 2000, Leonhardt et al., 2006, Ferk et al., 2010] suggest that volcanic glass is an excellent recording material for paleointensity studies. Use of volcanic glass enables several problems that cause failure or bias in paleointensity data to be overcome: Magnetic domain state bias affecting the different remanence acquisition processes in nature and in the laboratory [Leonhardt et al., 2004a] can be largely excluded as the remanence carriers are either single-domain (SD) or small pseudo-single-domain (PSD) grains [Geissman et al., 1983, Juárez et al., 1998, Smirnov and Tarduno, 2003, Leonhardt et al., 2006]. Further, some volcanic glasses have a pristine character with seemingly low alterations in geological time and in laboratory experiments [Pick and Tauxe, 1993]. Last, but not least their cooling histories are either comparable to those in the laboratory [Bowles et al., 2005] or a correction for cooling rate dependency [Fox and Aitken, 1980, Halgedahl et al., 1980] is possible by determining the natural cooling rates of the samples [Leonhardt et al., 2006, Ferk et al., 2010] via relaxation geospeedometry [Wilding et al., 1995, 1996a,b, Gottsmann and Dingwell, 2001a,b, Gottsmann et al., 2004, Potuzak et al., 2008, Nichols et al., 2009]. Thus, for SD particles that acquire weaker thermoremanent magnetizations (TRM) when cooled faster, paleointensity overestimates of more than 20% can be corrected for.

Problems can be encountered, however, when working with volcanic glass. Smirnov and Tarduno [2003] demonstrated that laboratory alteration causes bias in paleointensity experiments if the glass transition occurs below the blocking temperature of the remanence. Laboratory heating steps to temperatures above this transition can lead to alterations of magnetic minerals that would not necessarily be detected by alteration checks. Fortunately, determination of natural cooling rates via geospeedometry also yields the glass transition temperature T_g and thus by its comparison with blocking or Curie temperatures such alteration can often be ruled out.

In this study two other problems are examined: One is the devitrification of volcanic glass. The glass transition is a kinetic boundary below which the time required for melt relaxation increases greatly. Nevertheless, in geologic times sub T_g relaxation may become important. Hydration can additionally speed up crystallization. This might lead to magnetomineralogical changes and contemporaneous new remancence acquistion, which biases paleomagnetic experiments. The second problem is that during emplacement of obsidians significant strain, rotation and compression occur. Obsidian flows are often blocky lava flows and the blocks are often not *in situ*. Additionally, some obsidians have been compressed during their emplacement (e.g. Fig. 4.1). Care must be taken to ensure that paleointensities determined on samples from such rotated and/or squeezed blocks are reliable.

Here we present data from a 750 ka old partially devitrified obsidian at the Caldera Wall of Las Cañadas Caldera, Tenerife and results from a site within the Caldera, originating from

Figure 4.1: Obsidian block in Iceland that was squeezed during emplacement.

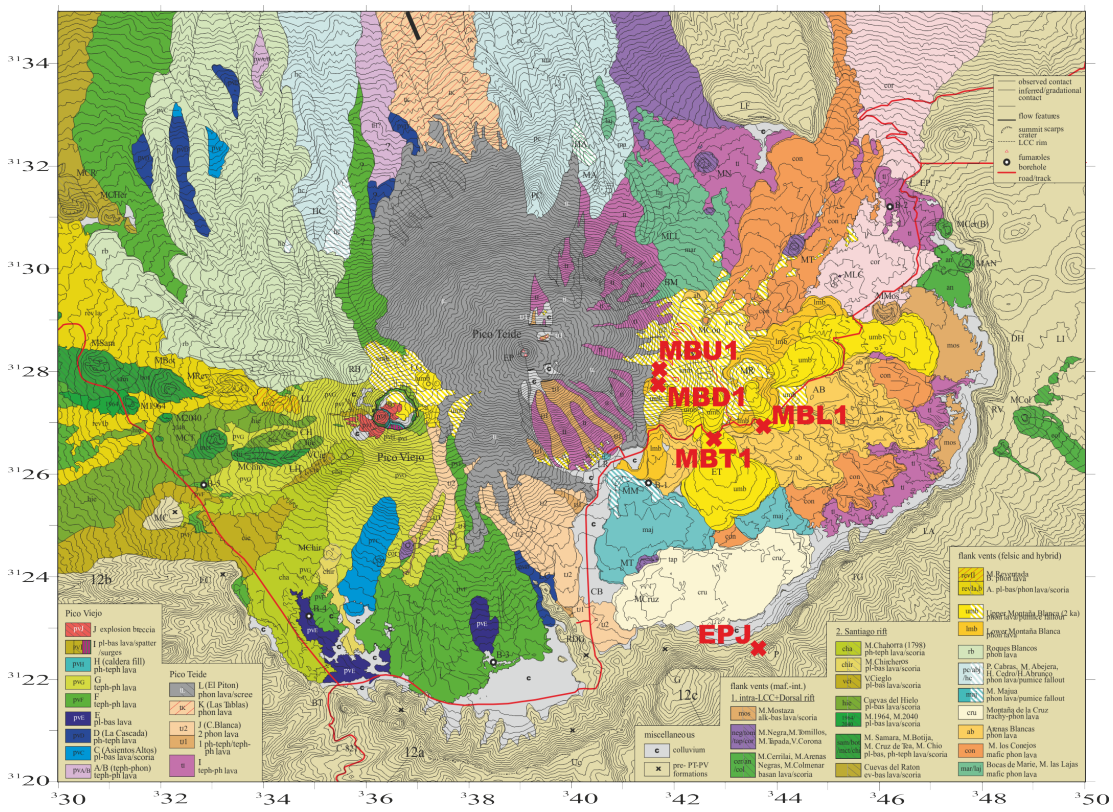

Figure 4.2: Geologic map of Las Cañadas Caldera from Ablay and Marti [2000] including the sampling sites (red crosses); coordinates refer to 2 km squares of the Spanish national grid (UTM projection, sector 28 North).

the ∼2 ka BP Montaña Blanca eruption, that shows emplacement rotation/compression and block break-up while cooling. Further we provide high quality anisotropy and cooling rate corrected data for 2065±17a BP at Tenerife.

4.2 Geology and sampling

Tenerife is the largest of the Canary Islands. Upper Miocene and Lower Pliocene basaltic series are found in the Anaga, Teno and Rocque del Conde massifs [Ancochea et al., 1990]. Later volcanic activity was concentrated on Las Cañadas central volcano, the NW-SE trending rift of Santiago del Teide and the Cordillera Dorsal, a SW-NE trending ridge linking Las Cañadas and the Anaga. The upper part of Las Cañadas volcano was destroyed and forms the so-called Las Cañadas Caldera, which was formed during different vertical and lateral collapses [e.g. Marti et al., 1994]. At its southern part the caldera wall is visible and reaches up to 500m above the rest of the edifice. Lavas from the Pico Teide (3718m) - Pico Viejo formation filled parts of the caldera and were also emplaced along the northern

slopes of the island (Fig. 4.2).
Samples were obtained using a water-cooled electrically driven drill on a field trip to Tenerife in September 2007. Whenever possible, sampling took place at sites where a gradient in cooling rates was suspected and where pristine clear glass with low crystal content was found (Fig. 4.2). Pictures of the different sites can be seen in Fig. 4.3. Two sites were sampled at El Pasajiron (EPJ, N28°13'24", W016°36'14"; all coordinates WGS84) at the southern caldera wall just to the east of Guajara, the highest point of the wall. A K-Ar date of El Pasajiron gives a date of 800 ka [Marti et al., 1994]. However, according to its stratigraphic position and the age of other units of the same eruption, a younger age of ∼750 ka is more probable. An age within the Bruhnes chron, i.e. the last 780 ka, is also supported by our normal directional data (section 4.5). At site EPJ1 we took four samples in a vertical profile of about 60 cm, and at site EPJ2 eight samples in another vertical profile of about 1.3 m height. Here, the uppermost samples EPJ2-1 to EPJ2-3 are in a fully devitrified part while EPJ2-4 to EPJ2-6 are in the partly devitrified middle of the outcrop and EPJ2-7 and EPJ2-8 are in the lowermost part consisting of fresh obsidian. The other four sites are at the Montaña Blanca (MB) complex, which is a flank vent complex at the eastern flank of Teide comprising MB and Montaña Rajada (MR) and resulting from the only well known post-caldera explosive eruption at 2065±17 BP (i.e. 115±17 BCE) [Ablay et al., 1995]. This age is a C14 age in calibrated years before present, with 95% confidence level and was calculated as weighted average and weighted standard deviation of the three C14 age determinations done by Ablay et al. [1995] using 1/standard deviation as weighting factor. The MB eruption involved effusion of lava and deposition of thick pyroclastic fallouts during a subplininan phase. Site MBT1 (MB Tabonal Negro 1, N28°15'29", W016°36'10") is within El Tabonal Negro. This fresh, blocky phonolitic lava flow represents the beginning of the eruption. As the partly overlying pumice is not baked or oxidized, perhaps only months may have separated these two phases of the eruption [Ablay et al., 1995]. Seven samples were taken as a horizontal profile on each of two big ∼2 m wide blocks that seemed to have broken apart in the middle. Samples were taken in more or less regular intervals of 10 to 20 cm within the black, glassy layers which are alternated with brown, more devitrified layers. The different blocks may represent parts of one original obsidian block that, still warm, was quenched from both sides and broke apart. The outsides of the two blocks are covered with clinker of up to 10 cm. Site MBU1 (Upper MB 1; 5 samples in a vertical profile, N28°16'7", W016°36'49") is an about 80 cm thick *in situ* lava flow at the top of MB. This lava flow belongs to the same phase of the eruption as El Tabonal Negro and is one of the few places at the pumice covered hill of MB, where blocks of lava crop out. Samples from the same site have been taken previously by Gottsmann and Dingwell [2001b] (name of sampling site in that publication: MB5) for relaxation geospeedometry. The two other sites are from the latter lava flow and dome effusion which was erupted subsequent to deposition of a pumice layer separating those flows from the lower flow. The nine samples of MBD1 (MB Dome 1, N28°15'57", W016°36'50") were taken at the western side of the uppermost dome structure at the MB fissure. The material is very homogeneous but less glassy. The samples span about 3 m in height. Site MBL1 (Lavas in block 1, N28°15'37", W016°35'34") lies just a few meters south of the

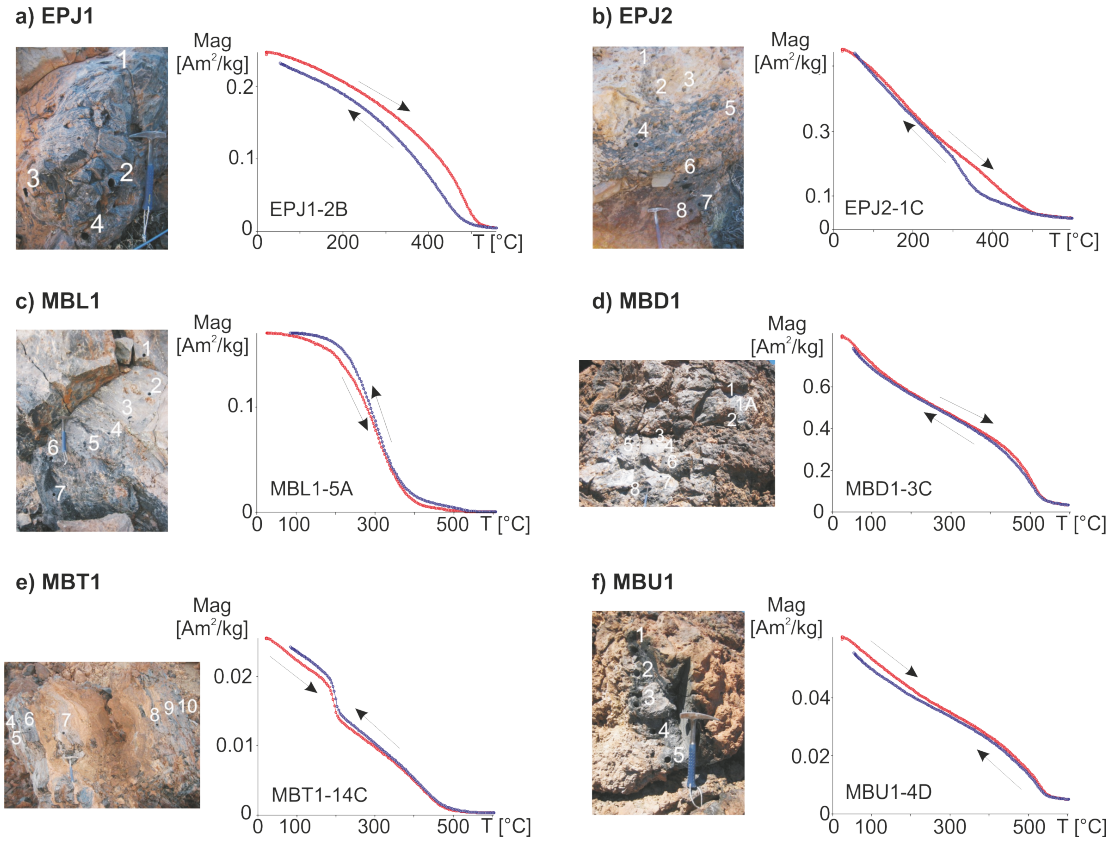

Figure 4.3: Pictures of the six different sites with sample positions indicated and respective thermomagnetic curves for each site.

road TF-21 and belongs to a blocky lava flow that was erupted from MR during the third phase of the whole eruption. Our 7 samples represent 1.5 m of the 3 m high block and range from very devitrified looking whitish material (MBL1-1 to MBL1-5) to a black and pristine glass layer at the bottom of the block (MBL1-6, MBL1-7).

From each of the samples we took some miniature cores of varying diameter (5 mm to 8 mm), that were subjected to a set of calorimeteric investigations, rockmagnetic measurements at room and high temperature, paleodirectional analyzes and paleointensity experiments including determination of the anisotropy of thermoremanence and the dependence on cooling rate.

4.3 Relaxation geospeedometry

Relaxation geospeedometry, i.e measurements of the heat capacity at constant pressure c_p, can be used to determine both the glass transition temperature T_g and the natural cooling rate. By passing through the glass transition, the melt changes from liquid-like

viscous to solid-like brittle behavior; it passes from metastable equilibrium to disequilibrium. Therefore, T_g does depend not only on the composition of the melt, but also on the quench rate. A record of the quench rate at the glass transition is frozen in the glass structure and can be accessed by reheating the sample together with parallel measurement of a structure dependent physical property such as heat capacity c_p. The concept of fictive temperature T_f is used to simplify the understanding of structural relaxation at the glass transition [Tool, 1946]. T_f expresses the temperature at which the temperature-dependent property of the glass is equal to that of the supercooled liquid. Above the glass transition the relaxation time τ to achieve equilibrium is short and thus the melt is in equilibrium: T_f equals the actual temperature T. At lower temperatures, τ increases and the melt departs from equilibrium where $T_f > T$. At this point the glass transition is entered and persists through a certain temperature interval. Below that interval the glass structure is frozen in and T_f is constant. The temperature at which the structure is frozen in depends on cooling rate: during faster cooling adjustment to new equilibrium is more restricted and hence, the structure is frozen in earlier. When reheating the sample, T_f depends both on the heating and on the previous cooling rate. T_f can be monitored by measuring c_p, first derivative of enthalpy H. Within the glass transition region c_p shows a peak during heating, which may be operationally defined as T_g (e.g. Fig. 4.4). As the heating curve depends on the previous cooling, an initial heating curve is modelled with four kinetic parameters that are obtained in successive heating/cooling runs with known rates. This enables a calculation of the natural cooling rate. Following the approach by Wilding et al. [1995] the Tool-Narayanaswamy [Narayanaswamy, 1971, 1988] equation for relaxation and the Debolt equation [Debolt et al., 1976] for fictive temperature were used for this modelling.

Specimens for relaxation geospeedometry were prepared by drilling cylinders of 6 mm diameter and cutting these into disks of approximately 1 mm. Then they were polished down to 55±2 mg, that is approximately the weight of the corundum standard (55 mg) which was used for quantitative measurements of c_p. The samples were dried for half an hour at 105°C. As far as possible no parts with visible alteration, devitrification or crystals were used. The measurements were done on a Netzsch Differential Scanning Calorimeter (DSC) 404 F1 Pegasus. The sample chamber was evacuated and flushed three times with high quality Argon 5.0 (99.999% pureness; concentrations: O_2 ≤2 ppm, H_2O ≤3ppm) before the insertion of the sample. During the measurement a constant flow of 25 ml/min Argon 5.0 prevented bulk oxidation and ensured constant atmospheric conditions. The sample was heated and cooled in the DSC with successive rates of 10 (only heated), 20 (cooled/heated), 15 (cooled/heated), 10 (cooled/heated) and 5 (cooled/heated) K/min. T_g is determined as the peak of the first (natural) run with 10 K/min heating rate. The four later runs (20, 15, 10 and 5 K/min) which are no longer influenced by natural cooling allow an estimation of the sample specific parameters. These can then be used to fit the first run, by adapting the previous, i.e. natural, cooling rate.

Relaxation geospeedometry was done on samples from all sites (Tab. 4.1). The best data were obtained for MBT1. Only MBT1-7C is an outlier with an extremly slow cooling rate of $2.0 * 10^{-6}$ K/min (10.5 K/year). For MBT1-1B the result of the measurement is

Table 4.1: Relaxation geospeedometry

Sample	T_g [±6°C]	natural cooling rate [K/min]
El Pasajiorn		
EPJ1-2B	560	0.0005
EPJ1-3B	609	0.0025
EPJ2-4B	669	0.0006
EPJ2-7B	682	0.0001
EPJ2-8B	682	0.004
Montaña Blanca		
MBD1-2B	625	0.02
MBD1-3C	624	0.07
MBD1-4B	627	0.38
MBD1-5B	669	0.0004
MBD1-6B	624	0.02
MBD1-7C	624	0.02
MBD1-8B	634	0.01
MBT1-1B	617	10
MBT1-2C	661	0.8
MBT1-3C	621	0.1
MBT1-4B	647	0.5
MBT1-5C	615	0.05
MBT1-6B	621	0.1
MBT1-7C	615	$2*10^{-6}$
MBT1-8B	636	0.05
MBT1-9	618	0.6
MBT1-10C	601	0.24
MBT1-11B	624	5
MBT1-12B	624	6
MBT1-13B	646	10
MBT1-14B	626	12
MBU1-1C	633	0.05
MBU1-3B	634	0.03
MBU1-4B	634	0.001
MBU1-5B	633	0.02

Glass transition temperatures T_g (peak of the first (natural) run with 10 K/min heating rate) and natural cooling rates of indicated samples.

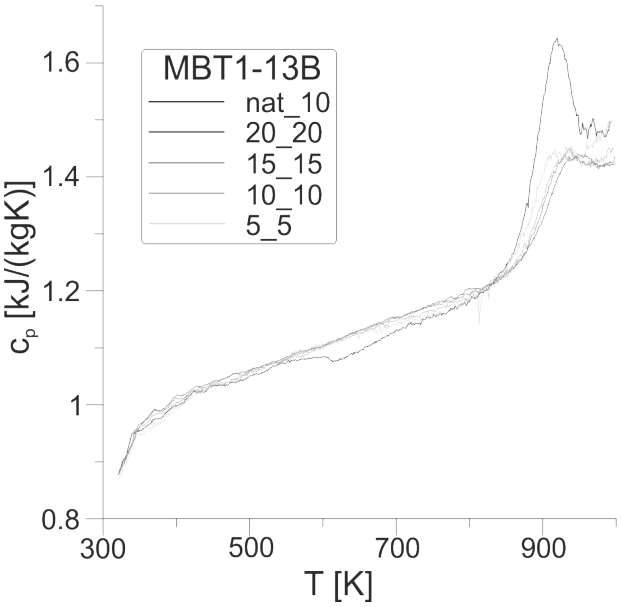

Figure 4.4: C_p curves for MBT1-13B as measured during heating. The different cooling/heating cycles are labelled: For example, nat_10 indicates previous, natural, cooling and then heating with a rate of 10 K/min.

promising, but its initial c_p curve is disturbed by reactions or phase transitions within the sample that are not yet understood. Therefore, influences on cooling rate estimation can not be ruled out. T_g is between 601°C for MBT1-10C and 661°C for MBT1-2C. At the outer rims of the two blocks high cooling rates of 10 to 12 K/min are observed, while in the middle where the two blocks lie next to each other low cooling rates of about 0.1 K/min are seen. This supports our field hypothesis that we are dealing with one block that has broken in two parts. The trend of the cooling rates in the interior of this whole block is asymmetrical to one side as the gradient of cooling rates is much higher on the left side. At MBU1 all samples show a large change in c_p of the supercooled liquid for the slow cooling cycle with 5 K/min at the end of the experiment. Nonetheless, it was possible to determine constant T_g of 633 - 634°C and the cooling rates range between 0.001 K/min and 0.05 K/min, which are in the same range as the data by Gottsmann and Dingwell [2001b]. Natural cooling rates of MBD1 range between 0.0004 K/min (0.58 K/day) and 0.38 K/min without any apparent trend and the T_g of these samples are between 624 and 669°C. Due to the low glass content of the MBL1 samples, no peak in c_p curves is found and thus, no results could be obtained for MBL1. Results for the glassy samples of the much older El Pasajiron sites are very good with the exception of EPJ1-1 and EPJ2-4. EPJ1-1 has too high a crystallinity to show a peak at T_g and c_p of EPJ2-4 changed after the first heating cycle. Natural cooling rates range between 0.0005 K/min (0.72 K/day) and 0.0025 K/min (0.15 K/h)for EPJ1 and between 0.0001 K/min (0.14 K/day) and 0.004 K/min (0.24 K/h) for EPJ2. Thus, cooling was considerably slower than for most MB samples. This could be

due to the fact that EPJ is a welded deposition with a high deposition rate and therefore, a thick layer that took longer to cool down. T_g for EPJ1 samples is between 560 and 609°C and for EPJ2 samples between 669 and 682°C.

4.4 Magnetic mineralogy and domain state

Rock magnetic measurements were performed to analyze magnetic mineralogy and domain state. Isothermal remanent magnetization (IRM) acquisition, isothermal backfield curves, hysteresis loops at room temperature and thermomagnetic curves were measured on a Variable Field Translation Balance (VFTB) using 5 mm diameter miniature cores. At least one sample of each site was heated in air stepwise to 420°C, 470°C, 520°C and, when necessary to reach the Curie temperature T_C, up to 560°C and 600°C. Between each of these steps additional backfield and hysteresis measurements at room temperature were done to test the thermal stability of the samples. Rockmagnetic data of all samples can be found in the appendix, Tab. B.1. Ore microscopy using oil objectives with magnifications of 50 and 125 was done on at least one sample per site that had previously been polished down to 1 μm.
Thermomagnetic curves (Fig. 4.3) yield T_Cs for EPJ1 of 500°C to 520°C and for EPJ2 of 450°C to 530°C. The thermomagnetic curves of EPJ2-1C and EPJ2-2D decline continously while those of all other samples drop relatively sharply at T_C. MBL1 samples lose most of their magnetization already at low T_Cs of 200°C to 350°C, but also have a small contribution of a second higher T_C at 400°C to 520°C. Specimens from MBD1 have a high T_C at about 530°C and a low T_C at 200°C to 390°C which, however, is not always very obvious. Three different T_Cs are observed in samples from MBT, though not each in every sample: One low T_C between 200°C and 240°C, one middle between 470°C and 530°C and a high one at 570°C. While the middle T_C is found in every sample, only sample MBT1-7C shows the high T_C and the low T_C is observed in samples MBT1-4C, MBT1-7C, MBT1-11A, MBT1-13A and MBT1-14C. All MBU1 specimens have a high T_C of ∼550°C and a second low T_C between 90°C and 240°C, which is not always very prominent.
Taken together, in all cases where T_g could be determined it is well above T_C and no alteration connected to $T_b > T_g$ [Smirnov and Tarduno, 2003] should occur during the paleointensity experiments. Further, heating and cooling curves from samples of all sites are almost reversible, at least when not heated far above the upper T_C. This already indicates the absence of any other alteration, which is further supported by hysteresis and backfield measurements conducted together with the stepwise heating: their parameters are almost identical after the different heating steps.

Plotted in a Day plot [Day et al., 1977] with domain state related boundaries and mixing lines by Dunlop [2002], single-domain (SD) or at least close to SD behavior is indicated for ∼65% of the samples (Fig. 4.5c and d). Only 15 of the 47 samples show grain sizes in the pseudo-single-domain (PSD) range for both M_{rs}/M_s (saturation of remanence/saturation magnetization) and B_{cr}/B_c (coercivity of remanence/coercivity). At MBL1 only sample MBL1-1 has a too low M_{rs}/M_s value while all the other samples plot clearly within the SD

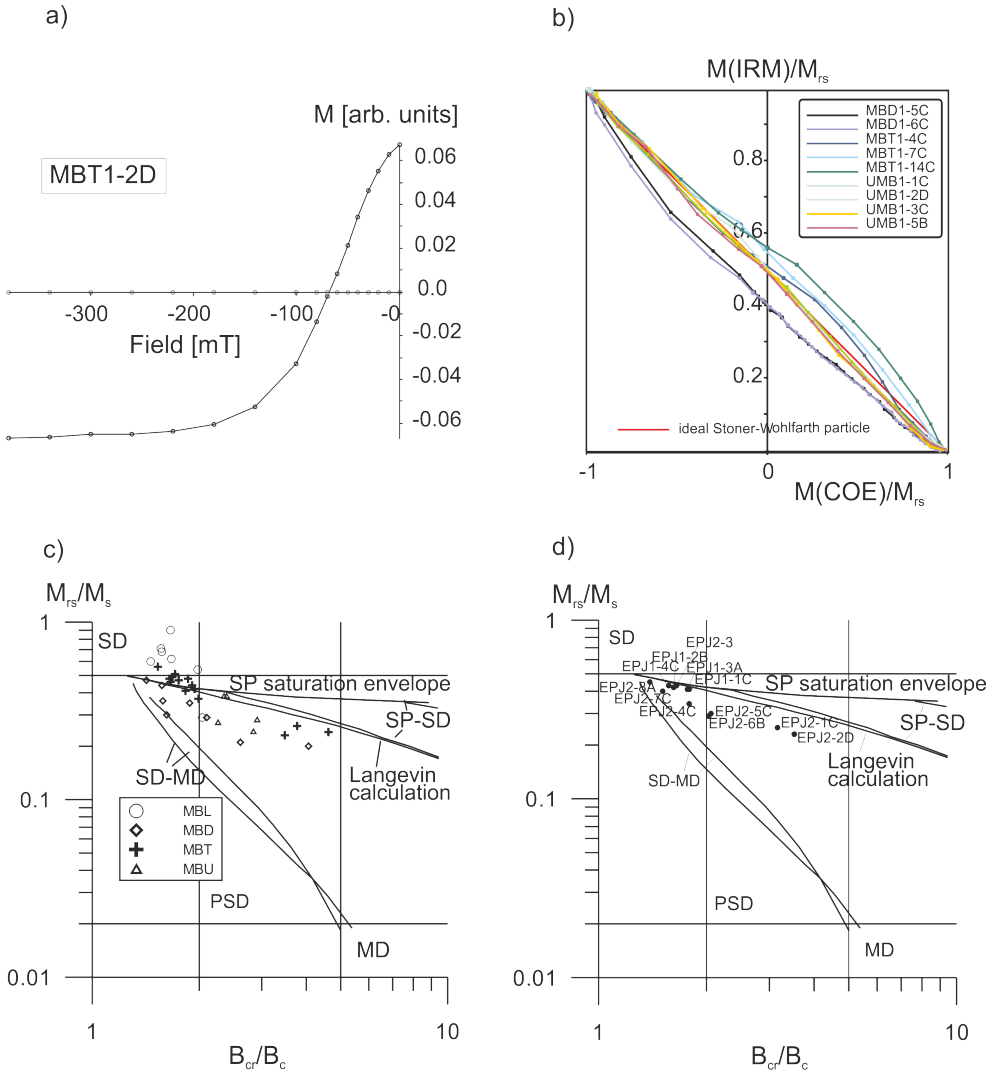

Figure 4.5: a) Backfield curve of sample MBT1-2D. b) Henkel plots [Henkel, 1964] of all Montaña Blanca (MB) samples that are in the PSD range of the Day plot. c) Day plot [Day et al., 1977] with domain state related boundaries and mixing lines by Dunlop [2002] of samples from c) MB and d) El Pasajiron.

panel. Similar to MBL1-1 also most samples from EPJ1, EPJ2, MBD1 and MBT1 have slightly too low M_{rs}/M_s values, but are still close to SD. The other samples from these sites as well as the samples from MBU1 lie within the PSD panel. A closer look at their position in the Day plot suggests an influence of superparamagnetic (SP) particles [Tauxe et al., 1996]. Further insight into the domain state of the specimens can be gained through Henkel plots [Henkel, 1964] (Fig. 4.5b): Here backfield and IRM data, i.e. remanence data, are plotted together. The diagonal of the plot represents ideal Stoner-Wohlfarth particles; that is, uniaxial non-interacting single-domain particles [Wohlfarth, 1958]. Not only for the samples within or very close to the SD panel, but also for those within the PSD panel the data are very close to the ideal line suggesting a predominant SD character of the remanence-carrying particles.
High B_{cr} values between 65 mT and 135 mT are observed for all samples. Thus, shape anisotropy is indicated. Only samples MBL1-1A, MBL1-2C and MBL1-3C have B_{cr} values as low as 35 mT and, thus, should not show any prominent anisotropy. Further the trend from high B_{cr} values for the nondevitrified samples to lower values for devitrified ones suggests a connection between devitrification processes and change in B_{cr}, e.g. a shortening of grains with previous uniaxial symmetry.
Unfortunately, it was very difficult to get information from ore microscopy, as the glassy matrix can not be resolved. However, a few grains of slightly larger sizes (mostly between 1 and 3 μm, in some cases up to 15 μm) were found to be distributed evenly about the samples of MB and EPJ. The brightness of these mostly rounded, sometimes elongated minerals changes under polarized light. As ore microscopy was unable to resolve the glassy matrix, magnetic force microscopy was done on some samples. However, even for this method, grain sizes were either too small or ferromagnetic particles too rare within the samples and thus, it was impossible to get any picture of magnetic domains.
As backfield and IRM curves for all sites saturate at low fields (i.e. mostly below 300 mT) (e.g. Fig. 4.5a), low coercive remanence carriers, as for example (titano-)magnetite are probable. For silicic melts Buddington and Lindsley [1964] found that titanomagnetites can only be responsible for relatively high T_Cs as no titanomagnetites with high titanium content are usually found within these. In contrast, low T_Cs are due to more titanium-rich hemoilmenites which can coexist in silicic melts together with the titanium-poor titanomagnetites [Buddington and Lindsley, 1964]. Although we are dealing with melts of phonolitic composition, this observation fits also to the results of ore microscopy, as hemoilmenites are optically anisotropic and often rounded or needle-shaped. Thus, the data suggest that the main remanence carriers of our samples are low-titanium titanomagnetites that are too small to be resolved using ore microscopy and within or close to the SD range. At MB these titanomagnetites are mostly accompanied by high-titanium hemoilmenites of slightly larger grain sizes: Those grains that were seen to change their brightness under polarized light. These generally contribute only very little to the whole remanence.

Table 4.2: Paleodirections

Locality or site	n/N	D [°]	I [°]	k	α_{95} [°]
El Pasajiorn	8/10	359.7	39.1	65	6.9
EPJ1	3/4	8.6	45.0	258	7.7
EPJ2	5/6	355.1	35.3	90	8.1
Montaña Blanca	17/19	357.4	47.7	125	3.2
MBL1	4/6	356.6	50.1	172	7.0
MBD1	8/8	355.8	47.8	127	4.9
MBU1	5/5	0.3	45.5	92	8.0

Mean directions (D, I) of the different sites and localities together with uncertainty values (k, α_{95}). n/N indicates number of directions used for calculation of mean (n) versus number of directions determined (N).

4.5 Paleodirections

Thermal demagnetizations to less than 10% of the NRM were done on at least 4 samples (inch cores) per site using a Schoenstedt furnace in the paleomagnetic laboratory of LMU Munich in Niederlippach. All magnetization measurements were carried out on a Molspin magnetometer. After each measurement of the remaining NRM the susceptibility was measured on a KLT-3 Minikappa bridge to detect alteration. Sometimes relative changes of up to 20% were observed, which were however not seen as continuous changes, but as sudden changes between two measurements, that came back to the original values at later measurements. These were therefor accorded to drifts in the instrument rather than to alteration. For most samples changes of only up to 10% were observed. After determination of the specimens' directions by principle component analysis (PCA) [Kirschvink, 1980], the mean direction of each site as well as of each locality (El Pasajiron, Montaña Blanca) were calculated using Fisher statistics [Fisher, 1953] (Tab. 4.2). All site mean directions are well defined with $k \geq 90$ and $\alpha_{95} \leq 8.1°$. Typical orthogonal projections and stereoplots with the resulting sample directions as well as the mean directions of each locality are given in Fig. 4.6.

Both sites at El Pasajiron as well as sites MBL1, MBD1 and MBU1 show northerly declinations D with somewhat varying inclinations I between 35.3° and 50.1°. This shows that not only the sites at El Pasajiron as well as MBD1 and MBU1 were cooled *in situ*, but also that the block at MBL1 did not rotate after cooling below T_C. At MBL1 two outliers (MBL1-5B and MBL1-6C) show eastward directions. Rock magnetically there is no obvious difference with the other samples. However, already in the field we have noted that reorientation of these samples may be difficult. Thus, these directions were not used

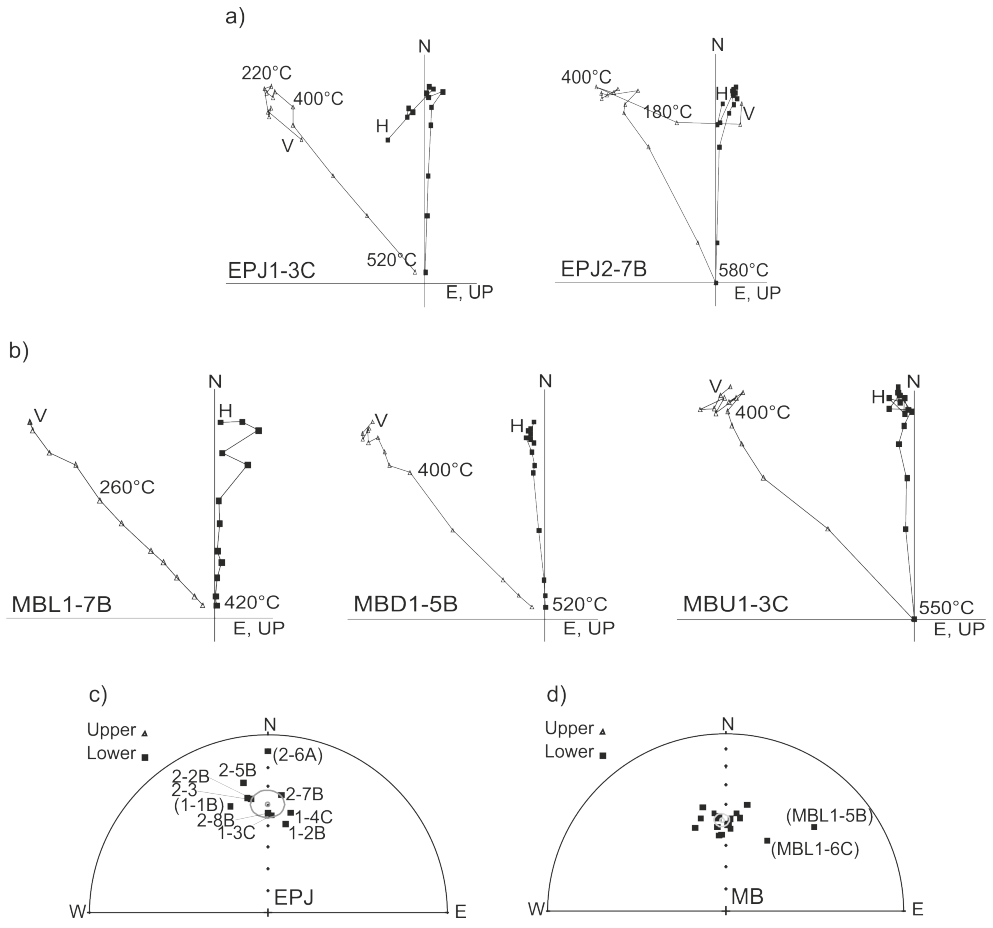

Figure 4.6: Orthogonal projections of one specimen per site at a) El Pasajiron (EPJ) and b) Montaña Blanca (MB). V and H indicate vertical and horizontal component, respectively. c) and d) show the stereographic projections of the different specimen directions and the calculated means (grey) of EPJ and MB. Specimen names in brackets mark directions not used for calculation of mean.

Table 4.3: Paleodirections of MBT1 samples

Specimen from MBT1	D [°]	I [°]
MBT1-2C	298.3	-1.8
MBT1-4B	325.4	-3.5
MBT1-7C	357.5	50.4
MBT1-8B	352.1	61.8
MBT1-10C	14.2	70.3
MBT1-12C	144.3	67.0
MBT1-14B	298.7	36.9

D and I as determined for specimens from MBT1.

for calculation of mean values. Further, data from site MBT1 was not included in the calculations as samples show varying directions througout the section. Paleodirectional data of this site and a more detailed analysis can be found in Tab. 4.3 and section 4.7.1. Taken together EPJ1 and EPJ2 give a mean direction for the 750 ka El Pasjiron with a declination of 359.7° and an inclination of 39.1°, while MBL1, MBD1 and MBU1 yield $D = 357.4°$ and $I = 47.7°$ for the 2 ka Montaña Blanca.

4.6 Paleointensity determination

In the following we concentrate on results for MB, while in section 4.7.2 data from EPJ are presented.

4.6.1 Thellier-type experiments

Paleointensity experiments on 5 mm and 8 mm diameter miniature cores were done in a MMTD20 thermal demagnetizer. For in-field steps laboratory fields of 30 ± 0.1 μT were applied during heating and cooling. The experiments followed the modified Thellier-technique MT4 [Leonhardt et al., 2004] for which zero-field steps are done first and which incorporates the commonly used pTRM checks, additivity checks [Krása et al., 2003] and pTRM tail checks [Riisager and Riisager, 2001]. Directional differences between the applied field and the NRM of the pTRM-tail check are taken into account according to Leonhardt et al. [2004a]. All determinations were analyzed using the ThellierTool4.21 software and its default criteria [Leonhardt et al., 2004]. This software allows full-vector treatment and application of check correction. Paleointensity data are summarized in Tab. 4.4, additionally quality parameters can be found in Tab. B.2 and Tab. B.3 in the appendix and respective plots of each site are given in Fig. 4.7.

Paleointensity determinations at sites MBU1, MBL1 and MBD1 are of good quality,

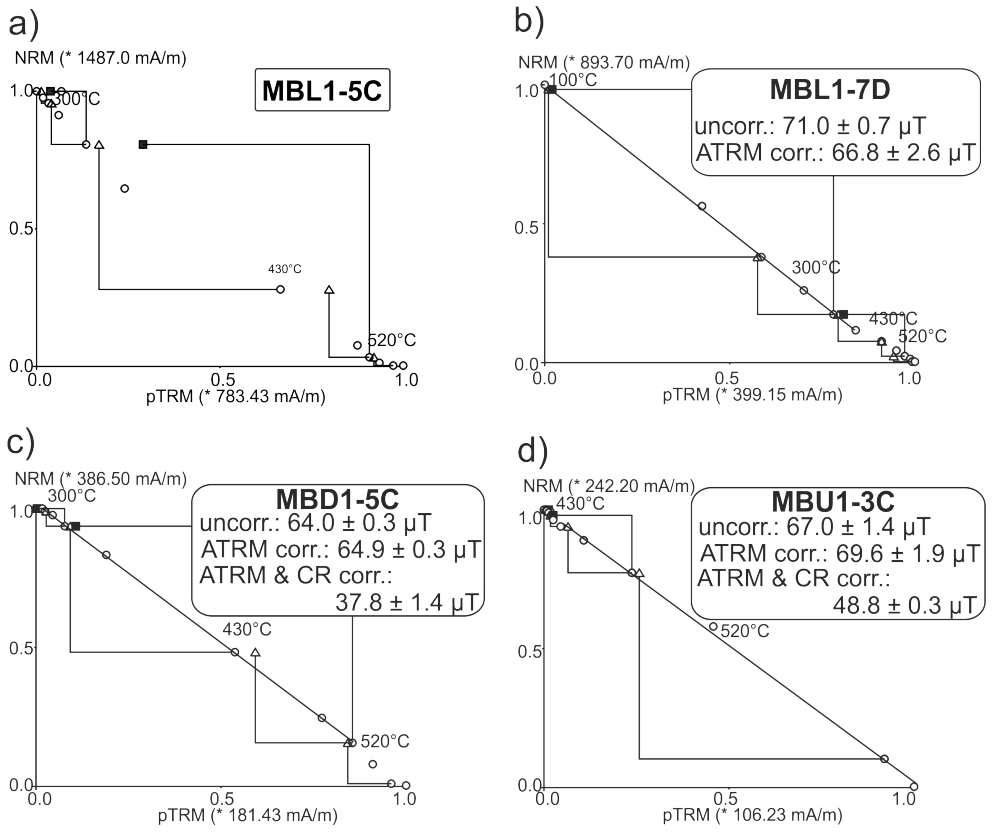

Figure 4.7: Respective NRM/pTRM diagrams (triangles: alteration checks, squares: additivity checks) for sites MBL1 (MBL1-5C rejected, MBL1-7D accepted), MBD1 and MBU1. Uncorrected and whenever possible ATRM and ATRM plus cooling rate (CR) corrected paleointensity values of the specimens are given.

giving a high success rate of 81% with 17 successful determinations out of 21 that had been performed. Four of these are class A and ten class B results according to the default criteria by Leonhardt et al. [2004]. Further three class C results were used due to good in-site agreement. For most of these determinations fractions f of the NRM [Coe et al., 1978] $\geq$0.82, only in two cases $f = 0.67$ (MBL1-1C) and $f = 0.41$ (MBD1-2D), were analyzed. Only for sample MBD1-2D has the whole range of the characteristic remanence seen in orthogonal projections not been analyzed. Gap factors g [Coe et al., 1978] are greater than 0.6, in most cases greater even than 0.7, and quality factors q [Coe et al., 1978] range between 7.5 and 141.5, mostly greater than 25. pTRM tails show no multi-domain (MD; both tail parameter $\delta(t)$ and relative intensity difference between repeated thermal demagnetizations $\delta(TR) > 7\%$) and only in two cases (MBU1-2D, MBU1-4D) minor PSD ($2\% < (\delta(t)$ and $\delta(TR)) < 7\%$) contribution. Alteration is absent in most specimens, as difference ratios DRAT [Selkin and Tauxe, 2000] are less than 4.3%.
Arithmetic means and standard deviations calculated from the paleointensity results of the different specimens yield mean values of 67.6$\pm$4.8 μT for MBL1, 64.7$\pm$7.2 μT for MBD1 and 63.3$\pm$2.9 μT for MBU1, which within error are identical. The weighted mean paleointensity (weighting factor: 1/standard deviation of the different sites) for Montaña Blanca using the data of these three sites gives 64.9$\pm$1.3 μT.

4.6.2 Magnetic anisotropy

A rock may be magnetically anisotropic, i.e. its ability to acquire a magnetization in a magnetic field can depend on the direction of this field. High B_{cr} values as determined during rock magnetic experiments suggest shape anisotropy in our samples. Fortunately, as weak field TRM is proportional to the field strength, the anisotropy tensor of TRM (ATRM tensor) can be obtained. Such determinations of the ATRM tensor were done on the same samples as previous paleointensity determinations, using again the MMTD20 demagnetizer. TRMs were imparted using in-field heating/cooling cycles to the upper end of the blocking spectra of the samples subsequently in +z, +x, -x, +y, -y and -z direction. Additionally, the +z treatment was repeated in the end to check for alteration. The measurements were analyzed following the approach of Veitch et al. [1984] and the results are again summarized in Tab. 4.4. After determining the ATRM tensor, the direction of the ancient field was calculated and the scaling factor f_{ATRM} to adjust the measured paleointensity by $H_{ATRM} = H_{UC} * f_{ATRM}$ (UC: uncorrected), is finally obtained by the relationship between ancient magnetization acquisition and laboratory magnetization acquisition in dependence of the ATRM tensor. An error estimate was obtained by not only determining f_{ATRM} from the averaged axes components but also seperately for positive (+x, +y, +z) and negative (-x, -y, -z) measurements, i.e. f^{pos}_{ATRM} and f^{neg}_{ATRM}. This way orientation errors and slight mineralogical changes are accounted for. The uncertainty of f_{ATRM} is then calculated by $\sigma(f_{ATRM}) = (|f^{pos}_{ATRM} - f^{neg}_{ATRM}|)$. The uncertainty σ_{ATRM} of the ATRM corrected intensity H_{ATRM} is a minimum maximum error including the uncertainty of the paleointensity determination and of f_{ATRM}.

Table 4.4: Paleointensity results and correction

Sample	Uncorr. paleointensity	ATRM correction		CR correction	
	H_{UC} [μT]	f_{ATRM}	H_{ATRM} [μT]	f_{CR}	$H_{ATRM,CR}$ [μT]
MBL1-1C	70.2±4.7				
MBL1-2C	61.0±1.7	1.154±0.019	70.4±3.2	-	
MBL1-3C	71,9±1.3	0.955±0.055	68.6±5.1	-	
MBL1-4C	63,9±1.8	1.026±0.005	65.6±2.2	-	
MBL1-5C					
MBL1-6A					
MBL1-7D	71.0±0.7	0.941±0.027	66.8±2.6	-	
MBL site mean	**67.6±4.8**		**67.8±2.1**		
MBD1-1A	65.2±1.2	0.979±0.001	63.8±1.2	-	
MBD1-1AD	72.8±0.8	0.995±0.037	72.4±3.5	-	
MBD1-2D	73.8±1.3	0.934±0.013	68.9±2.2	1.215±0.076	56.7±1.8
MBD1-3C	61.7±1.2				
MBD1-4D	63.2±2.0				
MBD1-5C	64.0±0.3	1.014±0.001	64.9±0.3	1.715±0.070	37.8±1.4
MBD1-6D	52.4±0.7	1.360±0.036	71.3±2.8	1.596±0.035	44.7±0.8
MBD1-7D					
MBD1-8C					
MBD site mean	**64.7±7.2**		**68.3±3.8**		**46.4±9.6**
MBT1-1C					
MBT1-3C	*62.2±0.9*	*1.098±0.060*	*68.3±4.7*	*1.466±0.104*	*46.6±0.1*
MBT1-4C					
MBT1-5A	*65.7±1.1*	*1.225±0.053*	*80.5±4.9*	*1.406±0.033*	*57.2±2.1*
MBT1-6D	69.5±1.8	0.991±0.002	68.9±1.9	1.373±0.092	50.2±2.0
MBT1-8C	*62.5±1.3*	*0.997±0.003*	*62.3±1.5*	*1.484±0.074*	*42.0±1.1*
MBT1-9	80.2±3.7	0.951±0.021	76.3±5.2	1.282±0.035	59.5±2.4
MBT1-10E	70.8±1.9	0.975±0.007	69.1±2.3	1.263±0.029	54.7±0.5
MBT1-11A	*56.1±0.9*	*0.986±0.003*	*55.3±1.0*	*1.188±0.023*	*46.6±0.0*
MBT1-12D	*63.7±3.0*	*1.033±0.000*	*65.8±3.1*	*1.162±0.050*	*56.6±0.2*
MBT1-13A	67.9±0.6	0.973±0.008	66.1±1.1	1.150±0.027	57.4±0.4
MBT1-14C	64.3±0.8	0.993±0.000	63.8±0.8	1.146±0.016	55.7±0.0
MBT site mean	**70.5±5.9**		**68.8±4.7**		**55.5±3.5**
MBT site mean (rot.)	***66.3±6.5***		***67.7±7.0***		***52.7±5.9***
MBU1-1D	65.6±1.3	0.994±0.003	65.2±1.5	1.298±0.072	50.2±1.6
MBU1-2D	62.9±2.5	0.955±0.001	60.1±2.4	-	
MBU1-3C	67.0±1.4	1.038±0.006	69.6±1.9	1.427±0.030	48.8±0.3
MBU1-4D	60.2±3.7	1.087±0.054	65.4±7.3	1.569±0.110	41.7±1.8
MBU1-5C	61.0±1.5	0.953±0.007	58.2±1.9	1.298±0.074	44.8±1.1
MBU site mean	**63.3±2.9**		**63.7±4.6**		**46.4±3.9**
MB loc. mean (without MBT1)	**64.9±1.3**		**67.0±1.3**		**46.4±0.0**
MB loc.mean (with unrot. MBT1)	**66.0±1.6**		**67.3±1.0**		**50.4±3.2**
MB loc. mean (includ. MBT1)	***65.1±1.0***		***67.1±1.0***		***48.4±2.1***

H_{UC}, H_{ATRM} and $H_{ATRM,CR}$ are the paleointensity values of the individual samples with associated errors for the uncorrected, ATRM corrected and ATRM and cooling rate (CR) corrected determinations, respectively. H_{ATRM} errors are calculated as maximum-minimum errors including the uncertainty of the uncorrected paleointensity σ_{UC} and of the ATRM correction factor f_{ATRM}. $H_{ATRM,CR}$ errors are calculated via full error propagation using the uncertainties of H_{UC}, f_{ATRM} and f_{CR}. Also shown are arithmetic means and standard deviations of the different sites and weighted means for the whole Montaña Blanca locality (using 1/(arithmetic standard deviation of site means) as weighting parameter; indicated as loc. mean). Data from rotated samples at site MBT1 is shown in italics and for site means indicated by (rot.). For locality MB paleointensity values are given that first are without MBT1, then are including unrotated MBT1 samples and then are including all MBT1 samples.

Relative differences in +z measurements are smaller than 3% and anisotropy correction could be performed (Tab. 4.4). For samples MBL1-1C, MBD1-3C and MBD1-4D no anisotropy or cooling (section 4.6.3) experiments were done. The resultant scaling factors f_{ATRM} of the other samples range between 0.93 and 1.36, although the majority of scaling factors is close to 1. For sites MBL1 and MBU1 resulting ATRM corrected mean paleointensites (again arithmetic mean and standard deviation) are almost the same as before correction: 67.8±2.1 μT (0.2% higher) and 63.7±4.6 μT (0.6% higher) respectively. However, at site MBD1 a 5.6% higher corrected value of 68.3±3.8 μT is observed. Within site scatter at MBL1 and MBD1 is reduced by anisotropy correction while at MBU1 a higher error after correction is observed. Taking all three sites together a sligthly larger (3.2%) weighted mean paleointensity of 67.0±1.3 μT is observed for Montaña Blanca after correction compared to the uncorrected value of 64.9±1.3 μT. Within error both values are identical and the error stays the same. This is due to the only marginal influence of ATRM scaling.

4.6.3 Cooling rate dependence

All our data suggest that we are dealing with remanence carriers within or close to the SD range. Theoretically [Halgedahl et al., 1980, Dodson and McClelland-Brown, 1980] and experimentally [Fox and Aitken, 1980, McClelland-Brown, 1984] it was found that an assemblage of identical, non-interacting SD particles acquires a larger TRM during slower cooling. However, even when dealing with only SD particles, the cooling rate dependency of TRM acquistion is not constant, but depends already on small changes in grain size and domain state. Leonhardt et al. [2006] and Ferk et al. [2010] showed that experiments which give the TRM dependency on cooling rate together with determinations of natural cooling rates from relaxation geospeedometry have to be done to correct overestimation of paleointensity.
Following the approach by Leonhardt et al. [2006], the same specimens as for Thellier-Thellier and anisotropy experiments were subjected to magnetic cooling rate dependency investigations that included two laboratory cooling rates. For fast cooling the cooling fan of the MMTD20 furnace was used like during the previous experiments, while for slow cooling the samples were cooled without fan operation. Laboratory cooling rates were determined on basaltic dummy samples across the glass transition intervals of our samples, i.e. between about 700°C and 550°C. By monitoring the temperature decrease versus time (using a thermocouple inside one of the basaltic samples) the mean cooling rates of our furnace in this temperature range were determined, i.e. the slope of the temperature decrease versus time curve between 700°C and 550°C was determined. A conservative estimate of the uncertainty in cooling rate determination is 10% for fast cooling and 5% for slow cooling.
First, a fast heating/cooling cycle with a cooling rate of ∼385 K/min was used to impart a TRM ($TRM_{f,1}$). Then a heating/cooling cycle with a 38.5-fold slower cooling rate of ∼10 K/min ($TRM_{s,1}$) and at the end, another fast one ($TRM_{f,2}$) in order to check for alterations during the experiment, were done. $TRM_{f,1}$ and $TRM_{f,2}$ of most samples differ

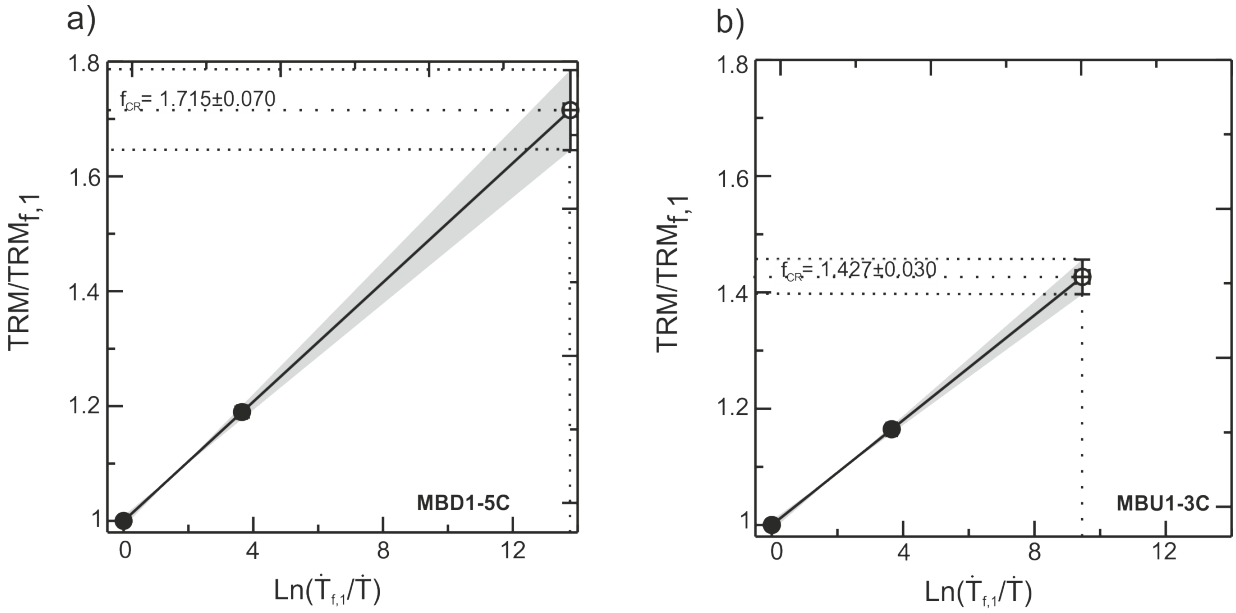

Figure 4.8: Cooling rate correction using the laboratory measured cooling rate dependency (solid symbols) and related uncertainties, as well as the linear extrapolation of the TRM dependency to the natural cooling rates as determined by relaxation geospeedometry (open symbols) for samples MBD1-5C and MBU1-3C.

by $\leq 2\%$ indicating no or very small alterations. Only four samples show differences of up to 5%. However, these samples also show differences between $TRM_{f,1}$ and $TRM_{s,1}$ $\geq$20% and thus, alteration in these samples should still be small enough to enable cooling rate corrections. Differences between $TRM_{f,1}$ and $TRM_{f,2}$ are used as error estimates for $TRM_{s,1}$ and $TRM_{f,1}$.

The TRM intensity for slow cooling is 7% to 31% larger than for fast cooling. This is higher than the theoretically predicted 5% to 7% overestimate per order of magnitude [Halgedahl et al., 1980, Dodson and McClelland-Brown, 1980]. TRM overestimates exceeding the theoretically predicted values were also observed for example in a study by Genevey and Gallet [2002] on archeomagnetic materials. A possible reason for the here observed overestimates of up to 31%, could be related to low-titanium titanomagnetites as remanence carriers and not SD magnetite or hematite as used in the theoretical studies. Titanomagnetites are characterized by different magnetic parameters, of which in particular the blocking temperature relationship, relaxation times and anisotropy are relevant for cooling rate dependencies.

The magnetic cooling rate dependency is extra-/interpolated to the natural cooling rates as determined by relaxation geospeedometery to correct the overestimation of the H_{ATRM} values (interpolation only for MBT1-14C which has a natural cooling rate of 12 K/min). To do this, the laboratory measured $TRM_{f,1}$ and $TRM_{s,1}$, both normalized to $TRM_{f,1}$, are plotted versus $\ln(\dot{T}_{f,1}/\dot{T})$ (Fig. 4.8). According to Halgedahl et al. [1980] such linear

extra-/interpolation is valid, if the remanence carriers are non-interacting SD particles that dominantly block close to the respective blocking temperature. As our samples are at least close to SD and unblock sharply within about 100 to 150°C, these conditions are fulfilled. The previous error estimates for inaccuracy of laboratory cooling rate and magnetization determinations allow a minimum/maximum error propagation towards the natural cooling rates (Fig. 4.8). The obtained cooling rate correction factor $f_{CR} = \mathrm{TRM}/\mathrm{TRM}_{f,1}$ is then used to correct the paleointensity values H_{ATRM} by $H_{ATRM,CR} = H_{ATRM}/f_{CR}$. Full error propagation, including the uncertainties of the paleointensity experiments as well as those of f_{ATRM} and f_{CR} gives the uncertainty $\sigma_{ATRM,CR}$ of the individual ATRM and cooling rate corrected paleointensity values. An application of cooling rate correction was only possible for samples whose natural cooling rates were determined successfully by relaxation geospeedometry. Thus, no cooling rate correction was possible for site MBL1 where the high crystal content suppressed any peak during calorimetry. At the other sites H_{ATRM} values are significantly reduced (Tab. 4.4). This results in arithmetic mean values of 46.4±9.6 μT at MBD1, 46.4±3.9 μT at MBU1 and a weighted mean value (weighting factor: 1/standard deviation of the different sites) of 46.4±0.0 μT for whole Montaña Blanca. The ∼20 μT reduction (28.5% for whole Montaña Blanca) relative to the non-corrected values underlines the pivotal importance of cooling rate correction for SD dominated materials.

4.7 Discussion

4.7.1 Emplacement rotations at site MBT

Some specimens of MBT1 show acquisition of TRM during emplacement rotations/squeezing and block break-up while cooling. This can be seen clearly in the curved orthogonal projections of the Thellier measurements (Fig. 4.9a) and is verified by field observation (Fig. 4.9b) and associated paleomagnetic directions (Tab. 4.3): Specimens MBT1-7C, MBT1-8B and MBT1-10C from the inner parts, which were the last to cool below T_C give northerly directions with inclinations between 50° and 70°. This corresponds relatively well to $D = 357.4°$ and $I = 47.7°$ for the other sites at MB. Thus, the inner part seems to be almost in the same position as during cooling. However, this does not account for the outer parts, where directions far from normal are recorded. At the left end of the site $D = 298.3°$, $I = -1.8°$ (MBT1-2C) and $D = 325.4°$, $I = -3.5°$ (MBT1-4B) are observed, while at the right end $D = 144.3°$, $I = 67.0°$ (MBT1-12C) as well as $D = 298.7°$, $I = 36.9°$ (MBT1-14B) are found.

Such rotations will not affect the resultant paleointensity if cooling occurs during a "normal" time range, i.e. external field variations are negligible. However, Arai plots with associated curved orthogonal projections are normally disregarded for paleointensity determination. Therefore, at first, only the paleointensity of specimens with linear parts in the orthogonal projections were analyzed (e.g. Fig. 4.9c), yielding a uncorrected mean value for MBT1 of 70.5±5.9 μT, an anisotropy corrected value of 68.8±4.7 μT and a ATRM

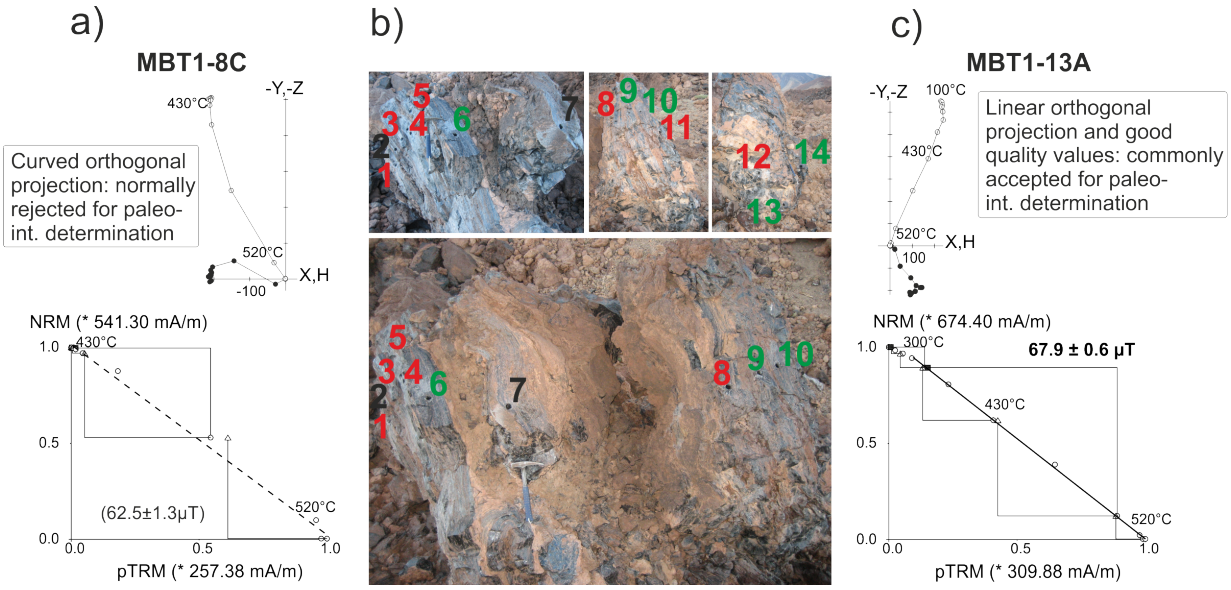

Figure 4.9: NRM/pTRM diagrams plots and respective orthogonal projections from the profile at MBT1. a) Plots of sample MBT1-8C, which normally would be rejected for paleointensity determination due to curved orthogonal projection. b) Pictures of MBT1 showing samples that are commonly accepted (green) and rejected (red) for paleointensity determination. c) Plots of sample MBT1-13A, which was accepted for paleointensity determination as orthogonal projection is linear and quality parameters were good.

and CR corrected value of 55.5±3.5 μT.
Arai plots of specimens with curved orthogonal projections, however, are often of very similar quality as those of the other MBT1 samples. Both samples with curved and with linear orthogonal projections show fraction of the NRM f≥0.84, only two times it is as low as 0.7 (MBT1-9) and 0.66 (MBT1-10E). MBT1-9 also shows a relatively low gap factor g=0.44 while all the other samples have g≥0.64. The quality factor q is mostly >16, again only MBT1-9 shows a low q=6.7 value. Taken together these data correspond to two class A, seven class B and only one class C result according to Leonhardt et al. [2004]. Due to the good quality of Arai plots of rotated samples, it was checked whether these data can be used by applying some pTRM model calculations using the phenomenological model by Leonhardt et al. [2004a] including some modification according to Fabian and Leonhardt [2010] (Fig. 4.10). If no rotations are implied the model yields the true "paleo"intensity (50 μT) for a SD remanence carrier (Fig. 4.10a). When only inclination changes constantly from 90° at 570°C to -90° at 0°C, while declination is kept constant, a slightly lower but within error true value is calculated (Fig. 4.10b). A constant change in direction during the whole cooling was applied as this is easily done in the computer calculation and gives a similar directional change during the blocking process as is observed in our samples. If, additionaly, declination changes constantly from 180° at 570°C to -180° at 0°C the intensity is underestimated by 1.2 μT (Fig. 4.10c). However, this results from the fact that a slight MD contribution has to be introduced to the model (inset Fig. 4.10) to enable computer calculations. Taken together, for SD remanence carriers paleointensity data from specimens with curved orthogonal projections should be reliable. Thus, taking these data into account a mean value of 66.3±6.5 μT is obtained.

However, if the recording material is anisotropic, as it is the case for many of our samples, then those coeval cooling rotations may become a nuisance. Usually, as mentioned before (section 4.6.2) anisotropy corrections are conducted using the ATRM tensor and the average direction of the selected linear segment in the Arai diagram, i.e. the resultant paleointensity is corrected. This technique may not be applicable when continuous changes of TRM acquisition directions are occurring. Indeed, it should be necessary to apply the anisotropy correction at each individual thermal step and its associated direction. This was done for all rotated MBT1 samples. As can be seen in Fig. 4.11 the paleointensity values do not change when comparing anisotropy correction of each step with anisotropy correction of the resultant paleointensity. Only uncertainty ranges are different, as for the latter (Fig. 4.11a) errors of both the paleointensity determination and of the correction factor are included, while for the former (Fig. 4.11b) only one of the paleointensity determination is included and the errors of the different correction factors for each step are left out. At least for samples with relatively small anisotropies a correction of the resultant paleointensity is therefore reasonable, which gives an anisotropy corrected mean value for MBT1 of 67.7±7.0 μT when all samples are included. Additonal application of CR correction gives an paleointensity of 52.7±5.9 μT. As all the data from site MBT1 are quite reasonable, they can also be included in calculation of an ATRM and CR corrected mean value for MB (including all samples from MBT1) yielding a ancient field value of 48.4±2.1 μT.

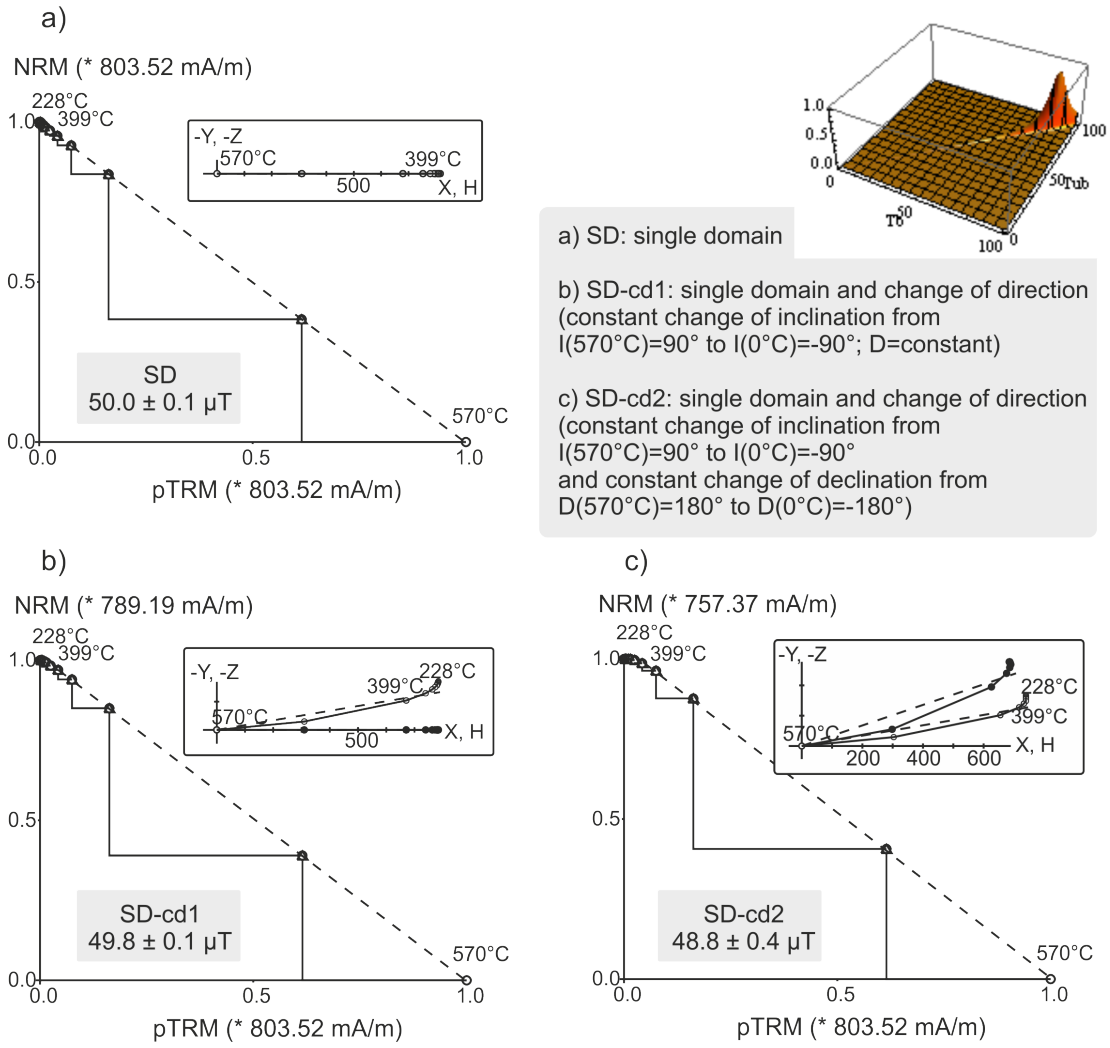

Figure 4.10: NRM/pTRM diagrams as calculated for a sample with SD remanence carriers (with minor MD contribution: inset), that a) was not rotated during emplacement, b) shows an constant change in inclination and c) shows constant changes in inclination and declination. a) and b) yield true paleointensity of 50μT, while c) gives slightly too low value.

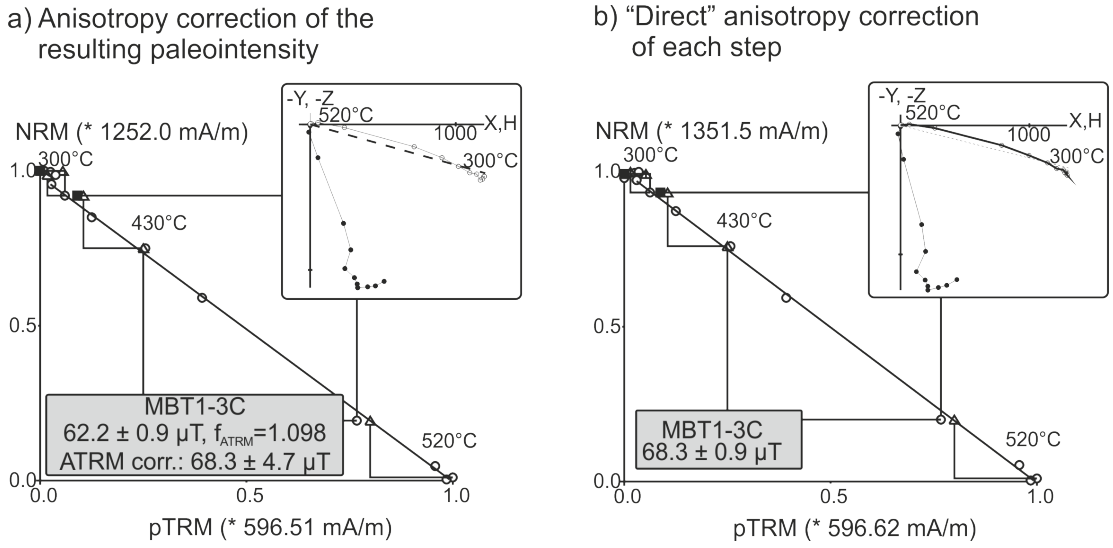

Figure 4.11: NRM/pTRM diagrams for MBT1-3C with anisotropy correction of a) the resultant paleointensity and b) each thermal step and the respective directions.

4.7.2 Devitrification at El Pasajiron

It was not possible to get good quality paleointensity data for El Pasajiron. Respective data (paleointensity values and quality parameters) can be found in Tab. B.3 of the appendix. Alteration occurs during all paleointensity experiments on samples from EPJ1. Nevertheless, if one analyzes the measurements, high paleointensity values of 60 to 68 μT are obtained. At EPJ2 alteration is not as strong as at EPJ1. However, increasing values of 17 to 38 μT are found for EPJ2-2B to EPJ2-6B (Fig. 4.12e) with especially the Arai plot of EPJ2-4C (28.7$\pm$0.6 μT) being of (seemingly) very high quality (Fig. 4.13a). EPJ2-7C and EPJ2-8C behave very similar to samples from EPJ1. They also yield high field values ($\sim$71 μT and $\sim$65 μT, respectively) and show non-linearity and failing pTRM checks which we interpret as alteration (Fig. 4.13b). No paleointensity value could be obtained for EPJ2-1C. To understand this at first sight astonishing variation in data, a closer look at the profile EPJ2 is needed: Site EPJ2 changes from clearly devitrified at the top to more glassy samples at the bottom. Both, a picture of site EPJ2 and different rockmagnetic parameters and values for paleointensity vs. profile height can be found in Fig. 4.12. It is important to mention that even though the profile changes from devitrified to more glassy, this may not account for each sample as during sampling we tried to find glassy parts even in the upper third. Further, there are differences between the surface and the inside of the rock. Some changes in rockmagnetic parameters with increasing alteration are observed. B_{cr} appears to get smaller with the increasing hydration from samples EPJ2-6B to EPJ2-1C (Fig. 4.12a). However, samples EPJ2-7C and EPJ2-8A show B_{cr} values almost as low as EPJ2-1C. Further, there is a trend towards more PSD-like behavior with increasing hydration (Fig. 4.12b and c, Fig. 4.5d). EPJ2-1 and EPJ2-2 are in the PSD range of the

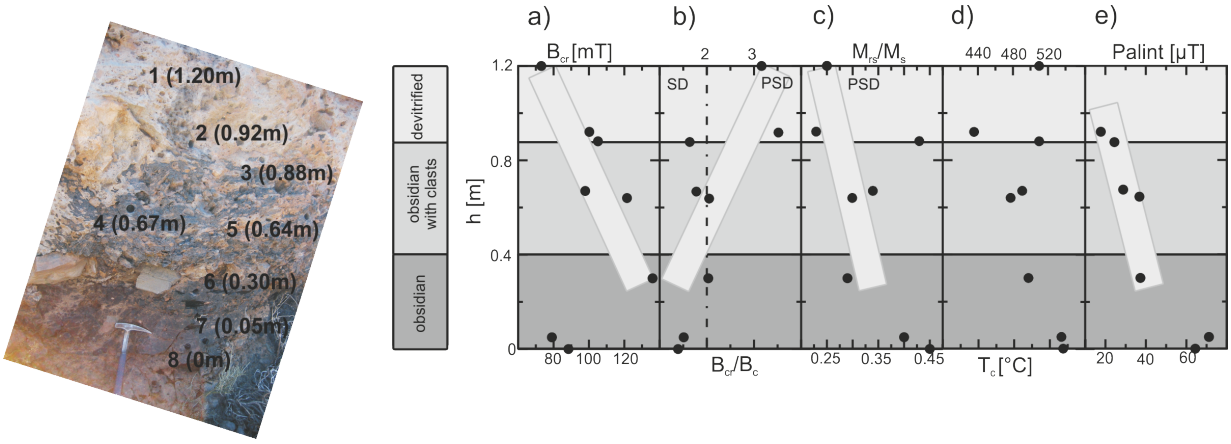

Figure 4.12: Picture of site EPJ2 together with rockmagnetic parameters and paleointensity values across the profile. Diagonal boxes in a), b), c) and e) show trends in data.

Day plot, while EPJ2-7C, EPJ2-8A and interestingly also EPJ2-3 have almost the same close to SD hysteresis parameters as samples from EPJ1. EPJ2-4C to EPJ2-6B already show a trend towards the two samples in the PSD range. There is no change in T_C that can be directly correlated to the change in devitrification (Fig. 4.12d).

Taken together, the rockmagnetic and paleointensity data suggest that during devitrification of the upper part of EPJ2 either new remanence carriers have grown or the old ones were altered, both leading to a change in NRM due to acquisition of a chemical remanence (CRM). Especially the increasing paleointensity values from the most devitrified samples to the more glassy samples support this hypothesis. The identical directions of EPJ1 and EPJ2 do not contradict this suggestion as northerly directions are found for the whole Brunhes chron and a later acquired CRM would give approximately the same direction as the primary remanence. Devitrified samples like EPJ2-4C carry a CRM which cannot be seen in the Arai plot and gives wrong paleointensities. The true field value at Tenerife 750 ka ago can only be obtained by those samples that are not devitrified. Hence, the field strength seems to have been approximately 60 to 70 μT (without inclusion of cooling rate dependency). However, as alteration is present in all samples yielding these high field values, calculation of a mean paleointensity for this time is not justified and further investigations, e.g. at other not devitrified sites at the Caldera Wall, are needed to get a reliable paleointensity value.

Even though paleointensity experiments for EPJ failed, it was tried to determine the ATRM tensor for samples from EPJ1 and EPJ2 to check whether the high differences in paleointensity are partly connected to anisotropy within the samples. However, a 2% to 10% difference in the two +z measurements indicates alteration and a meaningful determination of the ATRM tensor and of f_{ATRM} is, thus, not possible. As both paleointensity and anisotropy experiments for El Pasajiron sites had failed, no cooling rate experiments were done on these samples.

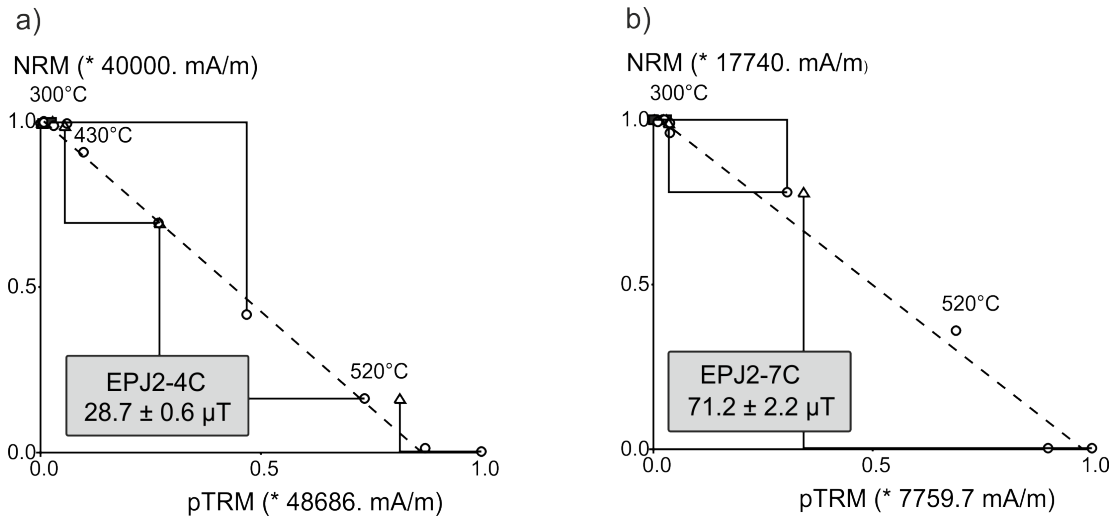

Figure 4.13: No obvious difference in quality can be found between paleointensity determinations of samples that a) show CRM overprint or b) carry the original TRM.

4.8 Conclusion

We have conducted a study of paleodirections and paleointensities on samples from Tenerife. For the 750 ka old El Pasajiron, at the southern Caldera wall, no good data could be obtained as during paleointensity experiments either alteration occured or potential CRM overprints were found for devitrified samples. When comparing paleomagnetic and rock magnetic data from different samples within the sites the following trends were found with increasing devitrification: Hysteresis and backfield properties showed a trend towards more PSD-like behavior and paleointensity was shown to decrease. A possible explanation for these features is the later acquisition of a CRM. This possible CRM is not easily identified

Table 4.5: VGPs, VDMs and VADMs of archeomagnetic studies and geomagnetic models at ∼115 BCE

Data set	Age (BCE)	Location	D [°]	I [°]	Int. [μT]	VGP Lat. [°N]	VGP Long. [°E]	VDM [10^{22}Am^2]	VADM [10^{22}Am^2]
this study	115±17	Tenerife	357.4	47.7	48.4±2.1	87.7	266.8	9.64±0.42	9.71±0.42
Kovacheva 1995	54±24	Spain	359.2	58.4	60.9±1.7	86.8	189.1	10.63±0.58	10.26±0.29
Kovacheva 1984, 1985-6	200±100	Morocco	1.8	53.0	56.6±5.3	87.6	136.0	10.57±1.64	10.32±0.97
Kovacheva 1984, 1985-6	50±50	Morocco	353.9	54.3	61.2±1.3	85.0	258.1	11.25±0.69	11.16±0.24
Bayes. Inv. Model	100	Tenerife	1.7	43.1	47.3±3.2	86.5	138.1	9.89±0.67	9.48±0.64
Bayes. Inv. Model	120	Tenerife	2.1	42.7	47.7±3.4	86.0	134.6	10.0±0.71	9.57±0.68
ARCH3K.1	120	Tenerife	2.6	46.3	49.5	87.6	87.6	10.0	9.93
ARCH3K.1	110	Tenerife	2.0	46.0	49.6	88.0	98.9	10.1	9.95
CALS3K.3	120	Tenerife	1.2	44.4	51.3	87.6	137.5	10.6	10.29
CALS3K.3	110	Tenerife	1.3	44.3	51.1	87.5	136.1	10.6	10.25
CALS7K.2	120	Tenerife	357.9	43.6	46.4	86.6	197.8	9.67	9.32
CALS7K.2	110	Tenerife	357.9	43.3	46.2	86.5	195.8	9.65	9.28

Locations, together with declination D, inclination I, paleointensity Int., virtual geomagnetic poles (VGP latitude and longitude), virtual dipole moments VDM and virtual axial dipole moments VADM of this study, 3 archeomagnetic studies (Spain: 42.27°N, 357.98°E [Kovacheva et al., 1995, Parés et al., 1992], Morocco: 35.50°N, 354.00°E [Kovacheva, 1984, 1985]) and four geomagnetic models (Bayesian inversion model for last 3000 years [Leonhardt et al., 2010], ARCH3K.1 [Donadini et al., 2009], CALS3K.3 [Korte et al., 2009] and CALS7K.2 [Korte and Constable, 2005]; all computed for Tenerife: 28.25°N, 343.4°E).

in the paleointensity experiments as it is not monitored by any of the performed checks. Indeed, some of the paleointensity determinations on apparently CRM overprinted samples are of high quality and would normally be regarded as reliable. Due to the possible CRM overprint no trustworthy data can be obtained from the devitrified samples. As the nondevitrified - and, thus, not CRM overprinted - samples altered during paleointensity experiments, their paleointensities can not be used either. However, they all yield values of 60 to 70 μT, hence, suggesting a strong field 750 ka ago. Further investigations for example at other not devitrified sites at the Caldera wall will have to show whether this is true. In conclusion, our data suggest that devitrified samples are prone to CRM overprinting and may not result in reliable paleomagnetic data. However, as our data set is very small and as alteration complicates the situation, further studies will have to prove whether the observed trends are found in other sections and are really connected to devitrification and/or hydration of glass and whether a CRM overprint truely exists. Nonetheless to be on the safe side when working with obsidian one should only sample nondevitrified sites as long as there are no other studies analyzing the reliability of devitrified samples.

Much better results were obtained for samples of the 115±17 BCE Montaña Blanca eruption. Paleointensity experiments are generally of high quality (section 4.6.1 and 4.7.1) and also anisotropy and cooling rate corrections were successful. Emplacement rotations and squeezing structures that are often found at obsidian outcrops were analyzed in detail at site MBT1. It was shown that paleointensity determinations of samples with curved orthogonal projections can be accepted when dealing with SD remanence carriers and that anisotropy correction can still be done for the resulting paleointenstity of our realtively weak anisotropic samples. The data of site MBT1 was included in the calculation of an ATRM and cooling rate corrected paleointensity, yielding a value of 48.4±2.1 μT. This corresponds to a Virtual Dipole Moment (VDM) of 9.64±0.42 $*10^{22}$Am^2 (uncertainty is a minimum/maximum error using the error bonds of the paleointensity, Tab. 4.5). Further, declination $D = 357.4°$ and inclination $I = 47.7°$ corresponding to a Virtual Geomagnetic Pole (VGP) of 87.7°N and 266.8°E were obtained. These values compare very well to both geomagnetic models and older paleointensity data (Tab. 4.5): The geographically closest paleomagnetic data for this time are some brick samples from Spain (54±24 BCE) [Kovacheva et al., 1995] that yield a paleointensity of 60.9±1.7 μT which corresponds to a VDM of 10.63±0.58 $*10^{22}$Am^2 and baked clay (200±100 BCE) and brick (50±50 BCE) from Morocco [Kovacheva, 1984, 1985] with paleointensities of 56.6±5.3 μT and 61.2±1.3 μT and VDMs of 10.57±1.64 $*10^{22}$Am^2 and 11.25±0.69 $*10^{22}$Am^2, respectively. No cooling rate or anisotropy correction were made for any of these data, though Kovacheva et al. [1995] explain that for the Spanish bricks neither of the two is necessary. As these sites are from more northerly latitudes, the paleointensities are all higher than our data. Two of the VDMs, however, are within error identical to our value and the third one is only slightly higher. This is a very good agreement, especially when the geographical distance and the age difference are taken into account. Additionally, a comparison with different geomagnetic field models by Leonhardt et al. [2010], Donadini et al. [2009], Korte and Constable [2005] and Korte et al. [2009] can be done. When these models are run for the geographical longitude and latitude of our sites very good agreement with our data is found, which

shows the validity of the geomagnetic models for that time and area. Only paleointensity and VDM data of CAL3K.3 [Korte et al., 2009] are out of the error bounds of our data, though still reasonably close. VGP latitudes of the models are very close to our data as well, whereas VGP longitudes are up to 180° off. This is due to the proximity to geographic north: Even though the poles are very close to each another, strong differences in VGP longitude may be observed. Last but not least, a comparison with today's field intensity at Tenerife, 38.5 μT, shows a decrease in intensity by 20% during the last 2 ka.

Acknowledgements

We thank Andy Biggin and Lisa Tauxe for their thorough reviews that strongly helped to improve the manuscript. We gratefully acknowledge Joan Marti for sharing his fundamental knowledge about geology and volcanology of Tenerife on the field trip in September 2007. We also thank him for providing the geological map of Tenerife and for giving fast and helpful answers to all our emails. Funding was provided by DFG grant Le1905/1-1 and FWF grant P21221-N14. D. B. Dingwell acknowledges the funding support of a LMUexcellent Research Professorship in experimental Volcanology (Bundesexzellenzinitiative) and ERC advanced grant EVOKES.

Chapter 5

Paleointensity on volcanic glass of varying hydration states

This chapter is a slightly modified version of a paper that has been submitted to Physics of the Earth and Planetary Interiors [Ferk et al., submitted]. Co-authors are J. S. Denton, R. Leonhardt, H. Tuffen, S. Koch, K.-U. Hess, and D. B. Dingwell.

Abstract

We have characterized the magnetic properties of variably hydrated volcanic glasses that were collected from rhyolitic deposits at Bláhnúkur, Torfajökull, Iceland. The glasses span the range from fresh obsidians to highly fractured perlites that contain >2 wt% meteoric water. Lava hydration plays a key role in the formation of perlite and, hence, these rocks are ideal to study hydration effects on remanence carriers and reliability of the paleomagnetic record. The total volatile content of the different samples was determined as a proxy for the degree of perlitization/hydration. This was compared to different rock magnetic parameters like coercivity of remanence, coercivity, saturation magnetization, saturation of remanence and Curie temperatures. It was found that coercivity of remanence, saturation magnetization and saturation of remanence decrease with increasing hydration, i.e. that magnetic remanence carriers get lost and that magnetic stability is reduced. Additionally, thermal demagnetization of a three component isothermal remanence revealed that mainly the high coercive material is destroyed within the more strongly hydrated samples while lower coercive material seems to be less affected. Grain sizes of all but one samples are in the pseudo-single domain range (the one exception shows multi-domain characteristics). It was impossible to unambiguously identify the remanence carriers, but titanomagnetites are most likely responsible for the lower coercivity component while hemoilmenites possibly represent the higher one. A modified Thellier method was used to determine paleointensity values. As most of the samples are hydrated it is not astonishing that the overall paleointensity data is not of very high quality. However, it is important to note that there are hydrated samples with well-defined Arai-diagrams. Allthough seemingly of high quality,

these paleointensity values are incorrect as there is a trend towards lower paleointensity values observed with increasing perlitization. We attempted to test for magnetic anisotropy and cooling rate dependency, but this was hampered by alteration during the experiments. Yet, it is argued that both, anisotropy and cooling rate dependency are unlikely to be responsible for the observed trend in paleointensity. Thus, even well-defined paleointensity values can be erroneous when obtained from hydrated glass. This emphasizes the need for unaltered samples and additional attention during paleointensity determinations.

5.1 Introduction

Much of the ongoing research in paleomagnetism is dedicated to the improvement of paleointensity determination. This goal is mainly pursued in two ways: the development of new paleointensity methods [Dekkers and Böhnel, 2006, Fabian and Leonhardt, 2010, Muxworthy and Heslop, 2011] and the search for ideal recording materials [Pick and Tauxe, 1993, Bowles et al., 2005, Leonhardt et al., 2006, Cottrell and Tarduno, 1999, Tarduno et al., 2007]. Both ways try to reduce problems that are often encountered during Thellier-Thellier paleointensity experiments [Thellier and Thellier, 1959] such as alteration (in geological time or in the laboratory experiment) [Valet et al., 1996], anisotropy of thermoremanence [Veitch et al., 1984], magnetic domain state bias [Leonhardt et al., 2004a] and different cooling histories in laboratory and nature [Leonhardt et al., 2006].
Volcanic glass is one of the materials that has been proposed to carry ideal magnetic remanence carriers, i.e. remanence carriers in the single-domain (SD) range that are stable during repeated heatings in the experiment and for which corrections of anisotropy of thermoremanence and cooling rate dependency via relaxation geospeedometry [Wilding et al., 1995, Gottsmann and Dingwell, 2001a, Wilding et al., 2004, Potuzak et al., 2008, Ferk et al., 2011b] are possible. However, in an earlier study on 750 ka year old rock from Tenerife we have found that devitrification of volcanic glass is challenging when determining paleointensity [Ferk et al., 2011b]: Changes in rock magnetic parameters (loss of remanence carriers and magnetic stability) leading to a decrease in recording accuracy of paleointensity with increasing devitrification suggested the presence of a chemical remanence (CRM) that had at least partially overprinted the original thermoremanence (TRM).
To investigate problems connected to hydration/alteration of volcanic glass in more detail we have sampled two sites at Bláhnúkur, Iceland, that exhibited varying degrees of perlitization. Perlite is volcanic glass that hosts abundant gently curved cracks (perlitic fractures) that surround cores of intact glass [McPhie et al., 1993] (Fig. 5.1). Lava hydration plays a key role in the formation of perlite. Denton et al. [in revision] suggested that major fractures in the glass are formed due to cooling contraction. Water travels along these fractures and diffuses into the glass through the fracture-glass interface leading to the formation of arcuate perlitic fractures. The most significant perlitization is likely to occur at temperatures just below the glass transition. Additional perlitization may occur at ambient temperatures if time-scales are long enough. The two outcrops studied here consist of hyaloclastites, perlitized and non-perlitized obsidians and microcrystalline rhyolite lavas all

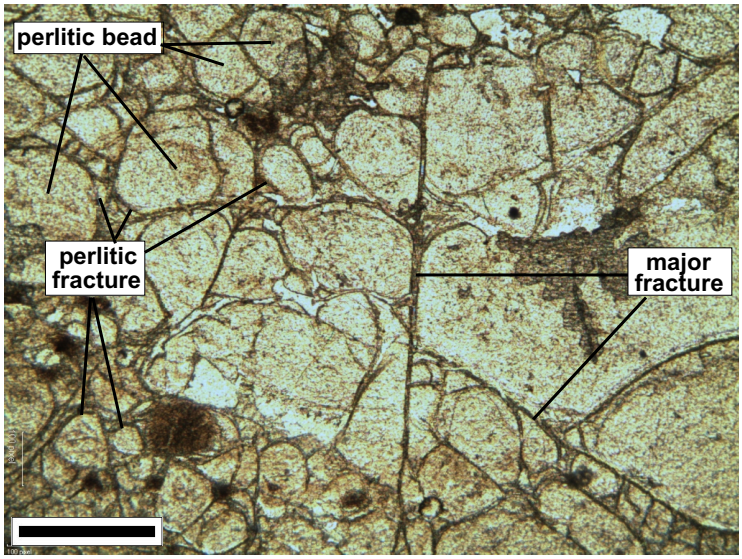

Figure 5.1: Thin section photograph of perlitized obsidian in plane polarized light. Major and perlitic fractures and perlitic beads are labelled. The scale bar is 0.5 mm long.

of which clearly show varying degrees of hydration. Hence, they are well-suited to analyze the influence of hydration/alteration on magnetic stability and magnetic remanence.

5.2 Geology and sampling

Torfajökull volcanic complex is the largest rhyolitic centre in Iceland [e.g. Tuffen et al., 2001] with more than 80% of lavas being silicic [Gunnarsson, 1998]. It is located at the intersection between the Eastern Rift Zone and the South Eastern Zone. Activity goes back to mid-Quaternary time forming a plateau of approximately 18x12 km^2. There are mainly subglacial and subaerial rhyolites, but also basaltic hyaloclastites present [Tuffen et al., 2001]. Bláhnúkur was formed during a small-volume effusive subglacial eruption in the last glacial period (115 to 11 ka ago) (Fig. 5.2) [Tuffen et al., 2001]. Outcrops consist of (sometimes perlitized) obsidian and microcrystalline rhyolite lava lobes in a pale grey perlitized hyaloclastite breccia [Tuffen et al., 2001, Denton et al., 2009].

Samples were taken on a field trip to Iceland in August 2008. We sampled two sites where pristine obsidian and obsidian with different degrees of perlitization (perlite) were found. Site C1B (Fig. 5.3) is a large outcrop (20 m long, 8 m high and 10 m deep) on the northern slope of Bláhnúkur (817 m elevation, N63°58'36.9", W019°04'43.2). The presence of columnar joints in the upper parts of the outcrop suggests the lava was constrained by an ice wall or now-eroded hyaloclastites; perlitized obsidian at the base indicates that the lava interacted with meltwater during cooling. The geometry of the outcrop is difficult to ascertain as it does not have a typical lobelike morphology. A largely microcrystalline interior is surrounded by an obsidian carapace as is the case in most lobes at Bláhnúkur.

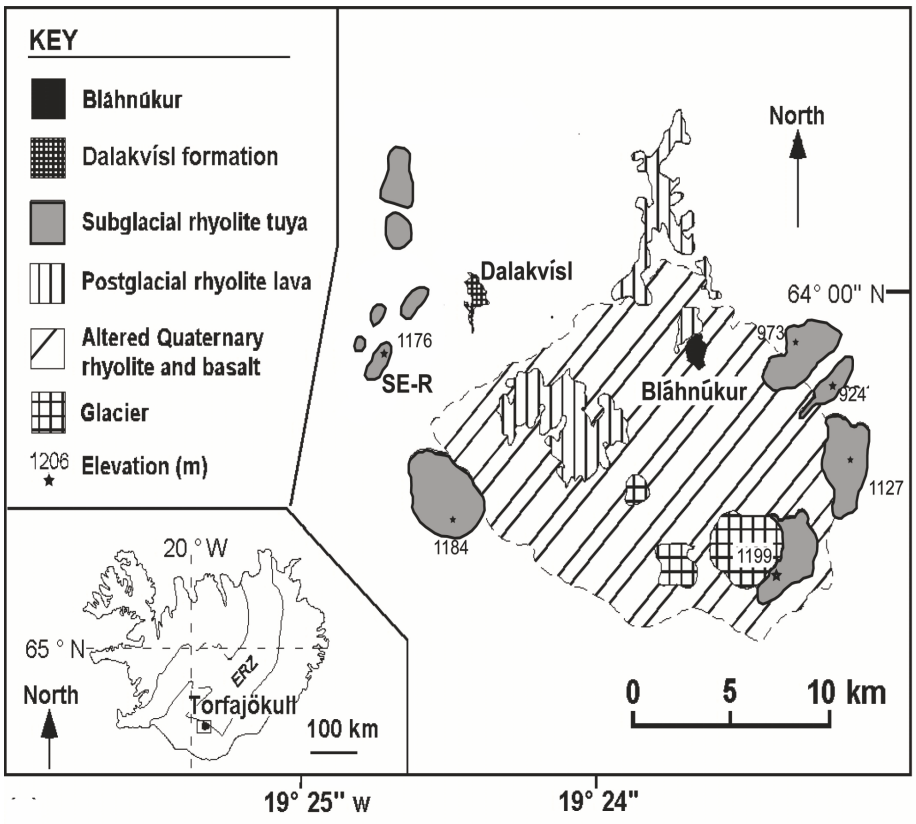

Figure 5.2: Map showing Bláhnúkur within Torfajökull central volcano (from Denton et al. [2009]).

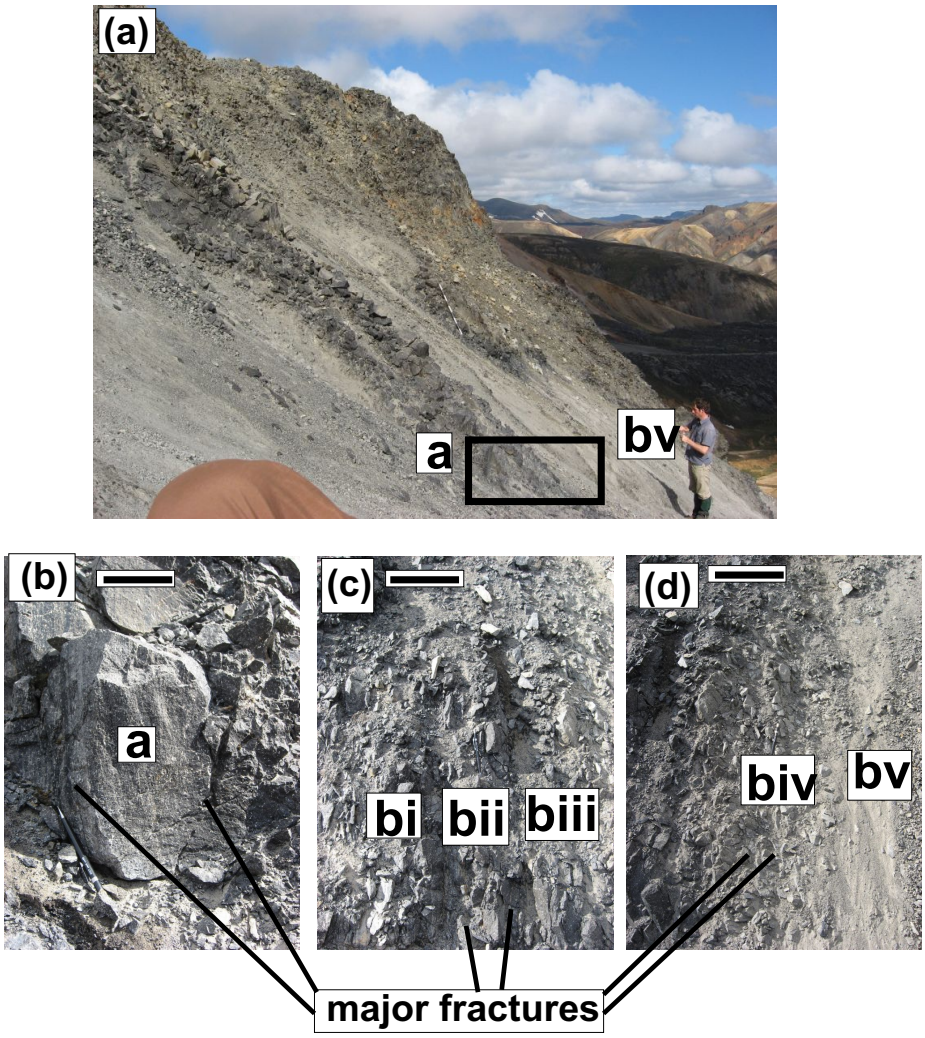

Figure 5.3: Photograph of locality C1B showing the relative position of the samples studied. The scale bar in the close-up images is 15 cm long. Modified from Denton [2010].

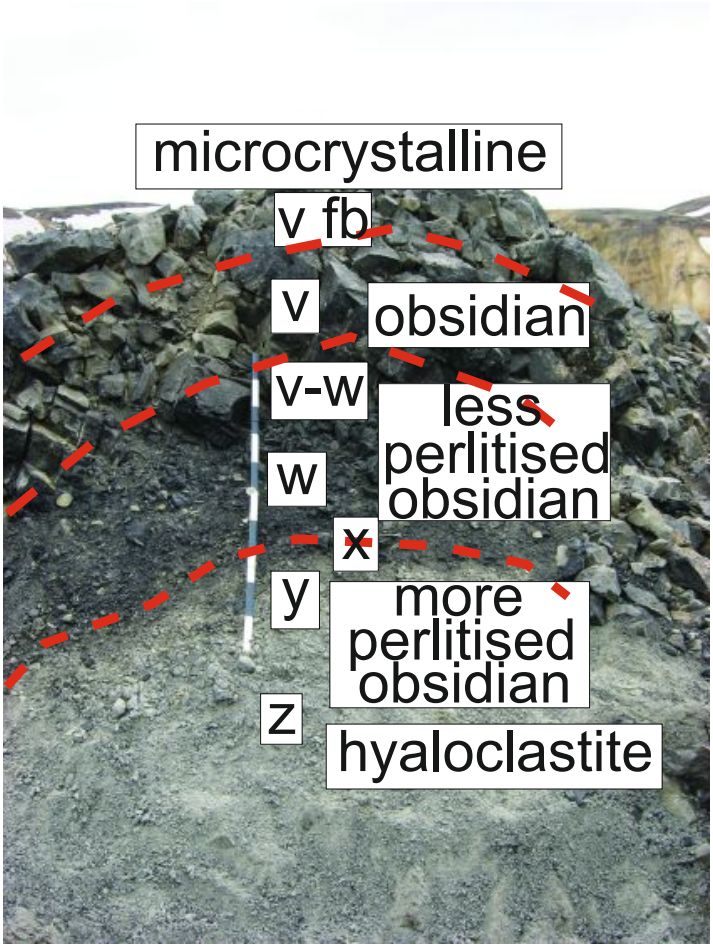

Figure 5.4: Field photograph of outcrop W2u showing the relative locations of the samples studied. The red dashed lines represent textural zone boundaries. Modified from Denton [2010].

The samples represent a sequence away from a well-defined contact between the perlitized margin and the surrounding hyaloclastite. The samples analyzed were named C1B a (flow banded transitional lava), bi (obsidian), bii (perlite), biii (perlite), biv (perlite) and bv (hyaloclastite). The lava lobe is vesicle and phenocryst-poor (less than 10%). The second site W2u (Fig. 5.4) is the upslope side of a small lobe on the apex of a south west to south trending ridge at Bláhnúkur (N63°31'29", W019°04'37.7", 860 m elevation) that is moderately to highly vesicular (up to 50%). It contains a hyaloclastite (W2u z) which grades into a large zone of brecciated perlitized obsidian (samples W2u x and W2u y), that gradually changes into a columnar-jointed perlitized obsidian (samples W2u w, W2u v-w). The perlitization gradually decreases in intensity until an unperlitized obsidian (W2u v) and a flow banded transition lava (W2u v fb) is reached.

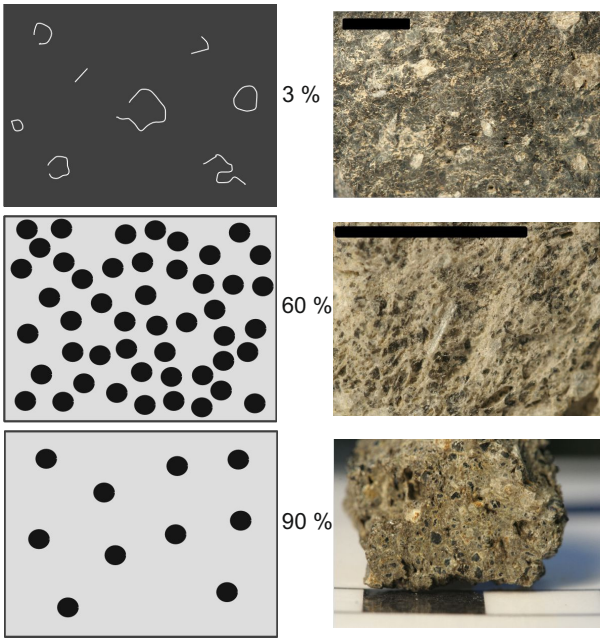

Figure 5.5: Examples of different degrees of perlitization: cartoons on the left, hand specimens on the right; black bar is 1cm. Modified from Denton [2010].

5.3 Degree of perlitization, volatile content and glass transition temperature

Degree of perlitization, fracture populations, volatile contents and thermal characteristics of the samples were analyzed in the course of a study by Denton et al. [in revision] on the formation of perlite. We only recapitulate those measurement procedures and those results that are of direct importance for the research presented here.

Field observation of perlitization was an estimate by eye of the proportion of grey hydrated material to black unhydrated material. The actual number i.e. 10% perlitized refers to 10% grey (hydrated) material and 90% black (unhydrated) material (Fig. 5.5). Visible perlitization in the field was quite variable and as a result the uncertainties are relatively large. Volatile contents and thermal characteristics of samples were analyzed by differential scanning calorimetry-thermogravimetric analysis-mass spectrometry (DSC-TGA-MS) using a TA Instruments SDT Q600 simultaneous DSC-TGA instrument coupled to an HPR-20 QIC Gas Analysis System mass spectrometer at Lancaster University. The DSC-TGA technique measures the weight loss and thermal characteristics of a sample while it is subject to a controlled heating programme. DSC-TGA measurements were done in oxygen-free nitrogen. The addition of a mass spectrometer allows the identification of the exsolved gases. Samples were crushed and sieved. The 125-500 μm size fraction was washed with acetone and then oven-dried at 50°C for about 1 hour [Newman et al., 1986]. After drying, the sample was transferred to a desiccator to minimize atmospheric water

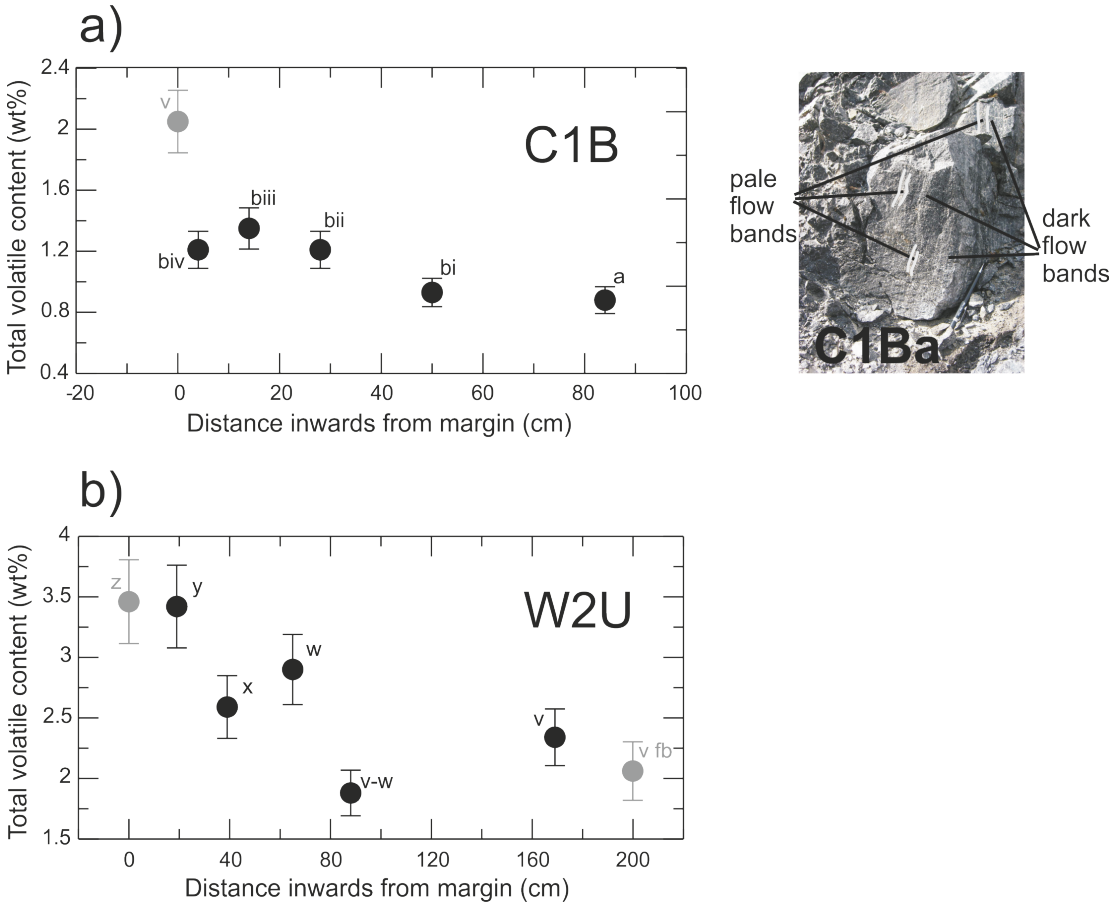

Figure 5.6: Total volatile content (with 10% error bounds) versus distance inwards from lobe margin at sites a) C1B and b) W2u. Grey symbols indicate samples for which no rock magnetic data are available. a) also shows a photograph with the relative proportion of pale (more crystalline) and dark (more glassy) flow bands in zone C1B a. The pencil is 15 cm long. Modified from Denton et al. [in revision].

adsorption before analysis. Approximately 50 mg of the sample were placed in a tared platinum cup on the DSC-TGA sample beam and heated at 5°C/min from ambient temperature to 1250°C. Total volatile loss (i.e. total volatile content; TVC) was calculated by subtracting the end weight from the start weight.
Additional simultaneous thermogravimetric (TGA) and calorimetric (DSC) measurements were carried out using a Netzsch STA 449 C at the University of Munich to determine the glass transition temperature. Here specimens of samples C1B bii, biii and biv and W2u v of approximately 37 mg were heated in a platinum crucible (with lid) with a heating rate of 25°C/min to 1000°C in Argon.

Lancaster TVC-data together with field estimates of degrees of perlitization is shown in Tab. 5.1 and in Fig. 5.6. Error bounds of TVC data in Fig. 5.6 are analytical errors,

Table 5.1: Hydration data

Site	Sample	Description	Degree of perlitisation (%)	TVC [wt %]
C1B	C1B a	flow banded transitional lava	0	0.88
	C1B bi	obsidian	0	0.93
	C1B bii	perlitized obsidian	2	1.21
	C1B biii	perlitized obsidian	10	1.35
	C1B biv	perlitized obsidian	40	1.21
	C1B v	hyaloclastite	N/A	2.05
W2u	W2u v fb	flow banded transitional lava	N/A	2.05
	W2u v	obsidian	0	2.34
	W2u v-w	perlitized obsidian	0-60	1.88
	W2u w	perlitized obsidian	0-60	2.90
	W2u x	perlitized obsidian	90	2.59
	W2u y	perlitized obsidian	90	3.42
	W2u z	hyaloclastite	N/A	3.46

Sample description, perlitization data (field estimate) and total volatile contents TVC. Modified from Denton et al. [in revision].

which are ±10%. Denton et al. [2009] showed that duplicate analyzes of perlitized obsidian often give different results due to heterogeneities of water partitioning. Better agreement is observed for non-perlitized obsidian. Hence, an additional ±10% uncertainty for the perlites needs to be considered. At C1B (Fig. 5.6a) the total volatile content decreases inwards from the lava lobe margin. The hyaloclastite (C1B v) is the most volatile-rich (2.05 wt.%). The three perlitized obsidians (C1B biv, biii, bii) show relatively similar total volatile contents (1.21-1.35 wt.%) indicating that the extent of hydration was uniform despite the range of field estimations of the degree of perlitization. The nonperlitized obsidian (C1B bi) is significantly less volatile-rich than the perlitized obsidians. A total volatile content of 0.93 wt.% for a non-perlitized obsidian is at the volatile-poor end of the range of volatile concentrations in non-perlitized Bláhnúkur obsidians [Owen et al., in revision, Tuffen et al., 2001]. The flow banded transitional lava (C1B a) has higher than expected total volatile contents considering the crystalline nature of the pale flow bands. However, as can be seen from the photograph in Fig. 5.6a the crystalline (pale) bands of C1B a are a smaller proportion than the more glassy flow bands (dark) so the bulk of the analyzed sample is glass. The field estimation of the degree of perlitization for W2u records a decrease from the lava lobe margin and this is also recorded in the total volatile content data (Fig. 5.6b). The hyaloclastite (W2u z) and the outermost perlite (W2u y) have very similar total volatile contents which is unusual when compared to other localities. Field estimations of perlitization suggest that perlitization is variable and this is also reflected by the total volatile content data as W2u w is more volatile-rich than W2u x. W2u v and W2u v fb are a non-perlitized obsidian and a non-perlitized flow banded transitional lava respectively and are both more volatile-rich than the innermost perlite (W2u v-w).

Table 5.2: Rock magnetic data

Site	Sample	TVC [wt %]	B_{cr} [mT]	S_{300}	M_{rs} [Am^2/kg]	M_s [Am^2/kg]	B_c [mT]	M_{rs}/M_s	B_{cr}/B_c	T_{c1} [°C]	T_{c2} [°C]
C1B	C1B a	0.88	41.55	0.89	0.018	0.395	1.72	0.05	24.12	329	461
	C1B bi	0.93	31.85	0.86	0.019	0.458	3.27	0.04	9.75	332	456
	C1B bii	1.21	24.69	0.89	0.015	0.412	3.10	0.04	7.98	329	461
	C1B biii	1.35	19.80	0.94	0.008	0.358	0.00	0.02	-	349	486
	C1B biv	1.21	13.09	1.00	0.009	0.394	1.74	0.02	7.54	312	476
W2u	W2u v	2.34	24.35	0.93	0.018	0.480	3.45	0.04	7.06	317	512
	W2u v-w	1.88	24.02	0.96	0.012	0.307	3.43	0.04	7.00	312	486
	W2u w	2.90	21.93	0.94	0.013	0.380	2.91	0.03	7.54	330	507
	W2u x	2.59	18.21	0.94	0.007	0.235	2.38	0.03	7.65	307	502
	W2u y	3.42	21.27	1.00	0.009	0.315	2.55	0.03	8.33	310	504

Total volatile contents TVC of the different samples together with remanence and hysteresis parameters (coercivity of remanence B_{cr}, Bloemendal parameter S_{300} [Bloemendal et al., 1992], saturation of remanence M_{rs}, saturation magnetization M_s, coercivity B_c, Day parameters M_{rs}/M_s and B_{cr}/B_c [Day et al., 1977]) and Curie temperatures T_{c1} and T_{c2} (determined from heating curve).

Calorimetric measurements at the University of Munich confirmed the TVC data from Lancaster. Additionally, an onset of the glass transition peak at 550°C (T_g) for samples C1B bii, biii and biv was observed, while there was no glass transition peak inferable for sample W2u v.

5.4 Magnetic mineralogy and domain state

For the magnetic experiments (rock magnetism, paleointensity etc.) mainly obsidian and perlitized obsidian samples were used. Additionally also sample C1B a (flow banded transitional lava) was measured, but no measurements were performed on samples C1B bv, W2u z and W2u v fb.

Rock magnetic measurements were performed to analyze magnetic mineralogy and domain state and their variance with degree of perlitization. Isothermal remanent magnetization (IRM) acquisition, isothermal backfield curves, hysteresis loops at room temperature and thermomagnetic curves were measured on a Variable Field Translation Balance (VFTB) at the University of Munich. After heating to 620°C, which - when compared to the onset of the glass transition peak at 550 °C (section 5.3) - probably is in or above the upper range of the glass transition, backfield and hysteresis measurements were repeated to check for alteration.

Overall samples from both C1B and W2u show very similar rock magnetic characteristics although changes with degree of perlitization are seen. Hysteresis loops are always very narrow (Fig. 5.7a) corresponding to values in the multi-domain (MD) range of the Day plot [Day et al., 1977] due to the very high B_{cr}/B_c values (Tab. 5.2). Henkel plots [Henkel, 1964], however, tell another story: For Henkel plots IRM and backfield, i.e. remanence data are used instead of the induced magnetization data from hysteresis that is used for Day plots. The diagonal in the Henkel plot represents ideal Stoner-Wohlfarth particles which are uniaxial non-interacting single domain (SD) particles [Wohlfarth, 1958]. Curves for all

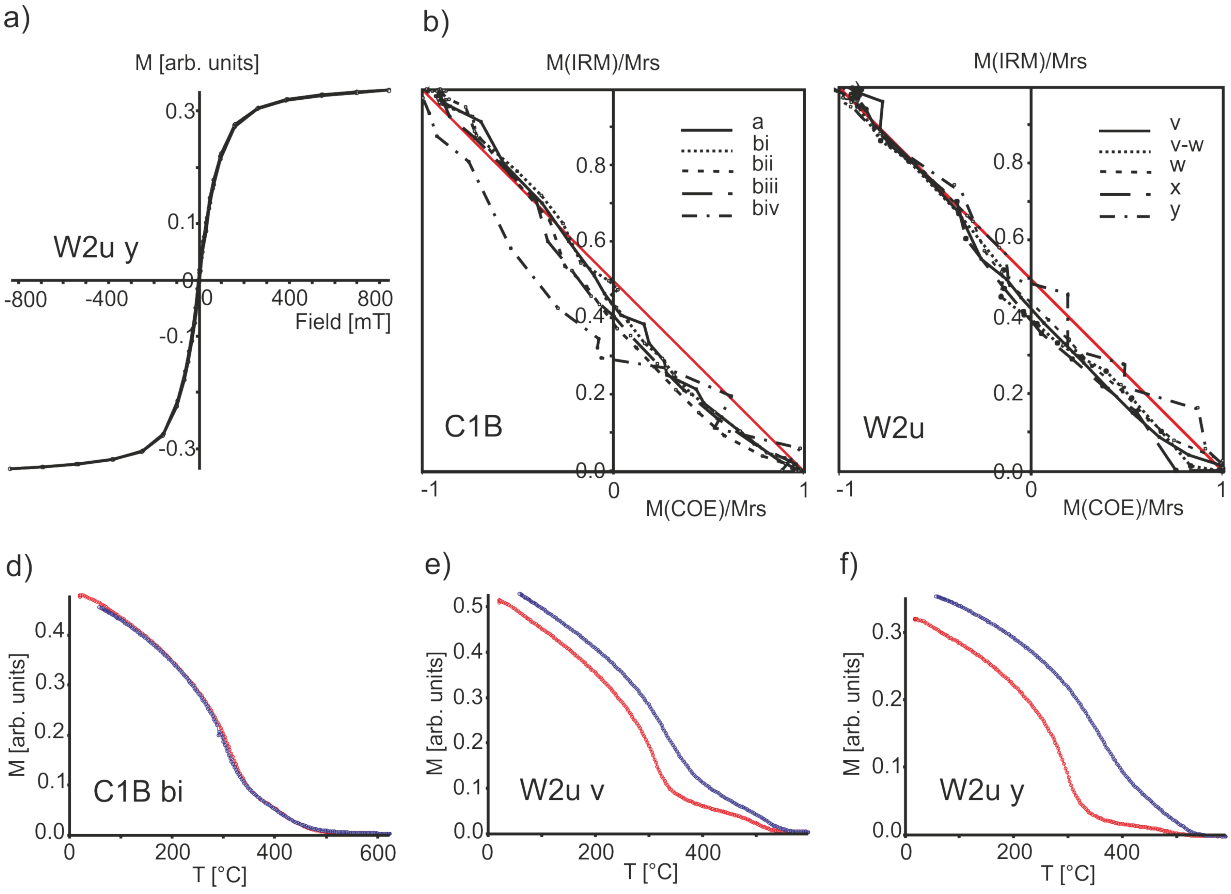

Figure 5.7: a) MD-like hysteresis plot of sample W2u y, small PSD-like Henkel plots of b) site C1B and c) site W2u. Varying alteration is observed in thermomagnetic curves of d) C1B bi, e) W2u v and f) W2u y.

Table 5.3: Backfield and hysteresis data after heating to 620°C

Site	Sample	TVC (wt %) [wt %]	B_{cr} [mT]	S_{300}	M_{rs} [Am^2/kg]	M_s [Am^2/kg]	B_c [mT]	M_{rs}/M_s	B_{cr}/B_c
C1B	C1B a	0.88	39.03	0.91	0.022	0.410	2.57	0.05	15.19
	C1B bi	0.93	29.92	0.86	0.020	0.459	3.55	0.04	8.42
	C1B bii	1.21	22.09	0.93	0.017	0.418	3.32	0.04	6.66
	C1B biii	1.35	17.21	0.95	0.010	0.371	0.00	0.03	-
	C1B biv	1.21	9.61	1.00	0.011	0.406	2.12	0.03	4.53
W2u	W2u v	2.34	18.97	0.97	0.022	0.533	3.69	0.04	5.14
	W2u v-w	1.88	23.51	0.93	0.014	0.321	3.93	0.04	5.98
	W2u w	2.90	20.33	0.93	0.014	0.387	3.03	0.04	6.72
	W2u x	2.59	16.07	0.95	0.008	0.254	2.57	0.03	6.25
	W2u y	3.42	16.79	1.00	0.010	0.351	2.60	0.03	6.47

Remanence and hysteresis parameters of the different samples as measured after heating to 620°C together with TVC data.

our samples (Fig. 5.7b and c) plot off but close to this line suggesting that one or more of these characteristics are not met, but differences are too small to support the presence of only MD remanence carriers. Instead SD/pseudo-single-domain (PSD) grains that may also be interacting or a SD/PSD-MD mixture are probably the main remanence carriers. Hysteresis plots of our samples are dominated by larger MD grains that do not or only slightly contribute to the remanence. Only sample C1B biv shows stronger deviations from the ideal line of the Henkel plot indicating a larger grain size of the remanence carriers or stronger interactions. Tail checks as done in the course of the paleointensity experiments (section 5.5) also suggest that the remanence carriers are mainly in the SD to PSD range. For C1B biv tail checks are again indicative of MD grains. All samples have two Curie temperatures T_C, one at 310-350°C and the other at 450-510°C (Tab. 5.2, Fig. 5.7d, e and f).

Curie and therefore also blocking temperatures T_B are, thus, always below the glass transition temperature at 550°C (section 5.3) and no alteration due to $T_B > T_g$ as mentioned by Smirnov and Tarduno [2003] is to be expected. There are only minor deviations between heating and cooling curves of almost all C1B samples (Fig. 5.7d). Samples C1B biv, W2u v, W2u v-w and W2u w show small alterations with a ∼50°C shift towards higher temperatures of the lower T_C in the cooling curve (Fig. 5.7e). This shift even increases to ∼100°C for samples W2u x and W2u y (Fig. 5.7f). Repeated backfield and hysteresis measurements after the thermomagnetic curves also show small changes (Tab. 5.3): the coercivity of remanence B_{cr} of all samples decreases by 2-6 mT (73-98% left) after heating and minor increases in coercivity B_c (4-40% increase, ∼1 mT), saturation magnetization M_s (0-12%) and saturation of remanence M_{rs} (8-28%) are observed. Some of these alterations might be connected to heating into the glass transition range where according to Smirnov and Tarduno [2003] "neocrystallization" sets in. However, their increases in M_s (140-300%) and M_{rs} (140-280%) are much higher than ours and their B_{cr} and B_c values increase where ours decrease and vice versa. Interestingly, there is no difference between W2u x/W2u y and the other samples even though these show highest deviations in the thermomagnetic curves. Alteration as recorded by hysteresis and backfield parameters is

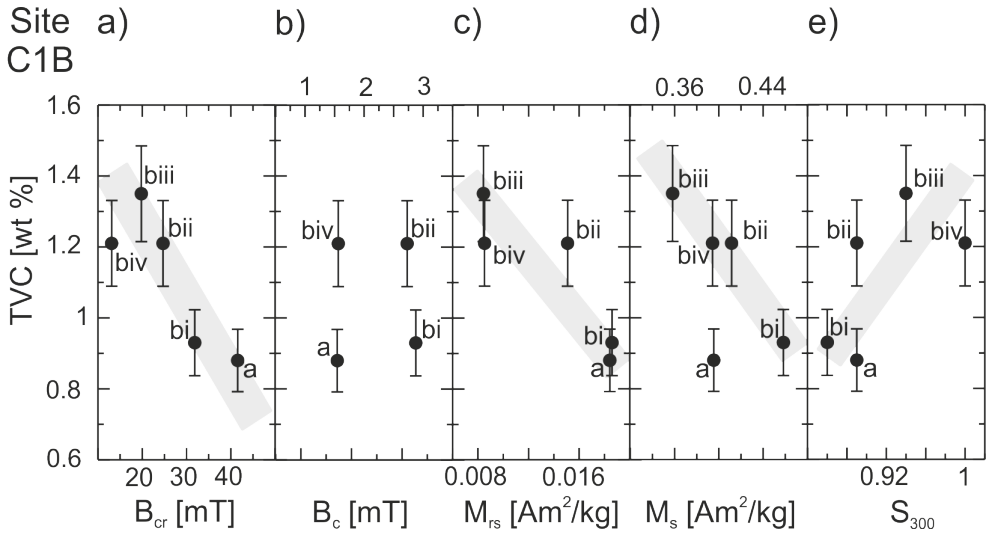

Figure 5.8: Site C1B: Total volatile content (with 10% error bounds) versus a) B_{cr}, b) B_c, c) M_{rs}, d) M_s and e) S_{300}. Grey boxes indicate identified trends.

of the same small amount in all samples.

When comparing the different samples of each site, there are some trends depending on the degree of hydration (Tab. 5.2, Fig. 5.8, Fig. 5.9): With increasing degree of perlitization B_{cr}, M_{rs} and M_s decrease, B_c and T_C stay constant and the S_{300}-parameter gets higher. Similar trends have been found by Ferk et al. [2011b] for 750 ka phonolitic rocks from Tenerife that showed varying degrees of devitrification. In almost all cases trends are seen more clearly at site C1B than at site W2u. Samples W2u v, W2u w and W2u y always show the trends very clearly while samples W2u v-w and W2u x smear it. A reason for this might be that TVC data was taken on the same samples, but obviously not on the same specimens as rock magnetic data. Field estimation of perlitization at site W2u (Tab. 5.1) showed large variances for W2u v-w (0-60%) and very high degrees of perlitization for W2u x. Therefore, much higher TVC values for both W2u v-w and W2u x are possible which would straighten the trends considerably. The least clear of the trends is the increase of S_{300}. An increase in S_{300} implies a loss of high coercive material and a stronger importance of low coercive material.

To check whether the stronger perlitized obsidians contain less high coercive material than the pristine obsidian or the transitional lava, a three component IRM was implied on specimens from C1Ba, bi, bii, biii, biv and W2u v. For the three component IRM first a 1500 mT IRM in z-direction, than a 300 mT IRM in x-direction and last a 50 mT IRM in y-direction were implied using a Magnetic measurements MMPM-9 pulse magnetizer at the University of Munich. In this way high, middle and low coercive material were activated separately. Then the unblocking spectra of the samples were measured by demagnetizing them in a MMTD20 thermal demagnetizer in the paleomagnetic laboratory of the University of Munich, Germany in Niederlippach and thermal decay curves of X, Y and Z

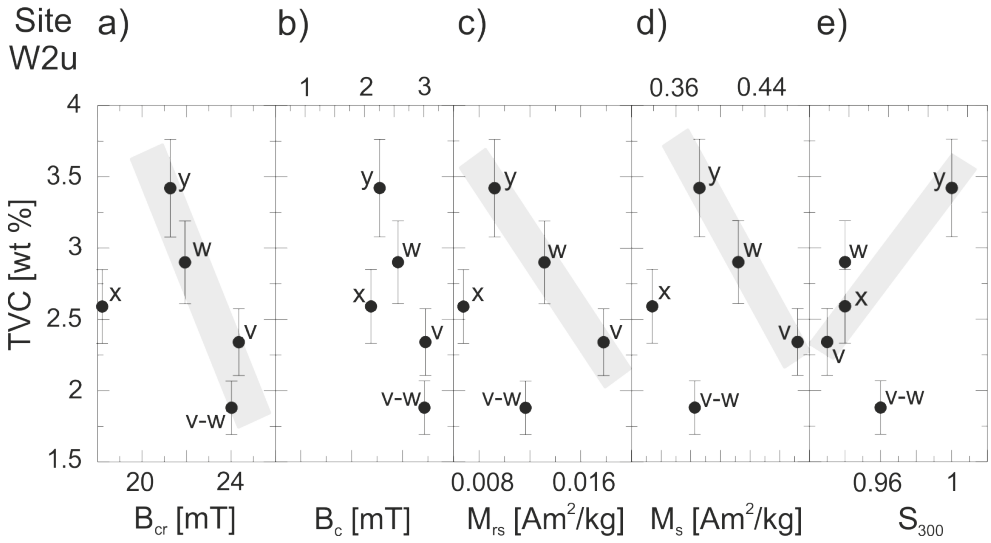

Figure 5.9: Site W2u: Total volatile content (with 10% error bounds) versus a) B_{cr}, b) B_c, c) M_{rs}, d) M_s and e) S_{300}. Grey boxes indicate identified trends.

component were plotted (Fig. 5.10). While for all samples the low coercive ($\leq$50 mT) Y-component contributed only very little to the whole magnetization, the importance of the middle coercive ($\leq$300 mT) X-component in comparison to the high coercive ($\leq$1500 mT) Z-component increases with increasing hydration. Though all components fully unblock only at temperatures of $\sim$500°C, a comparison of the magnetizations at 20°C is also interesting: X/Z at 20°C rises from 25% for the transitional lava C1B a to 96% for the strongly hydrated sample C1B biv. This finding suggests that the increase in S_{300} is real. Further, as absolute magnetization values for the X-component at 20°C are almost constant, the loss of remanence carriers and magnetic stability as implied by the decrease of B_{cr}, M_{rs} and M_s is mainly due to the loss of high coercive material while the lower coercive material seems to be less affected. The simultaneous decrease of M_{rs}/M_s (C1B: 0.05 to 0.02, W2u: 0.04 to 0.03) suggests an increase of grain size with increasing hydration.

In addition to the rock magnetic experiments, ore microscopy was performed on all C1B samples and on W2u v. The samples were polished in 5 steps with increasingly finer abrasive paper and 1μm diamond compound. Microscopy was done under reflected light with 125x magnification. Samples were examined with and without Fe-Fluid. No obvious differences between the samples were found. The grain size of most minerals is less then 10 μm (Fig. 5.11a, b, f) mostly $\sim$5 μm, but there are exceptions with some minerals being $\sim$30 μm x 30 μm (C1B bii, Fig. 5.11c) and others even $\sim$40 μm x 40 μm (C1B biv, Fig. 5.11d, e). There is a great variation in shapes: needles, angular and rounded shapes are found (Fig. 5.11). All minerals that could be resolved under the microscope change their brightness under polarized light (Fig. 5.11d, e). An accumulation of Fe-Fluid is only observed within cracks of one mineral in sample C1B biv (Fig. 5.11d).

Taken together the rock magnetic data suggest the occurence of two magnetic rema-

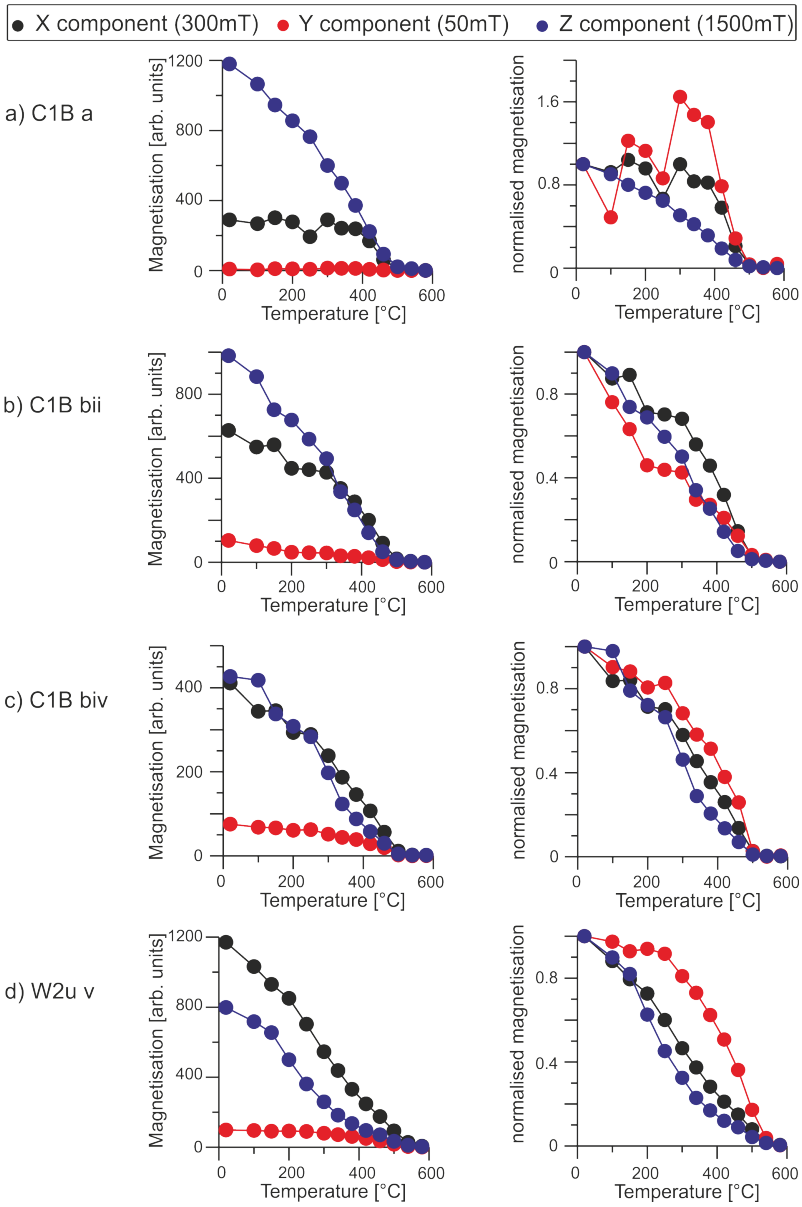

Figure 5.10: Decay curves (left column: absolute, right colum: normalized to initial magnetization values) for X (black, 300 mT), Y (red, 50 mT) and Z (blue, 1500 mT) component of a) C1B a, b) C1B bii, c) C1B biv, and d) W2u v.

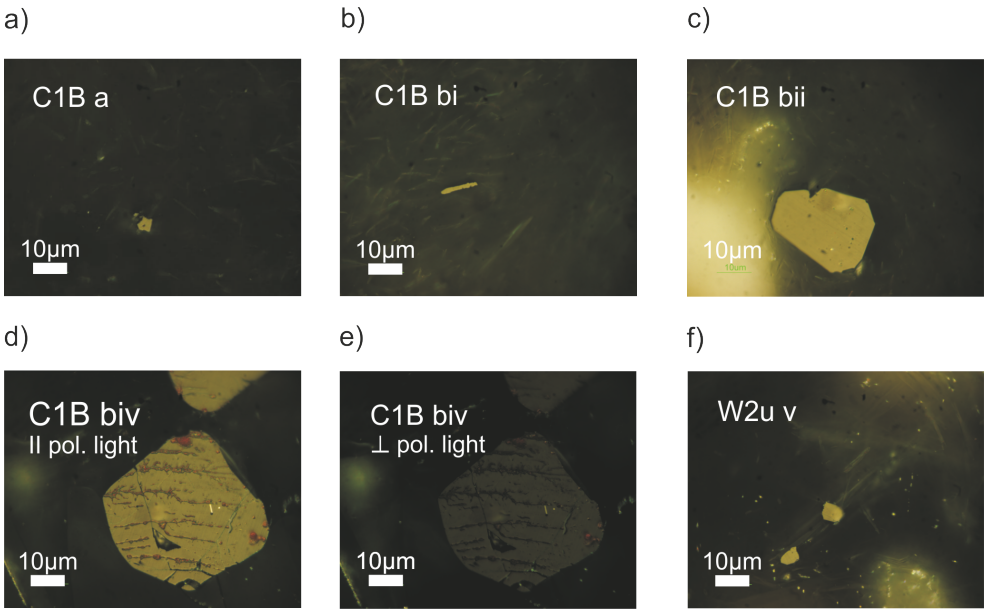

Figure 5.11: Images of ore microscopy (125x magnification) show a), b), c), f) variations in grain size and shape and d), e) behavior under polarized light.

nence carriers - one of middle and the other of high coercivity. The amount of higher coercive material is less when the material is more perlitized. Grain sizes are in the pseudo-single domain range, for one sample probably even in the multi domain range (C1B biv). The middle-coercive remanence carriers are probably titanomagnetites while hemoilmenites possibly represent the higher coercive component. It is, however, impossible to draw a definitive conclusion about the remanence carriers due to the present data.

5.5 Paleointensity determination

5.5.1 Thellier-type experiments

Paleointensity experiments were done in a MMTD20 thermal demagnetizer in the paleomagnetic laboratory of the University of Munich, Germany in Niederlippach. Unfortunately, at site W2u it was only possible to get a specimen of sample W2u v as all other samples crumbled during drilling. At site C1B cores could be drilled from all samples (C1B a to C1B biv). Paleointensity experiments were done on two sets of samples: The first one on 5 mm diameter cores (indicated by -0, e.g. C1B a-0) and the second one on 8 mm diameter cores (indicated by -1 and -2, e.g. C1B a-1 and C1B a-2). Laboratory fields of 50 ± 0.1 μT and 30 ± 0.1 μT were applied during heating and cooling for in-field steps of paleointensity experiments on the first and second sample set, respectively. All experiments followed the modified Thellier-technique MT4 by Leonhardt et al. [2004]. This is a zero-field first method that incorporates pTRM (partial TRM) checks (CK), additivity checks

(AC) [Krása et al., 2003] and pTRM tail checks (TR: repeated thermal demagnetization) [Riisager and Riisager, 2001]. Directional differences between the applied field and the NRM of the pTRM-tail check are taken into account according to Leonhardt et al. [2004a]. Paleointensity determinations were done using the ThellierTool4.21 software [Leonhardt et al., 2004]. This software allows full-vector treatment and application of check correction. Paleointensity data and quality parameters are summarised in Tab. 5.4 and different Arai plots are given in Fig. 5.12. Temperatures in the whole section 5.5 always refer to the temperature on the display of the MMTD20 thermal demagnetizer. The sample's temperature at high temperatures is 10 to 20°C lower.

As we are dealing with hydrated samples it is not astonishing that the over-all data quality is not very high. However, there are hydrated samples that seem to have good data quality. Orthogonal projections of samples C1B bi-0, bii-1, biv-0 and W2u v-0 are curved and only the uppermost temperature range (5 to 6 steps) can be used (e.g. Fig. 5.12b). Thus, the fraction of the NRM f [Coe et al., 1978] in these cases is 65-76%. For sample C1B bi-2 the paleointensity determination could be done only between 20°C and 440°C as alteration above these steps was too strong. Therefore a low fraction of NRM of 0.47 is observed for this sample. For all other samples f values between 0.72 and 0.99 are observed. The gap factor g [Coe et al., 1978] ranges between 61 and 86%. The smaller values are observed for samples with relative sharp unblocking between ∼350°C and 500-580°C . Quality factors q [Coe et al., 1978] of 4.5 to 33.1 are found. Unfortunately alteration occured in most of the experiments, but 2/3 of the analyzed ones show only minor to moderate alterations as indicated by relative check errors d(CK) of 1.0- 7.2%. Four paleointensity determinations with higher d(CK) values up to 13.3% are also found in Tab. 5.4 as they compare well to other data from the same sample. For sample W2u v-1 (Fig. 5.12f) only a check-corrected determination was possible and the result is only a rough estimate as one of the addivity checks does not fall on the previous pTRM value which would indicate successful check correction. Alteration during the experiments affects relative TR values d(TR), too. These are are between 0.6% and 11.8% which according to Leonhardt et al. [2004a] are characteristic of mainly PSD to MD grain sizes: They have calculated critical values to distinguish between SD, PSD and MD ranges: SD corresponds to d(TR) $\leq$ 2.5%, PSD to 2.5% $\leq$ d(TR) $\leq$ 7% and MD to d(TR) $>$ 7%. When alteration occurs these d(TR) values are not significant. However, even when just looking at samples with lowest d(CK) errors, there still seems to be a trend towards higher d(TR) values, i.e. towards larger grain sizes with increasing hydration, which supports our earlier findings in section 5.4. C1B biv-0 shows the biggest d(TR) value of 11.8. This MD characteristic is also shown by the curved Arai plots of the other two specimens from C1B biv (Fig. 5.12e).

Paleointensity results range between $31.9 \pm 1.1\mu$T and $57.0 \pm 3.9\mu$T and at site C1B there seems to be a trend connected to hydration: High values of $45.4 \pm 1.2\mu$T to $57.0 \pm 3.9\mu$T are found for specimens of the two least hydrated samples C1B a and C1B bi. Smaller values of $31.9 \pm 1.1\mu$T to $42.3 \pm 1.1\mu$T are found for samples C1B bii, C1B biii and C1B biv that are more strongly hydrated (Fig. 5.6a). We have found a similar behavior in our study on samples from Tenerife, which showed a decrease in paleointensity from ∼70μT to ∼17μT with increasing devitrification [Ferk et al., 2011b]. This was interpreted as an overprint by

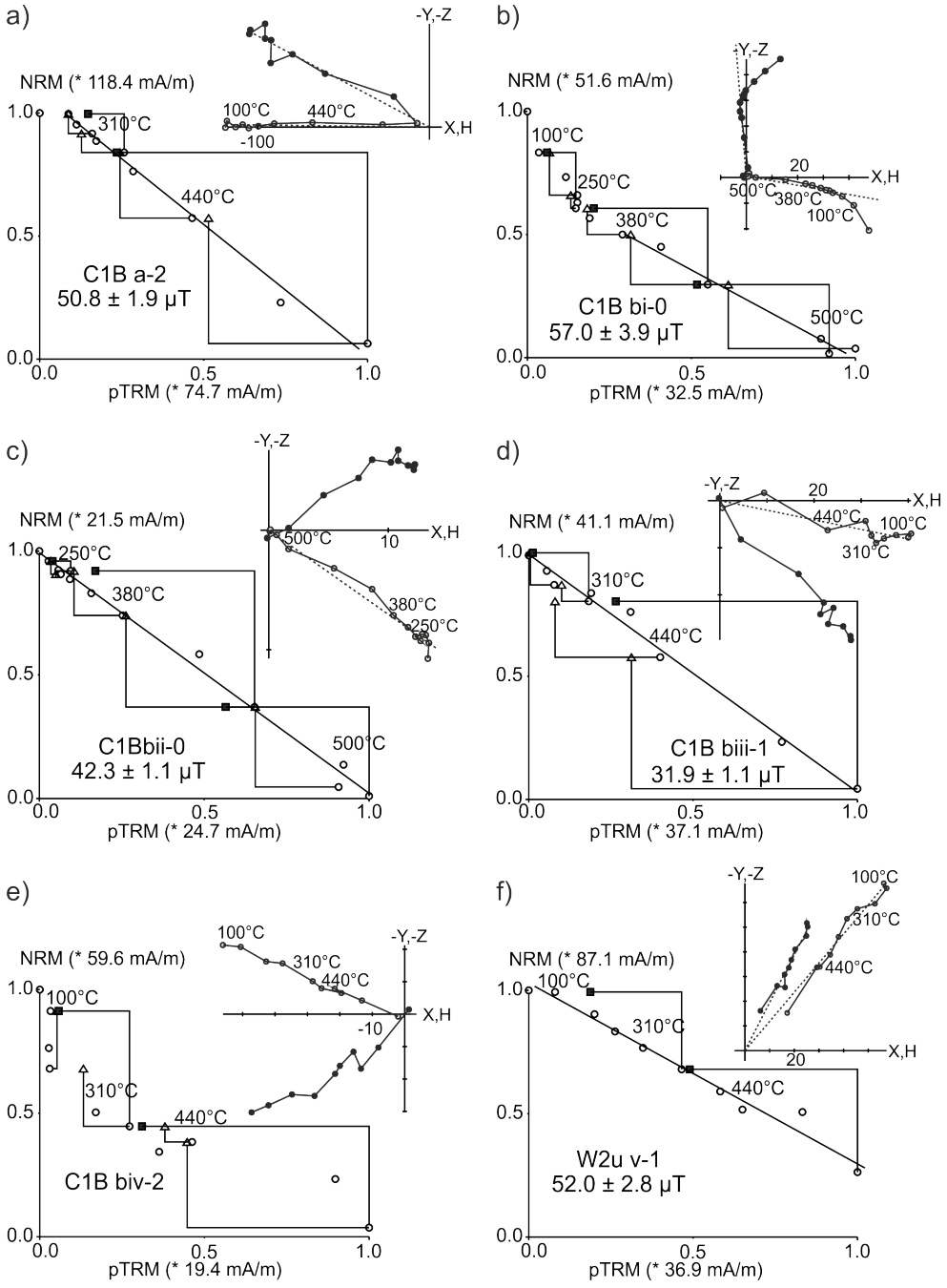

Figure 5.12: NRM/pTRM diagrams (triangles: alteration checks, squares: additivity checks) together with respective orthogonal projections for a) C1B a-2, b) C1B bi-0, c) C1B bii-0 and d) C1B biii-1, e) C1B biv-2 and f) W2u v-1. Temperatures indicate temperatures on the display of the MMTD20 thermal demagnetizer.

Table 5.4: Paleointensity data

Site	Sample	TVC [wt %]	H_{Anc} [μT]	ΔT [°C]	N	f	g	q	DRAT	d(AC)	d(TR)
C1B	C1B a-0	0.88	45.4 ± 1.2	20-580	13	0.96	0.80	28.7	4.5	13.5	4.0
	C1B a-1	0.88	49.2 ± 2.8	100-480	8	0.79	0.72	10.2	11.3	12.7	4.1
	C1B a-2	0.88	50.8 ± 1.9	100-520	9	0.88	0.78	18.7	2.9	6.0	6.4
	C1B bi-0	0.93	57.0 ± 3.9	380-580	6	0.68	0.66	6.7	6.0	5.7	4.6
	C1B bi-1	0.93	47.3 ± 3.0	20-520	10	0.93	0.78	11.3	2.8	4.9	6.9
	C1B bi-2	0.93	49.4 ± 3.7	20-440	8	0.47	0.80	4.9	8.1	9.7	0.6
	C1B bii-0	1.21	42.3 ± 1.1	20-580	13	0.99	0.84	33.1	1.0	8.3	6.5
	C1B bii-1	1.21	39.2 ± 1.9	310-520	6	0.76	0.71	11.0	10.0	7.5	10.3
	C1B biii-0	1.35	37.0 ± 1.7	20-540	12	0.98	0.75	16.1	5.9	2.8	9.0
	C1B biii-1	1.35	31.9 ± 1.1	20-520	10	0.96	0.78	21.5	7.2	7.8	7.6
	C1B biv-0	1.21	35.6 ± 3.5	380-580	6	0.75	0.61	4.7	4.6	2.3	11.8
	C1B biv-1	1.21									
	C1B biv-2	1.21									
W2u	W2u v-0	2.34	42.7 ± 4.3	420-580	5	0.65	0.71	4.5	13.3	10.6	4.4
	W2u v-1	2.34	52.0 ± 2.8	20-520	10	0.72	0.86	11.3	-	7.7	5.9

Ancient field intensity H_{Anc} and quality parameters (analyzed temperature interval ΔT, number of points used for determination of slope N, fraction of NRM f [Coe et al., 1978], gap factor g [Coe et al., 1978], quality factor q [Coe et al., 1978], difference ratio DRAT [Selkin and Tauxe, 2000], relative AC error d(AC), relative TR error d(TR)) together with total volatile contents TVC of the different samples. Temperatures indicate temperatures on the display of the MMTD20 thermal demagnetizer.

a CRM. Also here, it seems as if perlitization leads to a decrease in paleointensity that may be connected to a chemical remanent magnetization originating in the hydration process. One of the specimens from sample W2u v shows a similar high field value as samples from C1Ba and C1B bi while the other one gives a lower value more comparable to those from C1B bii - biv samples. However, as alteration occured in both experiments no conclusion can be drawn as to which result - if one at all - is more reliable.

5.5.2 Magnetic anisotropy

Additionally to the Thellier-type experiments, the influence of anisotropy of thermal remanence and of cooling rate were studied for the second set of samples (indicated by -1 or -2). This was done to clarify whether the observed trend in paleointensity is due to one of these effects rather than a consequence of the perlitization. The ability of some rocks to acquire a magnetization in a magnetic field depends on the direction of this field. Such rocks are called magnetically anisotropic. If the field during the paleointensity experiment is not parallel to the NRM, the laboratory TRM of such rocks is not of the same value even if the field strength is the same as during acquisition of the magnetization in nature. Fortunately, as weak field TRM is proportional to the field strength, the anisotropy tensor of TRM (ATRM tensor) can be obtained and a correction can be applied.
Determinations of the ATRM tensor were done on the same samples as previous paleointensity determinations, using again the MMTD20 demagnetizer. TRMs were imparted using in-field (30μT) heating/cooling cycles to the upper end of the blocking spectra of the samples subsequently in +z, +x, +y, -x, -y and -z direction. In the end, the +z treatment was repeated to check for alteration. The measurements were analyzed following the approach of Veitch et al. [1984] and the results are summarized in Tab. 5.5. After

Table 5.5: Anisotropy correction

Site	Sample	H_{UC} [μT]	ZP1/ZP2	f_{ATRM}	H_{ATRM} [μT]
C1B	C1B a-0	45.4 ± 1.2			
	C1B a-1	49.2 ± 2.8	0.98	0.983 ± 0.080	48.4 ± 6.7
	C1B a-2	50.8 ± 1.9	0.95		
	C1B bi-0	57.0 ± 3.9			
	C1B bi-1	47.3 ± 3.0	1.01	0.933 ± 0.051	44.1 ± 5.3
	C1B bi-2	49.4 ± 3.7	1.01	0.827 ± 0.243	40.8 ± 15.1
	C1B bii-0	42.3 ± 1.1			
	C1B bii-1	39.2 ± 1.9	1.06		
	C1B biii-0	37.0 ± 1.7			
	C1B biii-1	31.9 ± 1.1	1.10		
	C1B biv-0	35.6 ± 3.5			
	C1B biv-1				
	C1B biv-2				
W2u	W2u v-0	42.7 ± 4.3			
	W2u v-1	52.0 ± 2.8	1.16		

Uncorrected (H_{UC}) and ATRM corrected (H_{ATRM}) paleointensities. ZP1/ZP2 gives the relative difference between the first and second measurement in +z direction and f_{ATRM} is the anisotropy correction factor.

having determined the ATRM tensor, the direction of the ancient field is calculated and the scaling factor f_{ATRM} obtained by the relationship between ancient magnetization acquisition and laboratory magnetization acquisition in dependence of the ATRM tensor. The corrected paleointensity is obtained by $H_{ATRM} = H_{UC} * f_{ATRM}$ (UC: uncorrected). f_{ATRM} is calculated from the averaged axes components and its uncertainty is defined by $\sigma(f_{ATRM}) = (|f^{pos}_{ATRM} - f^{neg}_{ATRM}|)$, where the correction factors f^{pos}_{ATRM} and f^{neg}_{ATRM} have been calculated seperately for positive (+x, +y, +z) and negative (-x, -y, -z) measurements, respectively. The uncertainty σ_{ATRM} of the ATRM corrected intensity H_{ATRM} is a minimum/maximum error including the uncertainty of the paleointensity determination and of f_{ATRM}.

Comparison of the first and second +z measurement gives very promising results for C1B a-1 (2% difference), bi-1 (1%) and bi-2 (1%). The other samples (C1B a-2, bii-1, biii-1 and W2u v-1), however, show 5 to 16 % differences (Tab. 5.5). Alteration is therefore likely and the previous paleointensity results cannot be corrected for these samples. A correction was tried for the three samples with small changes in +z measurements. However, positive and negative correction factors differ by 5 to 25% (see also $\sigma(f_{ATRM})$ in Tab. 5.5). This also results in high uncertainties of the corrected paleointensities and it seems as if alteration is significant in these measurements, too. Therefore, it is impossible to say whether the trend observed in paleointensity data is due to magnetic anisotropy effects. However, it

Table 5.6: Cooling rate dependence

Site	Sample	SC1/FC1	FC2/FC1
C1B	C1B a-1	0.92	0.84
	C1B a-2	0.95	0.86
	C1B bi-1	1.03	0.86
	C1B bi-2	1.09	0.91
	C1B bii-1	1.18	0.95
	C1B biii-1	0.95	0.77
	C1B biv-1	0.86	0.96
	C1B biv-2	0.90	0.69
W2u	W2u v-1	1.14	1.34

Relative differences between slow (SC1) and first fast (FC1) cooling and between second (FC2) and first (FC1) fast cooling as determined on samples from the second paleointensity sample set.

is unlikely that anisotropy leads to a trend. Instead it normally causes increased scatter throughout a section.

5.5.3 Cooling rate dependence

Assemblages of identical, non-interacting SD particles have been found to acquire a larger TRM during slower cooling [Halgedahl et al., 1980, Dodson and McClelland-Brown, 1980, Fox and Aitken, 1980, McClelland-Brown, 1984]. Therefore, in earlier studies, dealing with SD or close to SD remanence carriers, we determined the cooling rate dependency of our volcanic glasses and corrected our paleointensities for it [Leonhardt et al., 2006, Ferk et al., 2010, 2011a,b]. However, a recent study by Yu [2011] shows no significant cooling rate effect in the remanence intensity of PSD magnetite and experiments by Fabian and Leonhardt [2009] also suggest that cooling rate effects for PSD carriers are negligible.
Nevertheless, determinations of the cooling rate dependency of TRM on the same samples as for paleointensity and anisotropy experiments were tried using two different cooling rates. For fast cooling (FC1, ≈30 min.) the cooling fan of the MMTD20 furnace was used like during the previous experiments, while for slow cooling (SC1, ≈8 h.) the samples were cooled without fan operation. After slow cooling the fast cooling was repeated (FC2) to check for alteration. Unfortunately, the samples altered significantly as indicated by 5 to 34% difference between the two fast coolings (Tab. 5.6). Even though the relative difference between SC1 and FC1 is sometimes even bigger, the high alteration prevents any meaningful corrections and, hence, hinders any stringent conclusions. However, as SC1/FC1 does not show any trend from unhydrated to hydrated samples, it is unlikely

that the observed trend in paleointensity data is connected to cooling rate depedency of TRM.
Since the cooling rate experiment failed, a detailed determination of the cooling rates during fast and slow cooling as well as a determination of natural cooling rates via relaxation geospeedometry was set aside.

5.6 Discussion and Conclusion

We have sampled two variably hydrated rhyolitic lavas from Bláhnúkur, Iceland. This has revealed the influence of hydration/alteration on the magnetic remanence carriers and on the reliablity of the magnetic record in volcanic glass. It was not possible to determine the remanence carriers unambiguously. However, a PSD/MD mixture of remanence carriers was found. One of the carriers is of middle and the other of high coercivity. With increasing perlitization a loss of the high coercive one takes place while the lower coercive material seems to be less affected. Simultaneously to this loss of magnetic remanence carriers and of magnetic stability an increase in grain size is observed.
Due to the perlitization of most samples, the quality of paleointensity data is not very high, but it is important to note that there are also hydrated samples with apparently good data quality. For example, the hydrated sample C1B bii-0 gives a well defined paleointensity (Fig. 5.12c) with good quality parameters (Tab. 5.4). However, within site comparison of the paleointensity results of samples with differing degrees of perlitization shows that there is a trend to lower paleointensity values with increasing degree of perlitization. Anisotropy and cooling rate experiments were done to check whether this trend is related to one or both of these biasing factors, but alteration during the experiments hampered interpretations. However, it is unlikely that magnetic anisotropy leads to a trend throughout a section. Instead, anisotropy normally results in larger scatter. Cooling rate also does not show a trend as the fraction between TRM of slow cooling and TRM of fast cooling (SC1/FC1) varies randomly over the section. This implies that the observed trend to lower paleointensity results is really connected to perlitization. Hence, even well defined paleointensity values can be too low when the determinations were done on hydrated samples.
Both rock magnetic and paleointensity data support the results of our earlier study on samples from a 750 ka year old devitrified site from Tenerife [Ferk et al., 2011b]. There devitrification of volcanic glass was found to cause a loss of remanence carriers, magnetic stability and recording accuracy of paleointensity. Both studies suggest that one has to be extremely careful when dealing with altered (hydrated or devitrified) glassy-looking samples. Hydrated volcanic glasses may in the field be identified by signs of perlitization (arcuate fractures) and of devitrification. Further, trends in the data (changes of B_{cr}, M_{rs}, M_s, S_{300} and paleointensity) throughout the section are suspicious. However, more problematic are sections that - unrecognized - are more or less equally altered. Equal alteration will most certainly falsify the paleointensity value, but this might stay undetected as no trend will be found and each paleointensity determination may be well defined.
One of many examples where this may play a role is the hydration of submarine basaltic

glasses (SBG). While there are also paleointensity studies on rhyolitic [Leonhardt et al., 2006], phonolitic [Ferk et al., 2011b] and pantelleritic [Ferk et al., 2011a] glasses, most paleointensity determinations have been done on SBG [Pick and Tauxe, 1993, Selkin and Tauxe, 2000, Bowles et al., 2005, Tauxe, 2006]. It has been questioned in the past whether the glass carries a primary TRM [Heller, 2002], but recent studies suggest that low-Ti titanomagnetite is formed at temperatures above both the glass and Curie temperature and therefore that the remanence is a total TRM [Burgess et al., 2010, Bowles et al., 2011]. However, over time the remanence carriers may be altered or hydrated. Helo et al. [2011] found more H_2O in host glasses from the East Pacific Rise than in the melt inclusions. This is indicative of post-eruptive hydration. Future studies will have to check whether such hydration affects the remanence carriers and leads to under- or overestimates of the true paleointensity.

Acknowledgements

Funding for A. Ferk and R. Leonhardt was provided by DFG grant Le1905/1-1 and FWF grant P21221-N14. H. Tuffen acknowledges support from NERC grants NE/G000654/1 and NE/E013740/1 and D. B. Dingwell the funding support of a LMUexcellent Research Professorship in experimental Volcanology (Bundesexzellenzinitiative) and ERC advanced grant EVOKES. J. S. Denton's fieldwork was funded by the Geological Society (Timothy Jefferson Field Research Fund). We further thank the Icelandic Environment Agency, the Icelandic Centre for research and the Icelandic Institute of Natural History for permission to conduct fieldwork in the Fjallabak Nature Reserve. Warm thanks to Nina Gegenhuber for help with sampling.

Chapter 6

Conclusion

On the basis of the here gathered data one has to answer the question "Volcanic glass - an ideal paleomagnetic recording material?" as asked in the title of this dissertation by saying "Yes, but...".
In the presented studies paleointensities have been determined on volcanic glass of various compositions and degrees of hydration: remelted (chapter 2) and natural phonolites (chapter 4), pantellerites (chapter 3), rhyolites and perlites (both chapter 5). Low alterations and remanence carriers in the SD or close to SD range were observed for the unhydrated phonolites with high glass transition temperatures. This led to high success rates in paleointensity experiments ($\geq$80%). For the remelted glass samples (chapter 2) a strong cooling rate dependency was observed which resulted in a field overestimate of 18%. After application of a cooling rate correction the value of the originally applied field was obtained and the validity and necessity of cooling rate correction could hence be verified. Anisotropy and cooling rate correction have also been applied to phonolitic samples from in-situ sites at Montaña Blanca (chapter 4). Additionally, it was possible to show that samples with SD remanence carriers from sites that rotated and/or broke during emplacement can be used for paleointensity determinations. Taken together corrected paleointensity data from Montaña Blanca gives a high quality field value for the Canary Islands 2 kyr ago that compares well with other data and geomagnetic field models in time and space. Further, paleointensity experiments on pantelleritic samples from Mayor Island, which also have SD remanence carriers, gave good results and a high success rate of 70% was achieved (chapter 3). However, repeated heatings to temperatures close to the glass transition between 405 °C and 489 °C introduced alteration into the experiments and therefore it was not possible to apply corrections to all paleointensities. It was tried to estimate the effect of cooling rate by comparison with the degree of overestimate of one of the samples and of another flow from Lipari [Leonhardt et al., 2006], but as already small changes in domain state affect the cooling rate dependency the cooling rate effect cannot be unambiguously determined. Nonetheless, the well defined paleointensity gives at least an upper limit for the paleointensity. This is of great value as the amount of available paleointensity data for the southern hemisphere is very low.
All these data are in agreement with earlier studies [Pick and Tauxe, 1993, Selkin and

Tauxe, 2000, Leonhardt et al., 2006] that suggest almost ideal behavior for volcanic glass. In all cases (remelted glass, natural phonolitic glass and pantelleritic glass) SD or close to SD remanence carriers are found and when the glass transition temperature is high enough alteration is small, too. Hence, success rates are large and the possibility to correct for cooling rate is another advantage. However, the studies on obsidians of various degrees of devitrification (chapter 4) and hydration (chapter 5) delimit the ideal characteristics of volcanic glass. In both cases a loss of magnetic remanence carriers and magnetic stability together with an increase of grain size of magnetic particles and a decrease of "apparent" paleointensity are observed. This suggests the presence of a chemical remanence or at least shows that during hydration/devitrification the samples altered; hence, the true paleointensity cannot be gained from them. Care has thus to be taken when sampling volcanic glass. If the whole section is altered to a common degree and this is not realised in the field, no trend will be seen in the data. As the altered samples often show well defined paleointensities a recognition of altered samples during the paleointensity experiment is unlikely. Taking these results for true will, however, lead to an underestimate of the real field intensity in the past. Helo et al. [2011] reported post-eruptive hydration of submarine basaltic glasses. An underestimate due to this hydration is a possible reason for the relatively low paleointensities for times older than 0.5 Ma that were determined on submarine basaltic glasses [e.g. Juárez et al., 1998, Selkin and Tauxe, 2000].
Hydration and devitrification are thus a large drawback when regarding the ideal characteristics of volcanic glass. However, when samples are taken with great care to assure that the samples are pristine or when even volatile measurements are done to exclude influence of hydration, one is likely to have high success rates in paleointensity experiments with very well defined paleointensity values that can be corrected for biasing effects like magnetic anisotropy or cooling rate dependency.

Appendix A

Supplementary material to chapter 2

The additional material to chapter 2 as presented here corresponds to the electronic supplement of publication Ferk et al. [2010].

A.1 Rock magnetic parameters and quality values of paleointensity measurements of the remelted glass samples

Tab. A.1:
Given are coercivity of remanence (B_{cr}), coercive force (B_c), saturation remanence (M_{rs}), saturation magnetization (M_s), Curie temperatures T_C, fraction of the NRM f [Coe et al., 1978], gap factor g [Coe et al., 1978], quality factor q [Coe et al., 1978], difference ratio DRAT (difference between pTRM*-check and related pTRM* acquisition normalized length of the selected segment) [Selkin and Tauxe, 2000] and normalized tail of PTRM d(t*) of the different samples.

Table A.1: Rock magnetic parameters and quality values of paleointensity measurements of the remelted glass samples

Sample	B_{cr} [mT]	B_c [mT]	M_{rs} [$*10^{-2}$Am^2/kg]	M_s [$*10^{-2}$Am^2/kg]	T_{C1} [°C]	T_{C2} [°C]	f	g	q	DRAT	d(t*)
LNN3-600-0.1	46.0	31.3	0.6	1.4	460	90	0.97	0.63	20.7	1.4	0.2
LNN3-600-0.5	43.6	22.0	0.6	2.7	445	85	1.00	0.45	20.0	2.3	0.4
LNN3-600-1	42.7	24.2	0.3	1.0	410	90	0.97	0.75	26.5	1.1	0.6
LNN3-600-5	40.6	24.9	0.6	1.6	420	80	0.99	0.48	25.4	0.5	4.5
LNN3-600-10	52.7	36.7	0.3	0.7	410	70	0.93	0.45	88.5	2.3	0.4
LNN3-600-15	50.8	27.6	0.1	0.4	450	70	0.95	0.5	33.0	1.1	2.1

A.2 Henkel plots of remelted glass samples

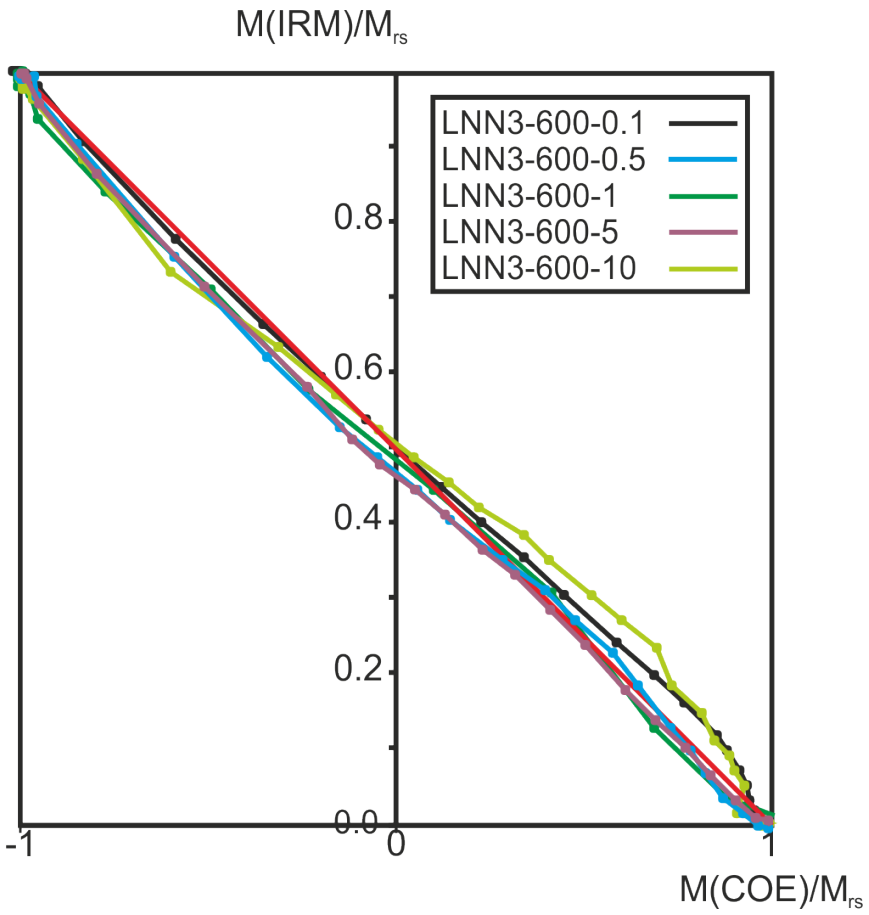

Figure A.1: Henkel plots of the different specimens. Red line represents the linear dependency of noninteracting uniaxial SD particles of Stoner-Wohlfarth type [Wohlfarth, 1958]. LNN-600-15 is only very weakly magnetized and the VFTB's IRM and backfield curve were too disturbed to calculate its Henkel plot.

Appendix B

Supplementary material to chapter 4

The additional material to chapter 4 as presented here corresponds to the electronic supplement of publication Ferk et al. [2011b].

B.1 Rock magnetic data for Montaña Blanca and El Pasajiron

Tab. B.1:
Backfield, hystersis, IRM acquisition and thermomagnetic data of samples from Montaña Blanca and El Pasajiron. Suffix-number after the sample indicates up to which temperature the sample was heated during stepwise heating (e.g. sample EPJ1-2B450 was heated to 450°C). Suffix n600 (or similar) indicates measurement after last heating to 600°C. Units of magnetic fields, magnetizations and weight are mT, Am^2/kg and mg, respectively. The table is split in two parts. The sample names are given in both parts. In addition the following parameters are given in the first part: weight, coercivity of remanence (B_{cr}), Bloemendal parameter (S_{300}), (para/diamagnetic) slope, saturation remanence (M_{rs}), saturation magnetization (M_s), coercivity (B_c), median destructive field of the difference curve (normal hysteresis loop-paramagnetic contribution, B_{rh}), saturation remanence/saturation magnetization (M_{rs}/M_s). The second part of the table gives coercivity of remanence/coercivity (B_{cr}/B_c), median destructive field of the difference curve/coercivity (B_{rh}/B_c), shape (quantitative measure dependent on the shape of the hysteresis loop: negative values indicate pot-bellied, positive values are related to wasp-waisted hysteresis curves), first and second Curie temperature in heating curve (T_{C1}(HC) and T_{C2}(HC), respectively, °C), area between the measured data and the ideal line for Stoner-Wohlfarth particel in Henkel plot (dE(h)), amplitude of extremum in difference between IRM acquisition and backfield measurement (dM(extr.)) and field value corresponding to dM(extr.) (B(dM)).

Table B.1: Rock magnetic data for Montaña Blanca and El Pasajiron

1.part

Sample	Weight	B_{cr}	S_{300}	Slope	M_{rs}	M_s	B_c	B_{rh}	M_{rs}/M_s
EPJ1-1C	1685	53,66	1,01	1,69E-07	0,000093	0,000223	29,92	53,71	0,41
EPJ1-2B450	354	86,32	0,98	6,28E-08	0,000094	0,000227	53,23	85,2	0,42
EPJ1-2B500	354	85,82	0,98	6,05E-08	0,000092	0,00022	52,71	84,49	0,42
EPJ1-2B550	354	85,72	0,98	5,93E-08	0,000093	0,000216	52,91	82,8	0,43
EPJ1-2B600	354	90,45	0,98	6,64E-08	0,0001	0,000222	57,23	86,41	0,45
EPJ1-2Bn600	354	95,4	0,97	6,71E-08	0,000101	0,000217	61,19	90,83	0,46
EPJ1-3A	186	93,5	0,98	5,09E-08	0,000075	0,000184	52,84	88,64	0,41
EPJ1-4C	365	87,87	0,98	6,26E-08	0,000105	0,000242	55,87	85,09	0,43
EPJ2-1C	273	73,09	0,94	4,05E-08	0,00001	0,000039	23,1	68	0,25
EPJ2-2D	248	100,34	0,94	4,81E-08	0,000018	0,000079	28,5	102,27	0,23
EPJ2-3	369	105,25	0,95	6,29E-08	0,000055	0,000127	63,72	102,33	0,43
EPJ2-4C	130	97,99	0,97	1,01E-07	0,000142	0,000424	54,85	94,14	0,34
EPJ2-5C	138	121,77	0,94	1,12E-07	0,000109	0,000371	59,24	117,31	0,3
EPJ2-6B450	292	135,97	0,92	1,39E-07	0,000125	0,000433	66,93	128,46	0,29
EPJ2-6B500	292	135,71	0,92	1,39E-07	0,000126	0,000438	66,62	127,27	0,29
EPJ2-6B550	292	131,8	0,92	1,33E-07	0,000124	0,000437	63,94	123,27	0,28
EPJ2-6B600	292	129,69	0,92	1,32E-07	0,000123	0,000433	63,23	121,48	0,28
EPJ2-6Bn600	292	126,8	0,92	1,35E-07	0,000126	0,000442	62,2	118,69	0,28
EPJ2-7C	363	79,06	0,99	9,89E-08	0,000222	0,000554	52,26	78,75	0,4
EPJ2-8A	98	88,4	0,99	6,82E-08	0,000174	0,000382	63,67	84,84	0,45
LB1-1A	316	36,06	1	1,26E-07	0,000033	0,000115	17,65	37,6	0,29
LB1-2C	454	32,61	1	2,74E-09	0,000067	0,000124	16,48	28,24	0,54
LB1-3C	443	38,66	1	-1,53E-09	0,000109	0,000159	24,61	33,26	0,68
LB1-4C500	227	59,18	0,99	8,45E-09	0,000135	0,000191	38,04	49,15	0,71
LB1-4C550	227	60,19	0,98	2,61E-09	0,00014	0,000196	38,37	51,53	0,71
LB1-4Cn550	227	59,23	0,98	-3,55E-10	0,000142	0,000193	37,39	48,9	0,74
LB1-5A	380	86,54	0,98	-1,96E-08	0,000158	0,000175	52,07	56,63	0,9
LB1-6A	158	116,38	0,95	2,18E-07	0,000072	0,00012	79,84	116,73	0,6
LB1-7D	414	91,29	0,97	-2,28E-10	0,000094	0,000151	54,74	79,88	0,62
MBD1-1A	152	92,58	0,95	9,03E-08	0,000078	0,000223	49,28	92,17	0,35
MBD1-1AD	200	94,49	0,95	8,73E-08	0,000079	0,000181	60,14	93,27	0,44
MBD1-2D	120	101,87	0,95	9,10E-08	0,000108	0,000231	71,61	103,71	0,47

1.part continued

Sample	Weight	B_{cr}	S_{300}	Slope	M_{rs}	M_s	B_c	B_{rh}	M_{rs}/M_s
MBD1-4D450	395	74,59	0,96	7,42E-08	0,000023	0,000079	36,35	74,34	0,29
MBD1-4D500	395	76,4	0,93	7,73E-08	0,000024	0,000081	36,49	74,11	0,3
MBD1-4D550	395	75,85	0,94	7,44E-08	0,000023	0,00008	36,17	75,45	0,29
MBD1-4D600	395	75	0,94	7,32E-08	0,000023	0,000079	35,64	72,37	0,3
MBD1-4Dn600	395	74,55	0,94	7,25E-08	0,000023	0,000079	35,25	72,38	0,29
MBD1-5C	313	78,85	0,96	7,03E-08	0,000015	0,000075	19,43	71,47	0,2
MBD1-6C	207	85,86	0,95	6,54E-08	0,000011	0,000052	32,88	86,89	0,21
MBD1-7D	168	89,78	0,97	8,19E-08	0,000051	0,000141	56,75	87,88	0,36
MBD1-8b	429	75,57	0,98	7,69E-08	0,000048	0,000159	46,53	74,29	0,3
MBT1-1C	412	71,67	0,99	4,87E-10	0,000081	0,000168	38,62	65,86	0,48
MBT1-2D	240	66,33	0,99	-7,78E-09	0,000126	0,000287	34,64	60,99	0,44
MBT1-3A	412	93,05	0,98	7,58E-08	0,000029	0,000053	60,86	88,63	0,56
MBT1-4C	250	96,01	0,99	1,15E-07	0,000028	0,000107	25,45	92,45	0,26
MBT1-5A450	206	72,24	0,99	8,93E-08	0,000078	0,000192	41,15	70	0,41
MBT1-5A500	206	74,27	0,97	8,64E-08	0,000079	0,000194	40,49	69,22	0,41
MBT1-5A550	206	74,2	0,96	8,70E-08	0,000079	0,000196	40,48	69,02	0,4
MBT1-5An550	206	74,78	0,96	8,87E-08	0,00008	0,000195	40,9	68,61	0,41
MBT1-6D	377	82,65	0,99	1,12E-07	0,000037	0,000078	47,36	77,35	0,47
MBT1-7C	378	69,66	0,98	8,44E-08	0,000008	0,000034	20,01	69,15	0,23
MBT1-8C	145	78,76	0,99	7,10E-08	0,00002	0,000045	47,44	74,69	0,46
MBT1-9	516	70,58	0,99	1,17E-08	0,000047	0,000128	35,52	69,99	0,37
MBT1-10E	252	75,37	0,99	1,08E-07	0,000035	0,000072	45,64	70,95	0,48
MBT1-11A	213	79,79	0,98	7,10E-08	0,000016	0,000039	41,22	72,27	0,42
MBT1-12D	236	83,32	0,98	7,19E-08	0,000017	0,000033	48,64	76,72	0,51
MBT1-13A	236	82,4	0,99	7,18E-08	0,000016	0,000033	49,17	76,13	0,49
MBT1-14C	338	91,19	0,98	7,85E-08	0,000011	0,000046	19,72	88,57	0,24
UMB1-1C	480	66,11	0,99	7,07E-08	0,000005	0,000016	22,68	68,86	0,28
UMB1-2D	202	88,97	0,97	5,36E-08	0,000005	0,000014	37,8	84,51	0,38
UMB1-3C	310	86,78	0,96	6,09E-08	0,000007	0,000017	36,31	82,63	0,38
UMB1-4D500	327	80,35	0,98	5,93E-08	0,000011	0,000041	35,92	83,09	0,27
UMB1-4D550	327	81,84	0,95	5,83E-08	0,000011	0,00004	36,04	83,47	0,27
UMB1-4D600	327	81,55	0,95	5,67E-08	0,000011	0,000039	36,11	82,71	0,27
UMB1-4D650	327	81,62	0,95	5,55E-08	0,000011	0,00004	36,07	78,43	0,29
UMB1-4Dn650	327	82,66	0,96	5,57E-08	0,000011	0,000039	35,77	84,18	0,27
UMB1-5B	349	78,25	0,98	5,29E-08	0,000003	0,000013	27,56	75,75	0,24

2.part

Sample	B_{cr}/B_c	B_{rh}/B_{cr}	shape	T_{c1}(HC)	T_{c2}(HC)	dE(h)	dM(extr.)	B(dM)
EPJ1-1C	1,79	1	-0,8	511	0	0,03	0,07	40
EPJ1-2B450	1,62	0,99	-0,9	0	0	0,09	-0,13	136
EPJ1-2B500	1,63	0,98	-0,92	0	0	999	0	0
EPJ1-2B550	1,62	0,97	-0,92	493	0	999	0	0
EPJ1-2B600	1,58	0,96	-0,91	516	0	999	0	0
EPJ1-2Bn600	1,56	0,95	-0,87	0	0	999	0	0
EPJ1-3A	1,77	0,95	-0,9	526	0	0,09	-0,14	117
EPJ1-4C	1,57	0,97	-0,94	512	0	0,08	-0,13	113
EPJ2-1C	3,16	0,93	-0,65	508	0	0,12	0,22	64
EPJ2-2D	3,52	1,02	-0,62	435	0	0,06	0,13	61
EPJ2-3	1,65	0,97	-0,87	508	0	0,04	0,09	81
EPJ2-4C	1,79	0,96	-1,08	489	0	0,05	0,09	68
EPJ2-5C	2,06	0,96	-1,11	476	0	0,06	-0,11	222
EPJ2-6B450	2,03	0,94	-1,17	0	0	0,03	-0,07	184
EPJ2-6B500	2,04	0,94	-1,19	0	0	999	0	0
EPJ2-6B550	2,06	0,94	-1,19	496	0	999	0	0
EPJ2-6B600	2,05	0,94	-1,19	496	0	999	0	0
EPJ2-6Bn600	2,04	0,94	-1,21	0	0	999	0	0
EPJ2-7C	1,51	1	-1,06	533	0	0,06	-0,11	129
EPJ2-8A	1,39	0,96	-1,07	535	0	0,07	-0,12	138
LB1-1A	2,04	1,04	-0,84	361	522	0,04	0,11	40
LB1-2C	1,98	0,87	-0,63	294	0	0,04	0,13	40
LB1-3C	1,57	0,86	-0,62	185	0	0,12	0,25	40
LB1-4C500	1,56	0,83	-0,6	242	0	999	0	0
LB1-4C550	1,57	0,86	-0,61	502	252	999	0	0
LB1-4Cn550	1,58	0,83	-0,6	0	0	999	0	0
LB1-5A	1,66	0,65	-0,64	356	0	0,1	0,19	80
LB1-6A	1,46	1	-0,7	198	366	0,09	-0,15	130
LB1-7D	1,67	0,87	-0,71	213	426	0,03	0,05	80
MBD1-1A	1,88	1	-0,86	528	387	0,09	-0,15	117
MBD1-1AD	1,57	0,99	-0,82	507	0	0,05	-0,11	120
MBD1-2D	1,42	1,02	-0,9	308	0	0,05	-0,12	126
MBD1-4D450	2,05	1	-0,95	0	0	0,14	-0,2	123
MBD1-4D500	2,09	0,97	-0,89	0	0	999	0	0
MBD1-4D550	2,1	0,99	-0,94	0	0	999	0	0
MBD1-4D600	2,1	0,96	-0,94	532	0	999	0	0

2.part continued

Sample	B_{cr}/B_c	B_{rh}/B_{cr}	shape	T_{c1}(HC)	T_{c2}(HC)	dE(h)	dM(extr.)	B(dM)
MBD1-4Dn600	2,11	0,97	-0,94	0	0	999	0	0
MBD1-5C	4,06	0,91	-0,65	533	263	0,14	-0,21	129
MBD1-6C	2,61	1,01	-0,97	533	0	0,15	-0,24	135
MBD1-7D	1,58	0,98	-1,07	528	0	0,08	-0,15	113
MBD1-8b	1,62	0,98	-1,27	522	0	0,04	0,09	55
MBT1-1C	1,86	0,92	-0,8	524	0	0,03	-0,08	110
MBT1-2D	1,91	0,92	-0,86	484	0	0,04	-0,08	100
MBT1-3A	1,53	0,95	-0,76	506	0	0,03	0,07	60
MBT1-4C	3,77	0,96	-0,66	206	498	0,04	0,1	70
MBT1-5A450	1,76	0,97	-0,93	0	0	0,05	-0,12	110
MBT1-5A500	1,83	0,93	-0,93	470	0	999	0	0
MBT1-5A550	1,83	0,93	-0,94	483	0	999	0	0
MBT1-5An550	1,83	0,92	-0,94	0	0	999	0	0
MBT1-6D	1,75	0,94	-0,77	497	0	0,07	0,17	80
MBT1-7C	3,48	0,99	-0,66	241	491	0,06	0,12	40
MBT1-8C	1,66	0,95	-0,85	494	0	0,04	0,1	80
MBT1-9	1,99	0,99	-0,9	515	0	0,03	0,07	80
MBT1-10E	1,65	0,94	-0,78	474	0	0,07	0,14	50
MBT1-11A	1,94	0,91	-0,81	194	484	0,08	0,15	80
MBT1-12D	1,71	0,92	-0,7	483	0	0,04	0,11	80
MBT1-13A	1,68	0,92	-0,77	473	209	0,09	0,17	50
MBT1-14C	4,62	0,97	-0,52	204	482	0,09	0,19	70
UMB1-1C	2,91	1,04	-0,66	545	238	0,04	-0,06	100
UMB1-2D	2,35	0,95	-0,67	542	0	0,04	-0,07	10
UMB1-3C	2,39	0,95	-0,71	549	0	0,02	-0,06	20
UMB1-4D500	2,24	1,03	-0,93	0	0	999	0	0
UMB1-4D550	2,27	1,02	-0,89	0	0	999	0	0
UMB1-4D600	2,26	1,01	-0,93	531	0	999	0	0
UMB1-4D650	2,26	0,96	-0,93	545	0	999	0	0
UMB1-4Dn650	2,31	1,02	-0,9	0	0	999	0	0
UMB1-5B	2,84	0,97	-0,81	552	0	0,04	-0,08	110

B.2 Paleointensity results and various quality parameters for Montaña Blanca

Tab. B.2:
The whole table is split in four parts. Sample name (Name), paleointensity (Paleoint, μT) and standard deviation (Stddev, μT) of each sample are given in each part of the table. Additionally, the first part gives minimum (T_{min}, °C) and maximum temperature (T_{max}, °C) of the temperature interval used for paleointensity determination, number of successive measurement steps used for paleointensity determination (N), slope of best fit line, standard deviation of fit/slope of fit, and fraction of NRM f [Coe et al., 1978]. The second part gives gap factor g [Coe et al., 1978], quality factor q [Coe et al., 1978], weighting factor w [Prévot et al., 1985], TRM (intersection between linear fit and x-axis, mA/m), true NRM (intersection between linear fit and y-axis, mA/m), inclination as calculated for an anchored-to-the-origin fit (Inc anchored, °) and declination as calculated for an anchored-to-the-origin fit (Dec anchored, °). The third part of the table gives maximum angular deviation as calculated for an anchored-to-the-origin fit (Mad anchored, °), inclination as calculated for a not-anchored fit (Inc free, °), declination as calculated for a not-anchored fit (Dec free, °), maximum angular deviation as calculated for a not-anchored fit (Mad free, °), angular difference between anchored and not-anchored solution (alpha, °), coordinates (CC: core coordinates) and type of paleointensity method (MT4, [Leonhardt et al., 2004]). The fourth part gives class of paleointensity determination (A, B or C as defined by Leonhardt et al. (2004); additional * indicates check correction), CK-error (difference between pTRM*-check and related pTRM* acquisition normalized to the TRM), CK-difference (CK-diff, cumulative difference of the individual checks from room temperature up to the maximum temperature used for the best fit line), difference ratio (Drat, difference between pTRM*-check and related pTRM* acquisition normalized length of the selected segment) [Selkin and Tauxe, 2000], tail parameter (d(t*), tail of pTRM parameter t* normalized to the NRM), differences between the first demagnetization step (TH) and the thermal repeat step (TR) regarding intensity and directional changes (d(TR)) and relative additivity check error d(AC).

Table B.2: Paleointensity results and various quality parameters for Montaña Blanca

1.part Name	Labfield	Paleoint	Stddev	Tmin	Tmax	N	slope	Std/slope	f
LB1-1C	30,00	70,2	4,7	200	460	7	-2,34	0,07	0,67
LB1-2C	30,00	61,0	1,7	20	430	8	-2,03	0,03	0,92
LB1-3C	30,00	71,9	1,3	20	300	5	-2,39	0,02	0,86
LB1-4C	30,00	63,9	1,8	20	490	10	-2,13	0,03	0,97
LB1-5C	30,00	0,0	0,0	20	580	0	0,00	0,00	0,00
LB1-6A	30,00	0,0	0,0	20	580	0	0,00	0,00	0,00
LB1-7D	30,00	71,0	0,7	100	390	6	-2,36	0,01	0,87
MBD1-1A	30,00	65,2	1,2	20	550	12	-2,17	0,02	1,00
MBD1-1AD	30,00	72,8	0,8	20	490	10	-2,43	0,01	0,92
MBD1-2D	30,00	73,8	1,3	300	460	5	-2,46	0,02	0,41
MBD1-3C	30,00	61,7	1,2	20	580	13	-2,06	0,02	0,98
MBD1-4D	30,00	63,2	2,0	20	580	13	-2,11	0,03	0,99
MBD1-5C	30,00	64,0	0,3	200	490	8	-2,13	0,00	0,82
MBD1-6D	30,00	52,4	0,7	300	580	9	-1,75	0,01	0,97
MBD1-7D	30,00	0,0	0,0	0	0	0	0,00	0,00	0,00
MBD1-8C	30,00	0,0	0,0	20	580	0	0,00	0,00	0,00
MBT1-1C	30,00	0,0	0,0	20	580	0	0,00	0,00	0,00
MBT1-3C	30,00	62,2	0,9	300	580	9	-2,07	0,01	0,97
MBT1-4C	30,00	0,0	0,0	20	580	0	0,00	0,00	0,00
MBT1-5A	30,00	65,7	1,1	20	580	13	-2,19	0,02	1,00
MBT1-6D	30,00	69,5	1,8	200	580	11	-2,32	0,03	0,97
MBT1-8C	30,00	62,5	1,3	20	580	13	-2,08	0,02	0,98
MBT1-9	30,00	80,2	3,7	460	580	5	-2,67	0,05	0,70
MBT1-10E	30,00	70,8	1,9	430	580	6	-2,36	0,03	0,66
MBT1-11A	30,00	56,1	0,9	250	520	8	-1,87	0,02	0,93
MBT1-12D	30,00	63,7	3,0	390	580	7	-2,12	0,05	0,84
MBT1-13A	30,00	67,9	0,6	300	580	9	-2,26	0,01	0,90
MBT1-14C	30,00	64,3	0,8	20	580	13	-2,14	0,01	0,98
UMB1-1D	30,00	65,6	1,3	350	580	8	-2,19	0,02	0,98
UMB1-2D	30,00	62,9	2,5	430	550	5	-2,10	0,04	0,87
UMB1-3C	30,00	67,0	1,4	430	580	6	-2,23	0,02	0,94
UMB1-4D	30,00	60,2	3,7	430	580	6	-2,00	0,06	0,89
UMB1-5C	30,00	61,0	1,5	430	580	6	-2,03	0,03	0,90

2.part

Name	Paleoint	Stddev	g	q	w	TRM	NRMt	Inc anch.	Dec anch.
LB1-1C	70,2	4,7	0,75	7,50	3,30	2857,10	6684,30	23,90	74,90
LB1-2C	61,0	1,7	0,78	25,40	10,40	259,60	527,60	-7,50	181,80
LB1-3C	71,9	1,3	0,60	29,60	17,10	5938,80	14223,20	-17,10	209,10
LB1-4C	63,9	1,8	0,84	29,10	10,30	487,00	1037,60	18,20	275,40
LB1-5C	0,0	0,0	0,00	0,00	0,00	0,00	0,00	0,00	0,00
LB1-6A	0,0	0,0	0,00	0,00	0,00	0,00	0,00	0,00	0,00
LB1-7D	71,0	0,7	0,68	63,40	31,70	378,10	894,20	-0,80	24,00
MBD1-1A	65,2	1,2	0,87	49,00	15,50	281,40	611,70	52,10	190,40
MBD1-1AD	72,8	0,8	0,86	68,40	24,20	352,40	855,20	-36,80	335,10
MBD1-2D	73,8	1,3	0,75	17,40	10,10	4415,50	10858,00	35,50	68,40
MBD1-3C	61,7	1,2	0,73	37,90	11,40	9214,50	18954,30	-74,40	358,20
MBD1-4D	63,2	2,0	0,84	26,50	8,00	2694,70	5676,30	-52,40	149,70
MBD1-5C	64,0	0,3	0,72	141,50	57,80	184,50	393,50	78,30	288,00
MBD1-6D	52,4	0,7	0,79	59,60	22,50	494,80	864,50	48,00	244,50
MBD1-7D	0,0	0,0	0,00	0,00	0,00	0,00	0,00	0,00	0,00
MBD1-8C	0,0	0,0	0,00	0,00	0,00	0,00	0,00	0,00	0,00
MBT1-1C	0,0	0,0	0,00	0,00	0,00	0,00	0,00	0,00	0,00
MBT1-3C	62,2	0,9	0,76	51,80	19,60	592,30	1228,30	15,60	73,80
MBT1-4C	0,0	0,0	0,00	0,00	0,00	0,00	0,00	0,00	0,00
MBT1-5A	65,7	1,1	0,84	48,90	14,70	581,70	1273,90	10,20	83,70
MBT1-6D	69,5	1,8	0,76	28,40	9,50	294,70	682,30	-64,70	171,20
MBT1-8C	62,5	1,3	0,68	32,60	9,80	263,70	549,00	-66,80	183,50
MBT1-9	80,2	3,7	0,44	6,70	3,90	528,30	1413,00	-32,30	141,40
MBT1-10E	70,8	1,9	0,64	16,40	8,20	248,10	585,80	-62,00	126,70
MBT1-11A	56,1	0,9	0,76	45,90	18,70	71,80	134,30	59,80	277,70
MBT1-12D	63,7	3,0	0,72	12,80	5,70	103,50	219,70	-36,30	333,10
MBT1-13A	67,9	0,6	0,80	79,20	29,90	310,90	703,90	-67,50	58,80
MBT1-14C	64,3	0,8	0,78	59,10	17,80	242,40	519,20	-69,70	355,20
UMB1-1D	65,6	1,3	0,70	35,10	14,30	2215,50	4840,90	48,90	53,40
UMB1-2D	62,9	2,5	0,69	15,30	8,90	2774,40	5817,10	-59,60	198,40
UMB1-3C	67,0	1,4	0,68	30,00	15,00	108,40	242,10	59,80	183,00
UMB1-4D	60,2	3,7	0,69	9,90	4,90	127,60	255,90	-49,90	175,30
UMB1-5C	61,0	1,5	0,74	26,50	13,20	1795,80	3653,70	40,30	46,70

3.part Name	Paleoint	Stddev	Mad anch.	Inc free	Dec free	Mad free	Alpha	Coordinates	Type
LB1-1C	70,2	4,7	2,50	24,30	72,60	5,50	2,20	CC	MT4
LB1-2C	61,0	1,7	4,00	-8,30	182,60	7,50	1,10	CC	MT4
LB1-3C	71,9	1,3	1,50	-17,50	208,70	2,50	0,50	CC	MT4
LB1-4C	63,9	1,8	4,40	18,00	274,20	6,80	1,20	CC	MT4
LB1-5C	0,0	0,0	0,00	0,00	0,00	0,00	0,00	CC	MT4
LB1-6A	0,0	0,0	0,00	0,00	0,00	0,00	0,00	CC	MT4
LB1-7D	71,0	0,7	1,70	-1,40	22,60	2,10	1,60	CC	MT4
MBD1-1A	65,2	1,2	1,70	52,30	189,90	2,70	0,40	CC	MT4
MBD1-1AD	72,8	0,8	4,30	-35,20	332,30	7,40	2,80	CC	MT4
MBD1-2D	73,8	1,3	0,90	35,70	68,50	2,20	0,30	CC	MT4
MBD1-3C	61,7	1,2	0,60	-74,40	358,50	1,20	0,10	CC	MT4
MBD1-4D	63,2	2,0	2,90	-51,20	149,90	5,00	1,20	CC	MT4
MBD1-5C	64,0	0,3	0,80	78,70	289,90	1,70	0,50	CC	MT4
MBD1-6D	52,4	0,7	2,50	48,20	243,10	3,40	0,90	CC	MT4
MBD1-7D	0,0	0,0	0,00	0,00	0,00	0,00	0,00	CC	MT4
MBD1-8C	0,0	0,0	0,00	0,00	0,00	0,00	0,00	CC	MT4
MBT1-1C	0,0	0,0	0,00	0,00	0,00	0,00	0,00	CC	MT4
MBT1-3C	62,2	0,9	2,50	16,80	73,50	3,60	1,30	CC	MT4
MBT1-4C	0,0	0,0	0,00	0,00	0,00	0,00	0,00	CC	MT4
MBT1-5A	65,7	1,1	6,30	11,60	83,60	10,00	1,50	CC	MT4
MBT1-6D	69,5	1,8	3,40	-64,40	174,30	6,00	1,40	CC	MT4
MBT1-8C	62,5	1,3	2,60	-67,80	182,80	5,20	1,00	CC	MT4
MBT1-9	80,2	3,7	5,40	-32,10	139,80	6,00	1,40	CC	MT4
MBT1-10E	70,8	1,9	4,20	-62,30	129,20	5,10	1,20	CC	MT4
MBT1-11A	56,1	0,9	4,10	63,20	278,10	7,50	3,50	CC	MT4
MBT1-12D	63,7	3,0	6,20	-37,80	335,20	7,80	2,30	CC	MT4
MBT1-13A	67,9	0,6	2,50	-67,50	59,50	3,70	0,30	CC	MT4
MBT1-14C	64,3	0,8	1,70	-69,40	355,20	3,50	0,20	CC	MT4
UMB1-1D	65,6	1,3	1,50	48,40	54,00	2,60	0,60	CC	MT4
UMB1-2D	62,9	2,5	1,00	-59,30	197,60	1,70	0,50	CC	MT4
UMB1-3C	67,0	1,4	1,50	59,80	183,20	2,60	0,10	CC	MT4
UMB1-4D	60,2	3,7	3,80	-50,00	176,20	6,40	0,60	CC	MT4
UMB1-5C	61,0	1,5	1,30	40,10	46,90	2,20	0,20	CC	MT4

4.part

Name	Paleoint	Stddev	Class	CK-error	CK-diff	Drat	d(t*)	d(TR)	d(AC)
LB1-1C	70,2	4,7	C	6,10	15,60	3,60	8,00	0,90	1,80
LB1-2C	61,0	1,7	B	1,80	9,50	0,90	2,70	1,00	4,40
LB1-3C	71,9	1,3	A	2,60	3,40	1,20	2,00	1,90	3,30
LB1-4C	63,9	1,8	B	3,60	6,70	1,60	2,40	0,40	6,60
LB1-5C	0,0	0,0		0,00	0,00	0,00	0,00	0,00	0,00
LB1-6A	0,0	0,0		0,00	0,00	0,00	0,00	0,00	0,00
LB1-7D	71,0	0,7	A	1,30	3,40	0,60	0,30	0,70	2,80
MBD1-1A	65,2	1,2	B	4,50	8,70	1,90	5,60	0,60	6,30
MBD1-1AD	72,8	0,8	A	2,20	1,90	0,90	1,90	2,40	1,80
MBD1-2D	73,8	1,3	B	4,70	8,50	4,30	3,70	0,90	2,90
MBD1-3C	61,7	1,2	B	3,60	6,30	1,60	9,20	0,90	2,60
MBD1-4D	63,2	2,0	B	5,50	3,40	2,40	2,20	2,00	6,50
MBD1-5C	64,0	0,3	B	5,60	9,20	2,90	7,10	0,70	2,80
MBD1-6D	52,4	0,7	B	5,40	0,90	2,70	0,90	0,50	0,90
MBD1-7D	0,0	0,0		0,00	0,00	0,00	0,00	0,00	0,00
MBD1-8C	0,0	0,0		0,00	0,00	0,00	0,00	0,00	0,00
MBT1-1C	0,0	0,0		0,00	0,00	0,00	0,00	0,00	0,00
MBT1-3C	62,2	0,9	B	4,50	8,70	2,00	3,80	2,30	2,90
MBT1-4C	0,0	0,0		0,00	0,00	0,00	0,00	0,00	0,00
MBT1-5A	65,7	1,1	C	8,60	8,60	3,60	5,50	1,20	8,80
MBT1-6D	69,5	1,8	A	2,90	2,30	1,20	0,90	4,00	2,50
MBT1-8C	62,5	1,3	B	6,50	4,60	2,90	0,70	5,00	1,00
MBT1-9	80,2	3,7	B	4,20	6,30	2,10	0,20	5,10	2,80
MBT1-10E	70,8	1,9	B	1,30	0,10	0,70	3,60	2,10	1,90
MBT1-11A	56,1	0,9	B	6,40	1,10	3,20	1,20	2,00	1,00
MBT1-12D	63,7	3,0	B	6,80	5,20	3,40	4,50	0,60	2,10
MBT1-13A	67,9	0,6	B	1,60	8,70	0,70	3,10	0,70	1,20
MBT1-14C	64,3	0,8	A	2,20	0,00	0,90	2,10	1,60	0,40
UMB1-1D	65,6	1,3	C	7,30	1,70	3,10	9,10	1,70	1,80
UMB1-2D	62,9	2,5	B	3,90	5,30	1,90	7,00	2,70	1,80
UMB1-3C	67,0	1,4	A	2,10	0,60	0,90	0,80	6,00	0,50
UMB1-4D	60,2	3,7	C	1,60	18,30	0,80	3,70	6,10	0,70
UMB1-5C	61,0	1,5	B	5,10	9,90	2,50	6,70	1,00	0,30

B.3 Paleointensity results and various quality parameters for El Pasajiron

Tab. B.3:
Please be aware that the data in this table are not for further use as alteration during the laboratory experiment and/or a probably present CRM falsify the results.
The whole table is split in four parts. Sample name (Name), paleointensity (Paleoint, μT) and standard deviation (Stddev, μT) of each sample are given in each part of the table. Additionally, the first part gives minimum (T_{min}, °C) and maximum temperature (T_{max}, °C) of the temperature interval used for paleointensity determination, number of successive measurement steps used for paleointensity determination (N), slope of best fit line, standard deviation of fit/slope of fit, and fraction of NRM f [Coe et al., 1978]. The second part gives gap factor g [Coe et al., 1978], quality factor q [Coe et al., 1978], weighting factor w [Prévot et al., 1985], TRM (intersection between linear fit and x-axis, mA/m), true NRM (intersection between linear fit and y-axis, mA/m), inclination as calculated for an anchored-to-the-origin fit (Inc anchored, °) and declination as calculated for an anchored-to-the-origin fit (Dec anchored, °). The third part of the table gives maximum angular deviation as calculated for an anchored-to-the-origin fit (Mad anchored, °), inclination as calculated for a not-anchored fit (Inc free, °), declination as calculated for a not-anchored fit (Dec free, °), maximum angular deviation as calculated for a not-anchored fit (Mad free, °), angular difference between anchored and not-anchored solution (alpha, °), coordinates (CC: core coordinates) and type of paleointensity method (MT4, [Leonhardt et al., 2004]). The fourth part gives class of paleointensity determination (A, B or C as defined by Leonhardt et al. (2004); additional * indicates check correction), CK-error (difference between pTRM*-check and related pTRM* acquisition normalized to the TRM), CK-difference (CK-diff, cumulative difference of the individual checks from room temperature up to the maximum temperature used for the best fit line), difference ratio (Drat, difference between pTRM*-check and related pTRM* acquisition normalized length of the selected segment), tail parameter (d(t*), tail of pTRM parameter t* normalized to the NRM), differences between the first demagnetization step (TH) and the thermal repeat step (TR) regarding intensity and directional changes (d(TR)) and relative additivity check error d(AC).

Table B.3: Paleointensity results and various quality parameters for El Pasajiron

1.part

Name	Labfield	Paleoint	Stddev	T_{min}	T_{max}	N	slope	Std/slope	f
EPJ1-1C	30,0	68,3	5,4	430	580	6	-2,3	0,1	0,9
EPJ1-2B	30,0	60,6	2,2	20	580	13	-2,0	0,0	1,0
EPJ1-3C	30,0	65,4	1,4	20	580	13	-2,2	0,0	1,0
EPJ1-4C	30,0	67,8	3,9	20	580	13	-2,3	0,1	0,9
EPJ2-1C	30,0	0,0	0,0	20	580	0	0,0	0,0	0,0
EPJ2-2B	30,0	17,9	0,4	350	580	8	-0,6	0,0	0,8
EPJ2-3	30,0	24,5	0,8	200	490	8	-0,8	0,0	0,5
EPJ2-4C	30,0	28,6	0,7	350	550	7	-1,0	0,0	1,0
EPJ2-5C	30,0	36,7	0,7	20	580	13	-1,2	0,0	1,0
EPJ2-6B	30,0	37,3	0,6	20	520	11	-1,2	0,0	0,8
EPJ2-7C	30,0	71,2	2,2	20	580	13	-2,4	0,0	1,0
EPJ2-8C	30,0	64,4	4,7	20	580	13	-2,2	0,1	1,0

2.part

Name	Paleoint	Stddev	g	q	w	TRM	NRMt	Inc anch.	Dec anch.
EPJ1-1C	68,3	5,4	0,7	7,9	4,0	8179,3	18607,5	39,0	8,1
EPJ1-2B	60,6	2,2	0,2	6,7	2,0	8390,0	16945,5	40,2	338,9
EPJ1-3C	65,4	1,4	0,7	33,8	10,2	788,0	1718,9	34,5	175,2
EPJ1-4C	67,8	3,9	0,4	5,5	1,7	9131,8	20621,2	-20,3	25,8
EPJ2-1C	0,0	0,0	0,0	0,0	0,0	0,0	0,0	0,0	0,0
EPJ2-2B	17,9	0,4	0,8	29,6	12,1	1868,2	1117,0	1,3	47,5
EPJ2-3	24,5	0,8	0,8	11,4	4,7	280,8	228,9	2,7	233,4
EPJ2-4C	28,6	0,7	0,8	30,3	13,6	42256,9	40237,0	-20,5	53,1
EPJ2-5C	36,7	0,7	0,7	36,9	11,1	5195,6	6358,8	-1,1	149,5
EPJ2-6B	37,3	0,6	0,3	13,8	4,6	7246,2	9002,5	-33,2	74,0
EPJ2-7C	71,2	2,2	0,7	21,9	6,6	7615,2	18066,7	-14,1	143,7
EPJ2-8C	64,4	4,7	0,6	7,3	2,2	82933,4	178008,4	-23,3	219,3

3.part

Name	Paleoint	Stddev	Mad anch.	Inc free	Dec free	Mad free	Alpha	Coordinates	Type
EPJ1-1C	68,3	5,4	2,4	39,0	7,0	3,3	0,8	CC	MT4
EPJ1-2B	60,6	2,2	3,4	40,1	339,0	6,1	0,1	CC	MT4
EPJ1-3C	65,4	1,4	2,9	34,4	176,1	5,1	0,8	CC	MT4
EPJ1-4C	67,8	3,9	2,5	-20,4	26,1	4,5	0,3	CC	MT4
EPJ2-1C	0,0	0,0	0,0	0,0	0,0	0,0	0,0	CC	MT4
EPJ2-2B	17,9	0,4	7,8	0,8	45,9	14,0	1,7	CC	MT4
EPJ2-3	24,5	0,8	3,0	3,5	232,9	12,2	0,9	CC	MT4
EPJ2-4C	28,6	0,7	3,3	-19,1	54,0	5,7	1,6	CC	MT4
EPJ2-5C	36,7	0,7	5,6	0,2	149,4	10,0	1,2	CC	MT4
EPJ2-6B	37,3	0,6	2,7	-32,5	77,2	9,9	2,7	CC	MT4
EPJ2-7C	71,2	2,2	2,1	-13,4	143,9	4,8	0,7	CC	MT4
EPJ2-8C	64,4	4,7	3,3	-22,7	219,0	7,7	0,7	CC	MT4

4.part

Name	Paleoint	Stddev	Class	CK-error	CK-diff	Drat	d(t*)	d(TR)	d(AC)
EPJ1-1C	68,3	5,4	C	20,0	27,4	9,4	3,4	1,7	11,4
EPJ1-2B	60,6	2,2	C	69,5	159,0	31,2	1,3	2,9	1,0
EPJ1-3C	65,4	1,4	C	15,7	19,8	6,6	2,1	1,8	8,0
EPJ1-4C	67,8	3,9	C	47,4	106,1	20,7	7,3	4,4	14,6
EPJ2-1C	0,0	0,0		0,0	0,0	0,0	0,0	0,0	0,0
EPJ2-2B	17,9	0,4	B	4,5	3,3	5,2	7,8	1,8	6,4
EPJ2-3	24,5	0,8	A	2,1	2,5	3,1	2,0	3,4	0,5
EPJ2-4C	28,6	0,7	B	6,5	5,8	4,8	2,2	4,9	6,3
EPJ2-5C	36,7	0,7	C	21,3	16,1	13,6	4,9	0,8	5,0
EPJ2-6B	37,3	0,6	B	5,8	6,4	4,7	1,3	2,7	1,6
EPJ2-7C	71,2	2,2	C	3,9	16,0	1,5	1,5	3,8	0,9
EPJ2-8C	64,4	4,7	C	12,9	31,5	5,7	4,6	2,6	3,5

Bibliography

G. J. Ablay and J. Marti. Stratigraphy, structure, and volcanic evolution of the Pico Teide-Pico Viejo formation, Tenerife, Canary Islands. J. Volcanol. Geotherm. Res., 103 (1-4):175–208, 2000.

G. J. Ablay, G. G. J. Ernst, J. Marti, and R. S. J. Sparks. The 2ka subplinian eruption of Montana Blanca, Tenerife. Bull. Volcanol., 57:337–355, 1995.

E. Ancochea, J. M. Fuster, E. Ibarrola, A. Cendrero, J. Coello, F. Hernan, J. M. Cantagrel, and C. Jamond. Volcanic evolution of the island of Tenerife (Canary Islands) in the light of new K-Ar data. J. Volcanol. Geotherm. Res., 44:231–249, 1990.

A. J. Biggin. How many paleointensity determinations are required from a single lava flow to constitute a reliable average? Geophys. Res. Lett., 30(11):98–101, 2003.

J. Bloemendal, J. W. King, F. R. Hall, and S.-J. Doh. Rock magnetism of late neogene and pleistocene deep-seasediments: Relationship of sediment source, diagenetic processes and sedimentlithology. J. Geophys. Res., 97:4361–4375, 1992.

J. Bowles, J. S. Gee, D. V. Kent, E. Bergmanis, and J. Sinton. Cooling rate effects on paleointensity estimates in submarine basaltic glass and implications for dating young flows. Geochem. Geophys. Geosys., 6:Q07002, doi:10.1029/2004GC000900, 2005.

J. A. Bowles, J. S. Gee, K. Burgess, and R. F. Cooper. Timing of magnetite formation in basaltic glass: Insights from synthetic analogs and relevance for geomagnetic paleointensity analyses. Geochem. Geophys. Geosys., 12(2):Q02001, doi:10.1029/2010GC003404, 2011.

M. D. Buck, R. M. Briggs, and C. S. Nelson. Pyroclastic deposits and volcanic history of mayor island. N. Z. J. Geol. Geophys., 24:449–467, 1981.

A. F. Buddington and D. H. Lindsley. Iron-titanium oxide minerals and synthetic equivalents. J. Petrol., 5:310–357, 1964.

K. Burgess, R. F. Cooper, J. A. Bowles, J. S. Gee, and D. J. Cherniak. Effects of open and closed system oxidation on texture and magnetic response of remelted basaltic glass. Geochem. Geophys. Geosys., 11(10):Q10007, doi:10.1029/2010GC003248, 2010.

A. Chauvin, Y. Garcia, P. Lanos, and F. Laubenheimer. Paleointensity of the geomagnetic field recovered on archaeomagnetic sites from France. Phys. Earth Planet. Sci., 120: 111–136, 2000.

R. S. Coe. The determinations of paleointensities of the Earth's magnetic field with emphasis on mechanisms which could cause non-ideal behavior in Thellier's method. Geomag. Geoelec., 19:157–179, 1967.

R. S. Coe, S. Grommé, and E. A. Mankinen. Geomagnetic paleointensities from radiocarbon-dated lava flows on Hawaii and the question of the Pacific nondipol low. J. Geophys. Res., 83:1740–1756, 1978.

R. D. Cottrell and J. Tarduno. In search of high-fidelity geomagnetic paleointensities: A comparison of single plagioclas crystal and whole rock Thellier-Thellier analyses. J. Geophys. Res., 105:23579–23594, 2000.

R. D. Cottrell and J. A. Tarduno. Geomagnetic paleointensity derived from single plagioclase crystals. Earth Planet. Sci. Lett., 169(1-2):1–5, 1999.

R. Day, M. D. Fuller, and V. A. Schmidt. Hysteresis properties of titanomagnetites: Grain size and composition dependence. Phys. Earth Planet. Inter., 13:260–266, 1977.

M. A. Debolt, A. J. Easteal, P. B. Macedo, and C. T. Moynihan. Analysis of structural relaxation in glass using rate heating data. J. Am. Ceram. Soc., 59 (1-2):16–21, 1976.

M. J. Dekkers and H. N. Böhnel. Reliable absolute palaeointensities independent of magnetic domain state. Earth Planet. Sci. Lett., 248(1-2):508–517, 2006.

J. S. Denton. The post-emplacement hydration and alteration of subglacially erupted obsidian to form perlite. PhD thesis, Lancaster University, 2010.

J. S. Denton, H. Tuffen, J. S. Gilbert, and N. Odling. The hydration and alteration of perlite and rhyolite. J. Geol. Soc., 166(5):895–904, 2009.

J. S. Denton, H. Tuffen, and J. S. Gilbert. Variations in hydration within perlitised rhyolitic lavas - evidence from Torfajökull, Iceland. Journal of Volcanology and Geothermal Research, in revision.

D. B. Dingwell. Structure and Dynamics of silicate melts, chapter Relaxation in silicate melts: some applications in petrology, pages 21–66. Mineral. Soc. of Am., Washington, D. C., 1995.

D. B. Dingwell and S. L. Webb. Relaxation in silicate melts. Eur. J. Min., 2:427–449, 1990.

M. H. Dodson and E. McClelland-Brown. Magnetic blocking temperatures of single-domain grains during slow cooling. J. Geophys. Res., 85:2625–2637, 1980.

F. Donadini, M. Korte, and C. G. Constable. Geomagnetic field for 0–3 ka: 1. new data sets for global modeling. Geochem. Geophys. Geosys., 10:Q06007, doi:10.1029/2008GC002295, 2009.

D. Dunlop. Theory and application of the Day plot (M_{rs}/M_s versus H_{cr}/H_c): 1. Theoretical curves and tests using titanomagnetite data. J. Geophys. Res., 107: doi:10.1029/2001JB000486, 2002.

K. Fabian and R. Leonhardt. Geomagnetic Field Variations, chapter Records of paleomagnetic field variations, pages 65–106. Springer, Berlin, 2009.

K. Fabian and R. Leonhardt. Multiple-specimen absolute paleointensity determination: An optimal protocol including ptrm normalization, domain-state correction, and alteration test. Earth Planet. Sci. Lett., 297:84–94, 2010.

A. Ferk, F. W. von Aulock, R. Leonhardt, K.-U. Hess, and D. B. Dingwell. A cooling rate bias in paleointensity determination from volcanic glass: An experimental demonstration. J. Geophys. Res., 115:B08102, doi:10.1029/2009JB006964, 2010.

A. Ferk, R. Leonhardt, K.-U. Hess, and D. B. Dingwell. Paleointensities on 8 ka obsidian from Mayor Island, New Zealand. Solid Earth, 2:259–270, 2011a.

A. Ferk, R. Leonhardt, F. W. von Aulock, K.-U. Hess, and D. B. Dingwell. Paleointensities of phonolitic obsidian: Influence of emplacement rotations and devitrification. J. Geophys. Res., 116:B12113, doi:10.1029/2011JB008397, 2011b.

A. Ferk, J. S. Denton, R. Leonhardt, H. Tuffen, S. Koch, K.-U. Hess, and D. B. Dingwell. Paleointensity on volcanic glass of varying hydration states. Phys. Earth Planet. Int., submitted.

R. A. Fisher. Dispersion on a sphere. Proc. R. Soc. London Ser. A., 217:295–305, 1953.

J. M. W. Fox and M. J. Aitken. Cooling-rate dependency of thermoremanent magnetisation. Nature, 283:462–463, 1980.

J. W. Geissman, N. G. Newberry, and D. R. Peacor. Discrete single-domain and pseudo-single-domain titanomagnetite particles in silicic glass of an ash flow tuff. Can. J. Earth. Sci, 20:334–338, 1983.

A. Genevey and Y. Gallet. Intensity of the geomagnetic field in western Europe over the past 2000 years: New data from ancient French pottery. J. Geophys. Res., 107(2285): doi:10.1029/2001JB000701, 2002.

A. Genevey, Y. Gallet, C. G. Constable, M. Korte, and G. Hulot. Archeoint: An upgraded compilation of geomagnetic field intensity data for the past ten millenia and its application to the recovery of the past dipole moment. Geochem. Geophys. Geosys., 9:Q04038, doi:10.1029/2007GC001881, 2008.

J. Gottsmann and D. B. Dingwell. Cooling dynamics of spatter-fed phonolite obsidian flows on Tenerife, Canary Islands. J. Volcanol. Geotherm. Res., 105:323–342, 2001a.

J. Gottsmann and D. B. Dingwell. The cooling of frontal flow ramps: a calorimetric study on the Rocche Rosse rhyolite flow, Lipari, Aeolian Islands, Italy. Terra Nova, 13:157–164, 2001b.

J. Gottsmann and D. B. Dingwell. The thermal history of a spatter-fed lava flow: the 8-ka pantellerite flow of Mayor Island, New Zealand. Bull. Volcanol., 64:410–422, 2002.

J. Gottsmann, A. J. L. Harris, and D. B. Dingwell. Thermal history of Hawaiian pa-hoehoe lava crusts at the glass transition: implications for flow rheology and emplacement. Earth Planet. Sci. Lett., 228:343–353, 2004.

B. Gunnarsson. Generation of Icelandic rhyolites: silicic lavas from the Torfajökull central volcano. J. Volcanol. Geotherm. Res., 83(1-2):1–45, 1998.

S. L. Halgedahl, R. Day, and M. Fuller. The effect of cooling rate on the intensity of weak-field TRM in single-domain magnetite. J. Geophys. Res., 85:3690–3698, 1980.

R. Heller. The variation of intensity of Earth's magnetic field with time. Phys. Earth Planet. Int., 131(3-4):237–249, 2002.

R. Heller, R. T. Merrill, and P. L. McFadden. The two states of paleomagnetic field intensities for the past 320 million years. Phys. Earth Planet. Int., 135:211–223, 2003.

C. Helo, M.-A. Longpré, N. Shimizu, D. A. Clague, and J. Stix. Explosive eruptions at mid-ocean ridges driven by CO_2-rich magmas. Nature geoscience, 4:260–263, 2011.

O. Henkel. Remanenzverhalten und Wechselwirkung in hartmagnetischen Teilchenkollektiven. Phys. Stat. Sol., 7:919–929, 1964.

B. F. Houghton and C. J. N. Wilson. Explosive rhyolitic volcanism: the case studies of Mayor Island and Taupo Volcanoes. N. Z. Geol. Surv. Records, 12:33–100, 1986.

B. F. Houghton, S. D. Weaver, C. J. N. Wilson, and M. A. Lanphere. Evolution of a Quaternary peralkaline volcano; Mayor Island, New Zealand. J. Volcan. Geotherm. Res., 51:217–236, 1992.

M. T. Juárez, L. Tauxe, J. S. Gee, and T. Pick. The intensity of the Earth's magnetic field over the past 160 million years. Nature, 394:878–881, 1998.

J. L. Kirschvink. The least-squares line and plane and the analysis of paleomagnetic data. Geophys. J. R. Astron. Soc., 62:699–718, 1980.

M. Korte and C. G. Constable. Continuous geomagnetic field models for the past 7 millennia: 2. CALS7K. Geochem. Geophys. Geosys., 6:Q02H16, doi:10.1029/2004GC000801, 2005.

M. Korte, F. Donadini, and C. G. Constable. Geomagnetic field for 0–3 ka: 2. a new series of time-varying global models. Geochem. Geophys. Geosys., 10:Q06007, doi:10.1029/2008GC002295, 2009.

M. Kovacheva. Some Archaeomagnetic Conclusions from 3 Archaeological Localities in Northwest Africa. C.R. Acad. Sci. Bulg., 37:171–174, 1984.

M. Kovacheva. Recherches archéomagnétiques sur trois sites archéologiques du Maroc. Bull. Archeol. Marocaine, 19:285–293, 1985.

M. Kovacheva, J. Pares, N. Jordanova, and V. Karloukovski. A new contribution to the archaeomagnetic study of a Roman pottery kiln from Calahorra (Spain). Geophys. J. Int., 123:931–936, 1995.

D. Krása, C. Heunemann, R. Leonhardt, and N. Petersen. Experimental procedure to detect multidomain remanence during Thellier-Thellier experiments. Phys. Chem. Earth, 28:681–687, 2003.

R. Leonhardt. Analyzing rock magnetic measurements: The RockMagAnalyzer 1.0 software. Comp. Geosci., 32:1420–1431, 2006.

R. Leonhardt and K. Fabian. Paleomagnetic reconstruction of the global geomagnetic field evolution during the Matuyama/Brunhes transition: Iterative Bayesian inversion and independent verification. Earth Planet. Sci. Lett., 253:172–195, 2007.

R. Leonhardt, C. Heunemann, and D. Krása. Analyzing absolute paleointensity determinations: Acceptance criteria and the software ThellierTool4.0. Geochem. Geophys. Geosys., 5:Q12016, doi:10.1029/2004GC000807, 2004.

R. Leonhardt, D. Krása, and R. S. Coe. Multidomain behavior during Thellier paleointensity experiments: A phenomenological model. Phys. Earth Planet. Inter., 147:127–140, 2004a.

R. Leonhardt, J. Matzka, A. R. L. Nichols, and D. B. Dingwell. Cooling rate correction of paleointensity determination for volcanic glasses by relaxation geospeedometry. Earth Planet. Sci. Lett., 243:282–292, 2006.

R. Leonhardt, K. Fabian, and E. Schnepp. Holocene global geomagnetic field reconstruction based on archeomagnetic data: Assessing error sources and uncertainties. Geophys. Res. Abstr., 12(Abstract EGU2010-9421), 2010.

R. A. Macdonald's. Nomenclature and petrochemistry of the peralkaline oversaturated extrusive rocks. Bull. Volcanol., 38:498–516, 1974.

J. Marti, J. Mitjavila, and V. Arana. Stratigraphy, structure and geochronology of Las Canadas Caldera (Tenerife, Canary Islands). Geol. Mag., 131(6):715–727, 1994.

E. McClelland-Brown. Experiments on TRM intensity dependence on cooling rate. Geophys. Res. Lett., 11:205–208, 1984.

J. McPhie, M. Doyle, and R. Allen. Volcanic Textures. A guide to the interpretation of textures in volcanic rocks. Centre of Ore Deposit and Exploration Studies, University of Tasmania, Hobart, 1993.

B. M. Moskowitz, M. Jackson, and C. Kissel. Low-temperature magnetic behavior of titanomagnetites. Earth Planet. Sci. Lett., 157:141–149, 1998.

A. R. Muxworthy and D. Heslop. A Preisach method for estimating absolute paleofield intensity under the constraint of using only isothermal measurements: 1. Theoretical framework. J. Geophys. Res., 116:doi:10.1029/2010JB007843, 2011.

O. S. Narayanaswamy. A model of structural relaxation in glass. J. Am. Ceram. Soc., 54: 491–498, 1971.

O. S. Narayanaswamy. Thermorheological simplicity in the glass transition. J. Am. Ceram. Soc., 71:900–904, 1988.

S. Newman, E. M. Stolper, and S. Epstein. Measurement of water in rhyolitic glasses : Calibration of an infrared spectroscopic technique. Am. Mineral., 71:1527–1541, 1986.

A. R. L. Nichols, M. Potuzak, and D. B. Dingwell. Cooling rates of basaltic hyaloclastites and pillow lava glasses from the HSDP2 drill core. Geochim. Cosmochim. Acta, 73: 1052–1066, 2009.

J. Owen, H. Tuffen, and D. McGarvie. A reconstruction of the palaeo-ice thickness at Bláhnúkur (Torfajökull, Iceland), using the magma degassing technique. Bull. Volcanol., in revision.

C. Papusoi. Effet de la vitesse de refroidissements sur l'intensité de l'aimantation thermoré manente d'un ensemble de grains monodomaines. An. Stiint. Univ. Al.I. Cuza Iasi Sect. Ib Tomul, 18:31–47, 1972.

J. M. Parés, R. De Jonge, J. O. Pascual, A. Bermúdez, and C. J. Tovar. Archaeomagnetic evidence for the age of a roman pottery kiln from calahorra (spain). Geophys. J. Int., 112:533–537, 1992.

F. J. Pavón-Carrasco, M. L. Osete, J. M. Torta, and L. R. Gaya-Piqué. A regional archeomagnetic model for europe for the last 3000 years, scha.dif.3k: Applications to archeomagnetic dating. Geochem. Geophys. Geosys., 10:Q03013, doi: 10.1029/2008GC002244, 2008.

T. Pick and L. Tauxe. Geomagnetic paleointensities: Thellier experiments on submarine basaltic glass from the east pacific rise. J. Geophys. Res., 98:17949–17964, 1993.

M. Potuzak, A. R. L. Nichols, D. B. Dingwell, and D. A. Clague. Hyperquenched volcanic glass from Loihi Seamount, Hawaii. Earth Planet. Sci. Lett., 270:54–62, 2008.

M. Prévot, E. A. Mankinen, R. S. Coe, and S. Grommé. The Steens Mountain (Oregon) geomagnetic polarity transition 2. Field intensity variations and discussion of reversal models. J. Geophys. Res., 90:10417–10448, 1985.

M. Prévot, M. E. Derder, M. McWilliams, and J. Thompson. Intensity of the Earth's magnetic field: Evidence for a Mesozoic dipole low. Earth Planet. Sci. Lett., 97:129–139, 1990.

P. Riisager and J. Riisager. Detecting multidomain magnetic grains in thellier paleointensity experiments. Phys. Earth Planet. Int., 125:111–117, 2001.

P. A. Selkin and L. Tauxe. Long-term variations in paleointensity. Phil. Trans. R. Soc. London, 358:1065–1088, 2000.

J. Shaw. A new method of determining the magnitude of the palaeomagnetic field: Application to five historic lavas and five archaeological samples. Geophys. J. R. astr. Soc., 39:133–141, 1974.

V. P. Shcherbakov, G. M. Solodovnikov, and N. K. Sycheva. Variations in the geomagnetic dipole during the past 400 million years (volcanic rocks). Izv. Russ. Acad. Sci. Phys. Solid Earth Engl. Trans., 38:113–119, 2002.

A. V. Smirnov and J. A. Tarduno. Magnetic hysteresis monitoring of cretaceous submarine basaltic glass during thellier paleointensity experiments: evidence for alteration and attendant low field bias. Earth Planet. Sci. Lett., 206:571–585, 2003.

R. J. Stevenson, R. M. Briggs, and A. P. W. Hodder. Emplacement history of a low viscosity, fountain-fed pantelleritic lava flow. J. Volcanol. Geotherm. Res., 57:39–56, 1993.

H. Tanaka, N. Komuro, and G. M. Turner. Palaeosecular variation for 0.1-21 Ka from the Okataina Volcanic Centre, New Zealand. Earth Planets Space, 61:213–225, 2009.

J. A. Tarduno, R. D. Cottrell, M. K. Watkeys, and D. Bauch. Geomagnetic field strength 3.2 billion years ago recorded by single silicate crystals. Nature, 446:657–660, 2007.

L. Tauxe. Long-term trends in paleointensity: The contribution of DSDP/ODP submarine basaltic glass collections. Phys. Earth Planet.Int., 156:223–241, 2006.

L. Tauxe and H. Staudigel. Strength of the geomagnetic field in the Cretaceous Normal Superchron: New data from submarine basaltic glass of the Troodos Ophiolite. Geochem. Geophys. Geosys., 5:Q02H06, doi:10.1029/2003GC000635, 2004.

L. Tauxe, T. A. T. Mullender, and T. Pick. Potbellies, wasp-waists and superparamagnetism in magnetic hysteresis. J. Geophys. Res, 101:571–583, 1996.

E Thellier and O Thellier. Sur l'intensité du champ magnétique terrestre dans le passé historique et géologique. Annales de géophysique, 15:285–376, 1959.

A. Q. Tool. Relation between inelastic deformability and thermal expansion of glass in its annealing range. J. Am. Ceram. Soc., 29:240–253, 1946.

H. Tuffen, J. Gilbert, and D. McGarvie. Products of an effusive subglacial rhyolite eruption: Bláhnúkur, Torfajökull, Iceland. Bull. Volcanol., 63(2-3):179–190, 2001.

J.-P. Valet, J. Brassart, I. Le Meur, V. Soler, X. Quidelleur, E. Tric, and P.-Y. Gillot. Absolute paleointensity and magnetomineralogical changes. J. Geophys. Res., 101(B11): 25029–25044, 1996.

R. J. Veitch, I. G. Hedley, and J.-J. Wagner. An investigation of the intensity of the geomagnetic field during roman times using magnetically anisotropic bricks and tiles. Arch. Sc. Genéve, 37:359–373, 1984.

M. C. Wilding, S. L. Webb, and D. B. Dingwell. Evaluation of a relaxation geospeedometer for volcanic glasses. Chem. Geol., 125:137–148, 1995.

M. C. Wilding, S. L. Webb, D. B. Dingwell, G. Ablay, and J. Marti. Cooling vartiations in natural volcanic glasses from Tenerife, Canary Islands. Contrib. Mineral. Petrol., 125: 151–160, 1996a.

M. C. Wilding, S. L. Webb, and D. B. Dingwell. Tektite cooling rates: calorimeteric relaxation geospeedometry applied to natural glass. Geochim. Cosmochim. Acta, 60: 1099–1103, 1996b.

M. C. Wilding, J. L. Smellie, S. Morgan, C. E. Lesher, and L. Wilson. Cooling process recorded in subglacially erupted rhyolite glasses: Rapid quenching, thermal buffering, and the formation of meltwater. J. Geophys. Res., 109(B08201):1–13, 2004.

E. P. Wohlfarth. Relations between different modes of acquisition of the remanent magnetization of ferromagnetic particles. J. Appl. Phys., 29:595–596, 1958.

S. Yang, H. Odah, and J. Shaw. Variations in the geomagnetic dipole moment over the last 12000 years. Geophys. J. Int., 140(1):158–162, 2000.

Y. Yu. Importance of Cooling rate Dependence of Thermoremanence in Paleointensity Determination. J. Geophys. Res., 116:B09101, doi:10.1029/2011JB008388, 2011.

Y. Yu and L. Tauxe. Testing the IZZI protocol of geomagnetic field intensity determination. Geochem. Geophys. Geosys, 6:Q05H17, doi:10.1029/2004GC000840, 2005.

Acknowledgements

There are many people that helped me during the course of this thesis. First of all I want to thank Roman Leonhardt who - at least for me - was pretty close to the perfect supervisor: Thanks, Roman, for on the one hand giving me the freedom to develop my own ideas and on the other hand for being there for me when I had questions or was struggling with a problem. Next I have to thank Don Dingwell who without hesitation accepted to be my official supervisor and who - though having an immense working load and millions of things to do - was always available for me. My warmest thanks to Kai-Uwe Hess who not only always has new ideas for further experiments and following projects, but also helped me with many experiments. My deepest thanks to Joanna Denton, Hugh Tuffen, Felix W. von Aulock and Stephan Koch whose contributions to the different papers are priceless and indispensable. Jo, Hugh, Felix, Roman, Nina Gegenhuber, Joan Marti, Uwe Kirscher, Khachatur Meliksetian and Sergei Karapetian: Thanks for the wonderful time I had on the field trips to Tenerife, Iceland and Armenia with you guys! Thanks to Stuart Gilder for letting me be a part of his work group even in times when I was neither a student nor an employee of the LMU. I am deeply indebted to Ramon Egli, Nikolai Petersen, Michael Winklhofer, Karl Fabian, Robert Scholger and Elisabeth Schnepp who helped me in various ways: experiments, theory, Mathematica programming, rock magnetic knowledge etc. I want to take the opportunity to again thank Joan Marti and Jo Gottsmann who repeatedly answered my questions and provided figures and data of their studies. Many thanks to the Institute of Rock Magnetism for giving me a fellowship for their laboratory. I especially want to thank Mike Jackson who not only dealed with bureaucracy but also introduced me to the measurements and helped me interpreting the data. Julia Linder, Kerstin Reimer, Michael Wack, Mike Volk, Maria Lenius, Simon Kremers, Tobias Megies: Thanks for all the procrastination: some gossip, a nice lunch and a lot of laughter keeps the spirit up.
Though nice supervisors and colleagues are essential to finish a thesis, there are also people from outside the university that helped to make this happen: Mama and Papa, thanks for not letting me know your worries about my future when I started studying geophysics and for instead supporting me in everything I did. Mama, Papa, Angelika and Günther, thanks for the countless babysitting hours and all your love for Ronja. Knowing that Ronja is in the best hands, has given me the possibility to work again after one year of maternity leave without feeling bad. Flo and Ronja: There's no way that all my thanks to you will fit on this page. So I just pick some: Thanks for being my family, my "Fels in der Brandung", for showing me that there's a life beside university, for letting me be like I am...